UNIVERSITY OF CALIFORNIA,
IRVINE

Ion Transport Phenomena at the Nanoscale in Different Model Battery Systems

DISSERTATION

submitted in partial satisfaction of the requirements
for the degree of

DOCTOR OF PHILOSOPHY

in Physics

by

Timothy Stephen Plett

Dissertation Committee:
Professor Zuzanna S. Siwy, Chair
Professor Phil Collins
Professor Reginald M. Penner

2017

DEDICATION

For Mike Oberle (1960-2015)
My first physics teacher
to whom I am forever grateful

TABLE OF CONTENTS

LIST OF FIGURES

LIST OF TABLES

ACKNOWLEDGMENTS

I am grateful for the opportunity to express my heartfelt thanks to those who were integral to my journey toward this moment.

Firstly, to my committee chair and advisor, Professor Zuzanna Siwy, I offer my thanks. As an advisor, she has been the embodiment of encouragement, patience, and charity. At a moment when I was most undeserving, she gave me an opportunity to work alongside one of her students, Dr. Trevor Gamble. Neither of us knew that decision would lead us to today and I am blessed to have had her guidance, perseverance, and academic insight influence my journey in research. Indeed, without her support, it is unlikely I would have completed this program with the level of success we achieved together or even at all.

I would also like to acknowledge Dr. Trevor Gamble, who went before me in this research and from whom I inherited technique and attitude in approaching research. His patience with me in the beginning and his willingness to endure my growing pains was crucial to my development as a researcher. He also gave me courage to step into leadership roles at NEES where he and I both served as student coordinators for a time, an experience which shall prove valuable after leaving grad school.

To my committee members, Professor Phil Collins and Professor Reginald M. Penner, I express gratitude for challenging me to be precise in language and clear in procedure. Their regular input and perspectives on my work opened doors to new insights and opportunities and highlighted the value of academic collaboration.

I also would like to thank fellow student researchers and post-docs, both current and former, both in the Siwy Group and those who participated in NEES. To those who have gone before, Dr. Laura Innes, Dr. Steve Buchsbaum, Dr. Mya Le Thai, Dr. Eleanor Gillette, Jill Pestana, Dr. Alexander Kozen, Dr. Tetyana Ignatova, Dr. Girija Chandran, William Mann, Wenjia (Josslyn) Cai: I offer my appreciation as you each have served as comrades-in-arms or mentors to me in pursuit of scientific knowledge, offering advice and perspective from a position I have now come to understand. To those who are with me now, Crystal Yang, Preston Hinkle, Dr. Yinghua Qiu, Gaurav Jha, Dr. Mina Abad, James Boyd, Juliette Experton, Jonathon Larson: my thanks in helping me endure and persevere to the end. As others involved in the daily challenges, struggles, and triumphs of research, your camaraderie has been a strength to lean on.

Additionally, I acknowledge the researchers at the Energy Frontier Research Center – Nanostructures for Electrical Energy Storage (NEES). Specifically, I would like to offer thanks to Dr. Gary Rubloff of UMD, Dr. Sang-Bok Lee of UMD, and Dr. Kevin Leung of Sandia National Labs, each of whom I have collaborated with on projects. I also would like to thank Dr. Elizabeth Lathrop who has been an effective liaison and source of help and insight in terms of student development and organization. Additionally, I offer thanks to the Thrust 1 PIs for their comments and support, especially Dr. Chuck Martin of University of Florida who routinely offered helpful suggestions and perspective on my findings.

I must also thank my family and friends who have supported me throughout the process of grad school: Stephen and Jeanile Plett, Anna Plett, Lydia and Brett Stroud, Daniel and Callie Kirk, Brian and Kayla Moseley (and Jack and Oliver), Nathan Lau, Timothy Johnson, Dr. Stephen and Sharon Crane, Daniel Quang, Logan Collier, Xiao Zheng, Ashley Uribe, and Jasmine Miller. Each of them supported me in a unique and positive way, rejoicing in my successes and comforting me in my setbacks. For their patience and acceptance, I am forever grateful. "No man is a failure who has friends." –Clarence, *It's a Wonderful Life*

The teachers and professors who led me on the path of science at the beginning are also deserving of praise. Foremost I acknowledge Mike Oberle and Connie Grosse, who were integral in the earliest stages of formal science education. I also give special thanks to Dr. John Silzel who modeled for me what it means to be a compassionate professor who also expected the very best from his students.

I also give a special thanks to the UCI Nihon Karate Club, Sensei Bruce Nguyen, Sensei Ray Galarze, Sensei Chad Eagan, and the Jinen-Kai Karate Organization. It is largely due to their efforts that I remained as healthy as I did throughout my time at UCI, both physically and mentally as the training regimen reminded me that I am both mind **and** body. To my sempais and kohais, I offer my appreciation for walking the path of Karate-Do with me.

Another organization which helped me succeed is Graduate Christian Fellowship at UCI through Christian Intervarsity. GCF was essential to some of my early friendships which endured through the process of grad school and encouraged my faith.

And finally, I offer this thesis to the Lord Jesus Christ, giving thanks to God the Father through him. It was by His provision and by His good pleasure that I came to UCI, learned humility and patience through failure, endured the challenges of research, and ultimately have come to this culminating moment. To Him be the kingdom, the power, and the glory, forever and ever. "For by grace you have been saved, through faith. And this is not your own doing; it is the gift of God, not a result of works so that no one may boast." *Gal. 2:8-9*

CURRICULUM VITAE

Timothy Stephen Plett

Education

2012	B.S. in Physical Sciences, emph. Physics, Biola University
2015	M.S in Physics, University of California, Irvine
2017	Ph.D. in Physics, University of California, Irvine Advisor: Zuzanna S. Siwy Thesis: *Ion Transport Phenomena at the Nanoscale in Different Model Battery Systems*

Experience

2012-14	Teaching Assistant, Department of Physics and Astronomy, University of California, Irvine
2013-17	Graduate Student Researcher, Siwy Research Group, University of California, Irvine
2014-17	Graduate Student Researcher, Nanostructures for Electrical Energy Storage Energy Frontier Research Center

Appointments

2015, 16	Adjunct Professor, Department of Chemistry, Vanguard University
2016	Teaching Associate, Department of Physics and Astronomy University of California, Irvine
2017	Adjunct Physics Instructor, Department of Physics, Cypress College
2017	Physics Instructor, Department of Physics Bakersfield College

FIELD OF STUDY

Ion Transport Phenomena in Nanopore Systems

PUBLICATIONS

Trevor Gamble, Karl Decker, **Timothy S. Plett**, Matthew Pevarnik, Jan-Frederik Pietschmann, Ivan Vlassiouk, Aleksei Aksimentiev, and Zuzanna S. Siwy, "Rectification of Ion Current in Nanopores Depends on the Type of Monovalent Cations: Experiments and Modeling" *The Journal of Physical Chemistry C*, **2014** 118 (18), 9809-9819, DOI: 10.1021/jp501492g

Timothy S. Plett, Trevor Gamble, Eleanor Gillette, Sang Bok Lee, and Zuzanna Siwy, "Ionic Conductivity of a Single MnO2 Mesorod at Controlled Oxidation States" *The Journal of Materials Chemistry A*, **2015**, 3, 12858-12863, DOI: 10.1039/C5TA03196F

Timothy S. Plett, Wenqing Shi, Yuhan Zeng, William Mann, Ivan Vlassiouk, Lane Baker, and Zuzanna S. Siwy, "Rectification of nanopores in aprotic solvents – Transport properties of nanopores with surface dipoles" *Nanoscale*, **2015**, 7, 19080-19091, DOI: 10.1039/C5NR06340J

Yinghua Qiu, Chih-Yuan Lin, Preston Hinkle, **Timothy S. Plett**, Crystal Yang, Jenu Varghese Chacko, Michelle A. Digman, Li-Hsien Yeh, Jyh-Ping Hsu, and Zuzanna S. Siwy, "Highly Charged Particles Cause a Larger Current Blockage in Micropores Compared to Neutral Particles" *ACS Nano* **2016** 10 (9), 8413-8422 DOI: 10.1021/acsnano.6b03280

Timothy S. Plett, Wenjia Cai, Mya Le Thai, Ivan Vlassiouk, Reginald Penner, Zuzanna S. Siwy, "Solid-State Ionic Diodes Demonstrated in Conical Nanopores" *J. Phys. Chem. C*, **2017**, 121 (11), pp. 6170-6176 DOI: 10.1021/acs.jpcc.7b00258

ABSTRACT OF THE DISSERTATION

Ion Transport Phenomena at the Nanoscale in Different Model Battery Systems

By

Timothy Stephen Plett

Doctor of Philosophy in Physics

University of California, Irvine, 2017

Professor Zuzanna S. Siwy, Chair

Lithium ion battery technology has flourished since its introduction into the consumer market. Not only has it helped revolutionize consumer electronics, it also compliments R&D into clean forms of energy harvest e.g. solar, wind, and hydro-electric. As demand for the technology grows, innovative approaches have been taken to improve capacity, output, and lifetime in Li-ion batteries. The approach studied in this research involves the inclusion of nanostructures, which have the potential to significantly increase capacity. While several techniques to fabricate nanostructures are understood, underlying phenomena governing ion transport in and around these nanostructures is only partially understood, which could directly impact design principles for such devices.

This thesis examines a variety of model systems which could serve to simulate environments found in proposed devices and answer questions regarding ion transport phenomena. The main components we studied from such battery systems were electrolyte and cathode materials. The electrolyte experiences different ion transport phenomena arising from the nanoconfinement of the cathode structures both around and inside the electrode material. Thus, having model systems to examine electrolyte and cathode material

separately and in tandem is useful for elucidating phenomena without the challenge of deconvolution resulting from other current-carrying mechanisms.

Our main tools for carrying out our research were synthetic nanopores. The nanopore structures afforded means to access nanoscale, control environment, and even fabricate components for study. By studying the current-voltage curves in these systems, we were able to draw meaningful conclusions about mechanisms of ion transport in these model systems. The main findings of this research include the inducement of positive surface charge on nanopore structures by organic solvent-based electrolytes by means of dipole and/or ion adsorption, positive evidence of gel electrolyte fitting current models of ion current rectification, and the impact of oxidation state and cycling in cathode material on ion transport through its porous media. Each of these findings is directly related to the thrust of the research and potentially provide insights for future battery design.

Introduction

The application of nanotechnology to the field of energy storage is a relatively recent development. A key result by Lee and Goodenough in 1999 showed that powders composed of nanoscale MnO_2 particles in 2 M KCl solution demonstrated sizeable capacitance, (~200 F/g) on the order of the best supercapacitors (carbon black) available at the time [1]. With the commercialization of the lithium-ion battery only eight years earlier [2], energy storage technologies were poised to make another leap forward. A variety of nanofabrication and assembly techniques have been developed since the time of the initial discovery and many have been utilized in creating model nanostructure architectures for battery cathodes [3-5]. Many designs have focused on densely packed structures, making use of conductive additives and scaffolding to boost electrical conductivity and, consequently, power density [6]. Materials with high degrees of porosity at the nanoscale, such as MnO_2, have also been favored to allow access of ions from electrolyte solution to cathodes. While such nanostructured materials have been exhaustively studied and characterized in terms of their electrochemical performance [7-8], an important feature of these structures still remaining for study is ion transport. Factors such as surface charge [9], confinement, ionic conductivity [8], and electronic conductivity [10] could influence device performance.

Synthetic nanopores offer a means to study ion transport phenomena in a controlled environment [11-15]. Their basic construction, a nanometer-scale hole embedded in a membrane from one atomic-layer in thickness to several microns, [16-37] offers means to study ionic current and other transport phenomena without the challenge of deconvoluting different contributing mechanisms as is generally the case for Electrochemical Impedance Spectroscopy [38]. Synthetic nanopores draw their inspiration from biological channels

found in cells, which are responsible for a wide variety of life-essential functions including, most notably, nerve signaling [39, 40]. Because of this, other applications of nanopores, aimed at biomimetic functions and sensing, have been pioneered [15, 41, 42]. Another analogous system for nanopores to mimic is that of electronic circuits, as ionic circuitry equivalents such as pn- junctions [43-45], pnp- and npn- transistors [46, 47], as well as diode and transistor-based logic circuits have been developed [48-50]. An important phenomenon that enabled the development of these technologies is ion current rectification. For nanopores, this most commonly occurs by means of asymmetry in a pore's geometry e.g., the case of conically-shaped nanopores, and the presence of surface charges [15, 20, 23-28, 51, 52]. In such an arrangement, the ionic concentrations become voltage-dependent; for one voltage polarity, concentration of both types of ions in solution exceed bulk concentrations, while a depletion zone is formed at the opposite polarity [53-56].

However, the large majority of nanopore systems have focused on biomimetic, or aqueous electrolytes, which generally include inorganic salts. This is reasonable since water-based electrolytes are well understood in terms of their solution chemistry and electrochemistry [11,12]. But for battery systems, aqueous electrolytes can only serve as an initial model for behavior as most electrolytes utilized in real applications are based on organic solvents [57-59], gel [60, 61], or even conductive solids e.g. LiPON or $LiPO_4$ [62]. These electrolytes have not been submitted to the same level of rigorous study in nanopores as aqueous electrolytes, with a few exceptions [63]. Thus, their behaviors in nanoconfined environments, such as those found in recently studied nanofabricated battery cathodes, is relatively unknown. Experiments aimed at elucidating ion transport behavior in cathode materials as well as for both organic and solid electrolytes in nanoconfinement form the

basis of this thesis [64-66], which seeks to demonstrate that many phenomena observed in well-studied aqueous systems translate to organic and solid electrolyte systems under similar conditions.

Chapter 1: The Effect of Surface Dipoles and Aprotic Solvents on Nanopore Rectification

Synthetic nanopore systems offer many technological benefits, such as the improvement of sensing techniques, development of nanofluidic devices, and fabrication of ionic circuits [41, 67]. As an experimental platform, nanopores play a major role in the design of model systems. Some biomimetic systems nanopores have been used for include voltage and pH sensitive gating as well as other selective transport behaviors and sensing applications [15, 41, 42]. A key advantage afforded by certain nanopore systems, i.e. conically shaped nanopores and glass nanopipettes, is access to the sub-100nm scale length, which is advantageous in many of these techniques [15, 20]. However, most of these systems operate in electrolyte conditions composed of aqueous salt solution, a direct link to biological systems. Additionally, multiple efforts have been made to gather modeling and experimental data for predicting and explaining transport phenomena in aqueous solutions [11, 12]. Some studies have explored exceptions, such as ionic liquids and organic solvent/electrolyte systems [68, 69], which have exhibited phenomena deviating from the norm.

Among these phenomena, one of the most interesting effects observed with nanopores is the peculiar behavior of ionic current rectification. As was described in the introduction, this rectification can be caused by the asymmetry of the pore's geometry, e.g. the case of conically shaped nanopores, and the presence of surface charges [15, 20, 23-28, 51, 52]. Ionic concentrations in an asymmetric and charged nanopore are voltage-dependent [53-56]; for one voltage polarity, concentration of both cations and anions exceed the values in the bulk, while for the opposite voltage polarity a depletion zone is created (Figure 1.1).

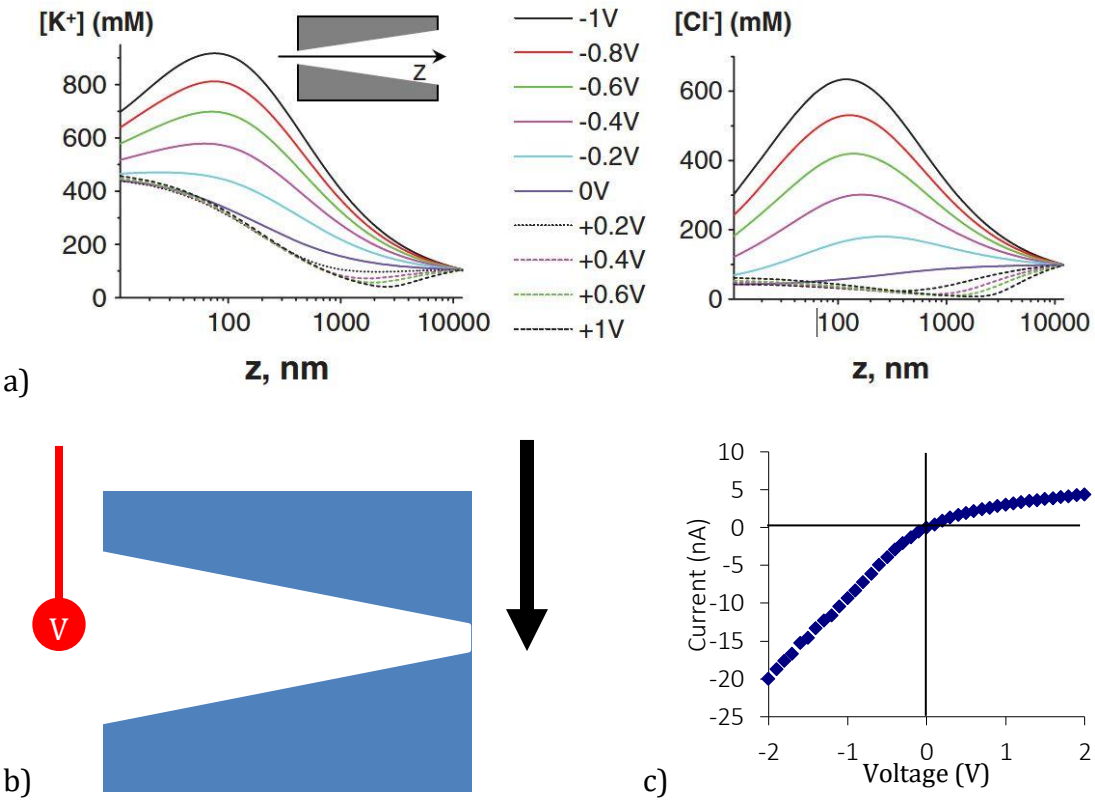

Figure 1.1 An illustration of the concept of nanopore rectification, reproduced from Powell et al (Phys. Rev. Lett. 2009) [133]. **(a)** Modeling captures the principle of voltage dependent ionic saturation and depletion. The parameters for the model are 500nm base, 5nm tip with a surface charge, σ, -0.5*e*/nm^2 **(b-c)** provide a functional undestanding of the principle. **(b)** A simple schematic of a conically-shaped nanopore. The length scale of most conically shaped pores in polymer materials is between 400-1000nm at the base and 10nm-50nm at the tip. **(c)** Data from a polyethylene terephthalate (PET) pore with a base of 426nm and a tip of 15nm in 1 M KCl with pH 8. Rectification is clear; negative voltage is favored over postive voltage, which is consistent with negative surface charge. This is expected for PET, which features deprotonated carboxyl groups at pH 8 after being chemically etched with NaOH.

This effect has been confirmed for nanopores in a variety of materials that possess similar geometry and surface charge characteristics. Ion current rectification has also been observed in geometrically symmetric nanopores with patterned surface charges such that there was a junction between two zones with positive and negative surface charges [43-45, 70-73]. A report has also been published showing rectification of currents carried by large organic ions in glass pipettes, and proposed that surface adsorbed electrolyte ions can cause effective

charge inversion [74]. In most cases, the sub-100nm length scale is necessary to induce this effect to a measurable extent, which is most easily achieved in the conically-shaped pores and nanopipettes.

Additionally, the sub-100nm length scale of conically shaped pores offers another opportunity for nanopores to serve as model systems for ion transport, specifically in nanostructured battery components [9, 64]. Recently, discoveries have been made in the field of electrical energy storage, which utilize model nanostructures and architectures to increase energy storage and power density in lithium ion battery technology [1]. This has generated new interest and efforts toward understanding the transport properties of lithium at the nanoscale, leading to new experiments with nanopores in order to address these queries [75]. One reported series of experiments with conical nanopores in polyethylene terephthalate (PET) showed that this rectification behavior was dependent on the cation used to probe the pore. This was linked to the cation's likelihood to 'dwell' near the charged surface of the pore wall, causing modulation of the effective surface charge. As revealed by the molecular dynamics simulations, a larger number of lithium ions stayed adsorbed close to the surface compared to sodium and potassium ions, leading to lowest rectification in lithium chloride. Recent work has also been done on how standard electrolyte (aq. KCl) transports through nano-fabricated battery materials, (manganese oxide), revealing this cathode material is porous in nature and possesses nano-voids with excess surface charge [9]. However, these experiments were conducted in aqueous solutions, which are not ideal or representative of lithium ion battery technology, which rely on the use of organic solvents to resist electrode degradation and improve capacity retention and cycle life [57-59].

In this chapter, we propose a method utilizing conical nanopores in polycarbonate [27] films, polyethylene terephthalate [23] films, and glass nanopipettes [20,21] to compare the behavior between aqueous solutions and solutions utilizing propylene carbonate (PC), an organic solvent commonly used in lithium ion battery studies [57]. The intent is to examine the effect of nanoconstrictions on lithium transport in a solvent environment similar to that used in traditional battery experiments. We also seek to examine the effect of solvent on ion transport properties, which has heretofore not been closely studied, utilizing glass nanopipettes in experiments to widen the scope of examined organic solvents. From these data, we postulate a new mechanism of ion current rectification via finite dipole moment on pore walls [77], originating from solvent adsorption.

Section 1.1 – *Nanopore Fabrication and Characterization*

Polymer pores used in this study and others appearing in this work were prepared using the track-etching technique [28]. The films were irradiated with single U ions accelerated to 11.4 MeV/u at the UNILAC linear accelerator of the GSI Helmholtzzentrum fur Schwerionenforschung in Darmstadt, Germany [77]. This procedure has been shown to create damage tracks in the polymer, regions where the chemical bonds have been broken or weakened by the passage of the heavy ion. Such damage tracks have been visualized with a staining agent, RuO_2, and measured using electron microscopy to be about 5-10nm in diameter [78]. These damage tracks are further weakened by exposure to UV light [79, 80], which serves to agitate the weakened chemical bonds in the damage track.

The films are then subjected to wet chemical etching, which can be controlled based on the bulk etch rate of the material, e_{bulk}. Because of the weakened and broken chemical

bonds in the damage track, the track has a different and faster etch rate, e_{track}, than that of the bulk. This allows us to control the nanopore shape based on etching conditions [24, 27]. For fabricating a cylindrical pore, which will be used later in this thesis, the pore is immersed in etchant at a heightened temperature (e.g. 50-70^{o}C). These etching conditions cause the $e_{track} >> e_{bulk}$ (~1 μm/min vs. 10nm/min), which result in a nearly cylindrical pore. We must acknowledge, however, that smoothness of cylindrical pores depends on the material and pore diameter. Studies have shown that pores etched in semi-crystalline polymers such as polyethylene terephthalate (PET) demonstrate striking undulations along the axis of the pore [81], whereas pores in more amorphous polymers like polycarbonate are smooth [82].

Conical pores are etched using asymmetric etching conditions [27]. Films are loaded into a custom-made conductivity cell and exposed to etchant on one side only and a stopping solution on the other, and monitored with a voltage to identify membrane breakthrough. This causes asymmetric etching of the pore and produces a conical shape as has been previously reported. For etching in PET pores, a standard solution of 9 M NaOH was used and has been measured to have a bulk etch rate of 2.14 nm/min in PET [24]. For polycarbonate pores, the etchant used was 8 M KOH with a solvent composition 80/20 H_2O and ethanol (v/v). This was done in compliance with a publication by Fujimoto et al. [83] that established the chemical bulk etching rate for two standard polycarbonate membranes, 1.69 and 1.78μm/h for Lupilon and Makrofol foils respectively. Since our polycarbonate membranes are custom-produced, we estimated our chemical bulk etch rate to be an average of the two rates reported, yielding ~1.74μm/h, or ~30nm/min. These etch rates were used in calculating base and tip size for our conical nanopores.

Figure 1.2 Cartoon of the etch process for both cylindrical and conical pores. **(a)** A damage track is made through a membrane. **(b-c)** Etching processes for a cylindrical pore and conical pore. In the cylindrical pore fabrication **(b)**, the damage track etches through very rapidly by comparison to the bulk, allowing an even etching of the entire pore, which gradually widens. In the conical pore case **(c)**, the track etch rate is slowed to the point where the bulk etching of the inner membrane can occur at a more comparable pace, which results in the conical shape over time.

Our glass nanopipettes were fabricated from quartz capillaries (Sutter Instruments, Novato, CA) with 1mm outer diameter and 0.7 mm inner diameter. Two pipettes were produced by pulling a single capillary using a P-2000 CO_2-laser pipet puller (Sutter Instruments, Novato, CA). The puller program parameters used were: heat – 690; filament – 3; velocity – 45; delay – 165; pull – 190. These parameters produced nanopipettes with tip size around 35nm, which were characterized by scanning transmission electron microscopy (FE-SEM, FEI Quanta-FEG, Hillsboro, OR).

To characterize the polymer pores, linear portions of current-voltage curves are used to calculate pore size based on the system resistance. In a cylindrical pore, the calculation is straightforward, working from the standard equation for resistance based on solution resistivity (1 M KCl ρ = 0.1 at room temperature) and the pore size,

$$R = \rho \frac{L}{A} = \rho \frac{4L}{\pi a^2} \qquad (1.1)$$

where a is the opening diameter of the pore (which is calculated) and L is the length of the pore ($L \sim$ foil thickness, 10nm for polycarbonate, 12nm for PET). In a conical pore, the system resistance is calculated approximating the pore shape with a truncated cone [24]:

$$R = \rho \frac{L}{A} = \rho \frac{4L}{\pi a_t a_b} \qquad (1.2)$$

The large opening, a_b, corresponded to the side in contact with the etchant (KOH, NaOH) and was estimated based on the respective bulk etch rates, allowing us to calculate tip size, a_t. These calculations are used throughout this work to calculate polymer pore sizes (Fig. 1.3)

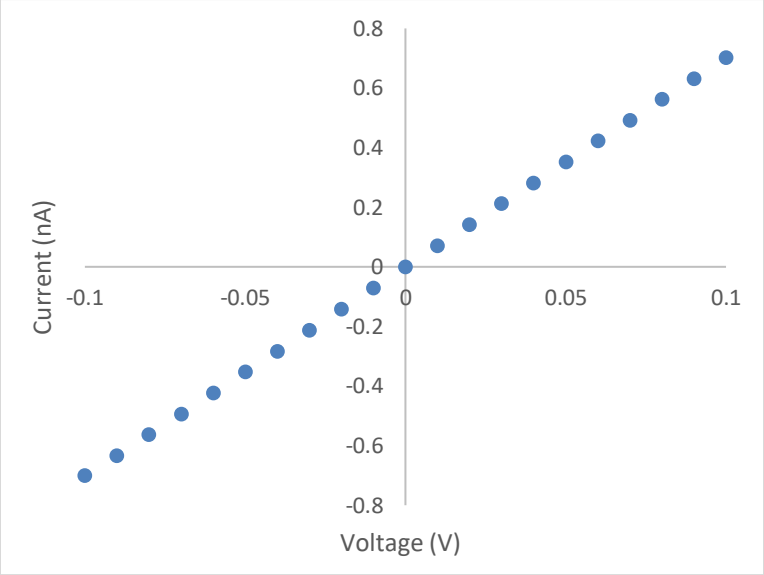

Figure 1.3 Sizing scan from a conical nanopore which had been etched for 186 minutes (by etch rate of 2.14) yielding a_b = 397.5nm. When Eqn. (1.2) is applied to this data, the calculation results in a_t = 13nm

Section 1.2 – *Aqueous $LiClO_4$ Contrasted with $LiClO_4$ in Propylene Carbonate*

The initial investigation sought to contrast aqueous salt solutions with propylene carbonate (PC) based solutions. Figure 1.3 shows current-voltage curves of a single conically shaped polycarbonate nanopore with the narrow opening diameter of 10 nm, and the wide opening of 540 nm, recorded in aqueous solutions of three different monovalent salts. As expected and shown before in the literature, single conical nanopores in polycarbonate films behaved similarly to their polyethylene terephthalate (PET) counterparts [23-25], in that they showed ion current rectification (Fig. 1.4).

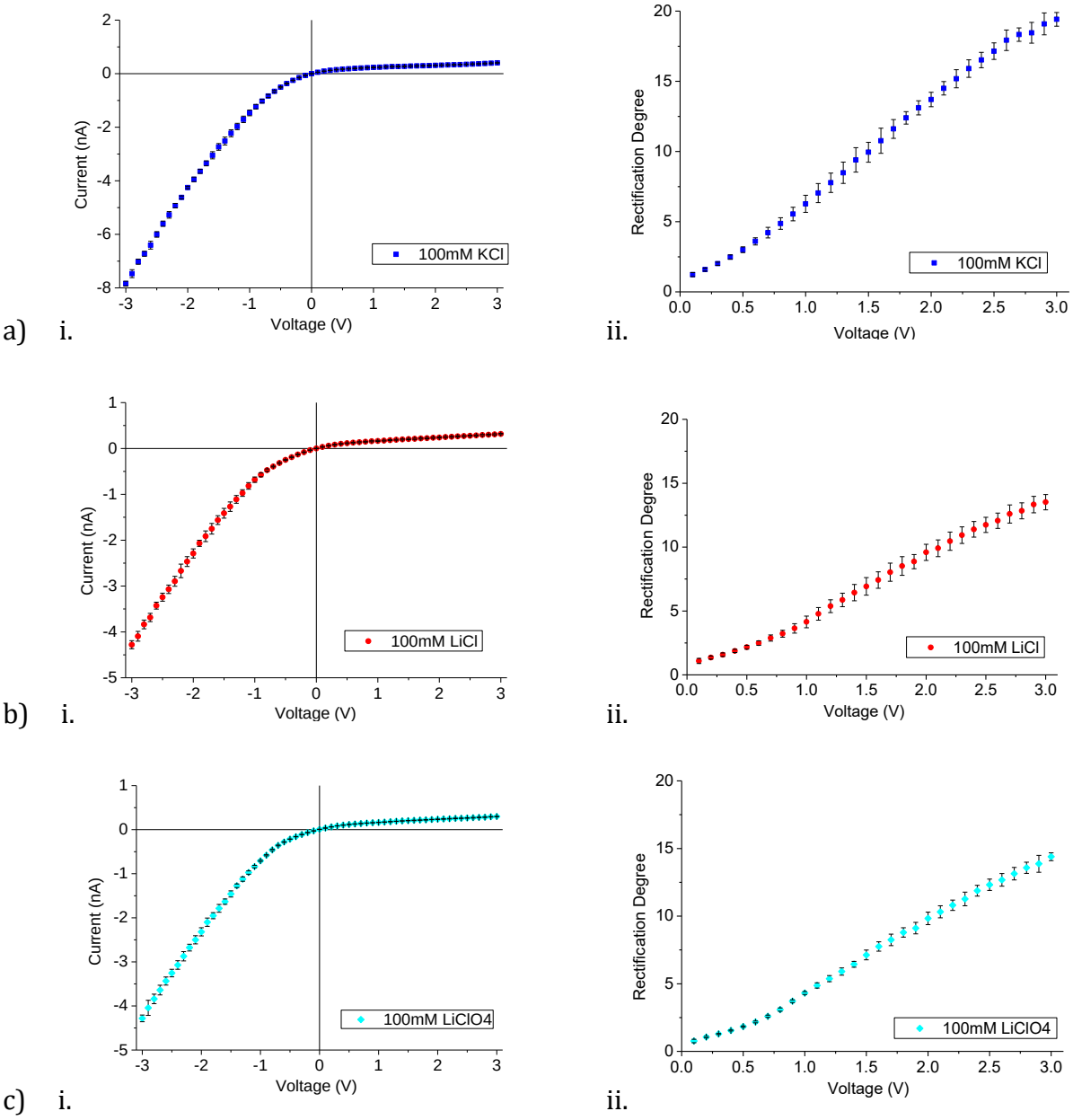

Figure 1.4 Current-voltage curves and rectification degrees recorded in a single polycarbonate nanopore with opening diameter of 10 nm (tip) and 540 nm (base). Recordings were made in aqueous solutions of **(a)** 100 mM KCl, **(b)** 100 mM LiCl, and **(c)** 100 mM LiClO4. Rectification degree in this figure was calculated as a ratio of currents for negative and positive voltages i.e. $R = |I_{-2V}|/|I_{+2V}|$.

It is because pores in these two polymer materials contain carboxyl groups which, in aqueous neutral and basic solutions, render the pores negatively charged. The current rectification results from the conical shape and excess surface charge of the pore walls. In

aqueous solutions, ion current through single polycarbonate conically shaped nanopores examined here showed similar dependence on type of salt as reported before for PET nanopores [75]. Namely, magnitude of ion currents and rectification in KCl were consistently higher than values observed with LiCl or $LiClO_4$ (Figure 1.4). Lower rectification in lithium salts is attributed to ability of the lithium ions to lower the effective surface charge of surfaces covered with carboxyl groups [75].

In the propylene carbonate solutions however, a new effect emerged that was unexpected. Because propylene carbonate is protophobic in nature [84], carboxyl groups on the pore walls cannot deprotonate since the donated protons would not solvate. Without deprotonation, the carboxyl groups would not render the pore walls any net charge which, as mentioned above, is responsible for the rectification phenomenon observed in conical nanopores. Thus, it was hypothesized that the response for the nanopore in these solutions would be linear. However in the tested propylene carbonate salt solutions, the conical nanopores (n = 50) consistently exhibited rectification in lower concentrations of salts. Furthermore, the rectification occurred in the opposite direction from the aqueous solutions i.e. with the same electrode configuration, positive currents were higher than negative currents. Figure 1.5 shows the effect in $LiClO_4$ solutions over a wide range of concentrations in two nanopores, with tip opening diameters of 11 nm (polycarbonate) and 15nm (PET). Similar to the experiments in aqueous solutions, there is concentration dependence as well as tip size dependence in the response of a pore [15, 54]. As tip size grew larger, the onset of this 'reverse' rectification occurred in lower concentrations. Note that inverted rectification was shown before for polymer pores in aqueous solutions only in cases when the pore walls carried excess positive surface charge [15, 44, 48].

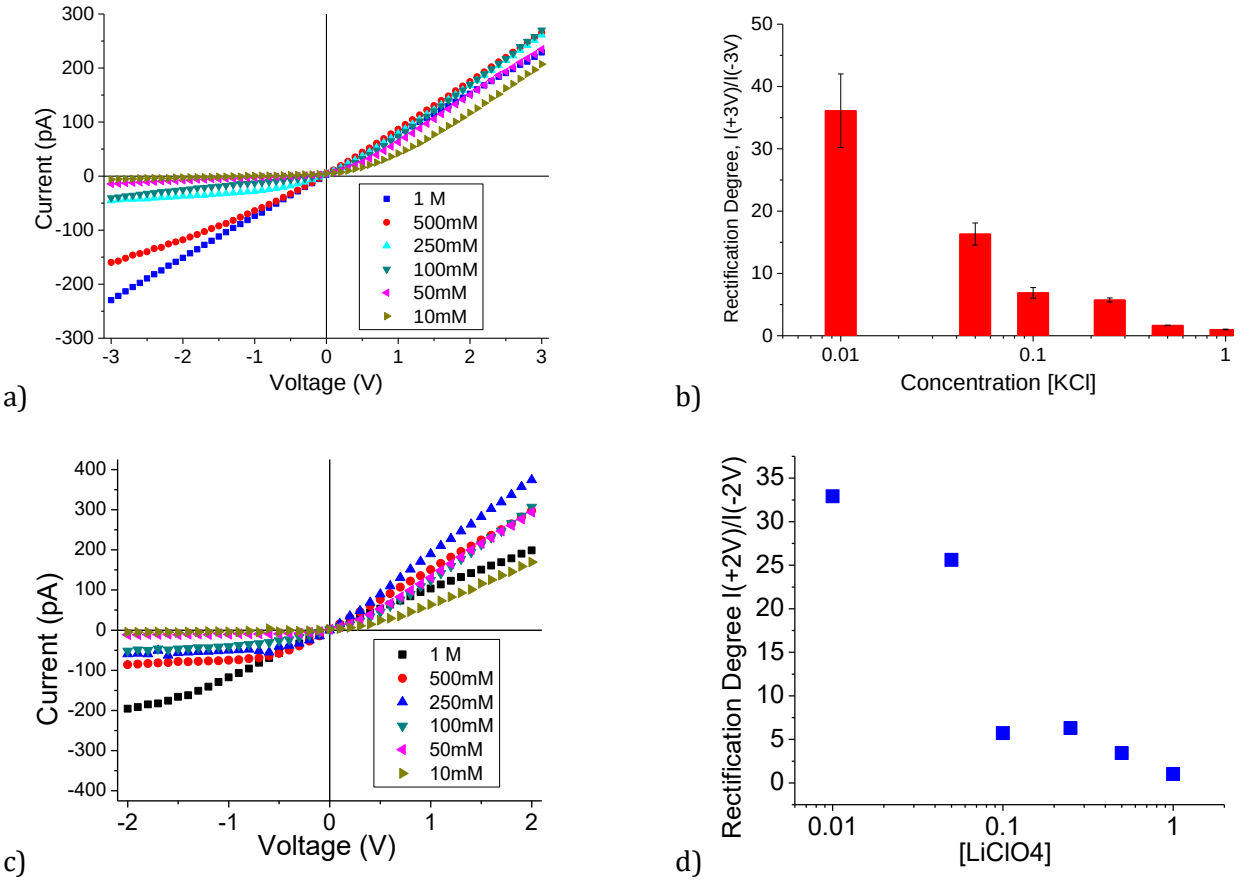

Figure 1.5 (a) Current-voltage curves recorded in a range of $LiClO_4$ concentrations in propylene carbonate for a single conical polycarbonate nanopore with the tip opening of 11nm and the wide opening of 470 nm. **(b)** Rectification degree calculated as a ratio of currents in +3V and -3V. **1.4 (c-d)** show similar data for a PET pore with tip opening of 15 nm and base opening of 1280nm.

In order to test whether the inverse rectification of current recorded with the simple inorganic salt of $LiClO_4$ could be observed in a conically shaped rectifying nanopore system other than polymers, we tested the behavior of glass nanopipettes. In aqueous solutions, walls of glass pipettes are negatively charged due to deprotonation of silanol groups. Figure 1.5 shows current-voltage curves recorded in 100 mM $LiClO_4$ and 10 mM $LiClO_4$ propylene carbonate solutions. Similar to the recordings in polycarbonate and PET pores (Figure 1.4), current-voltage curves recorded in propylene carbonate are inverted compared to measurements performed in the water solution [20, 21, 55, 74].

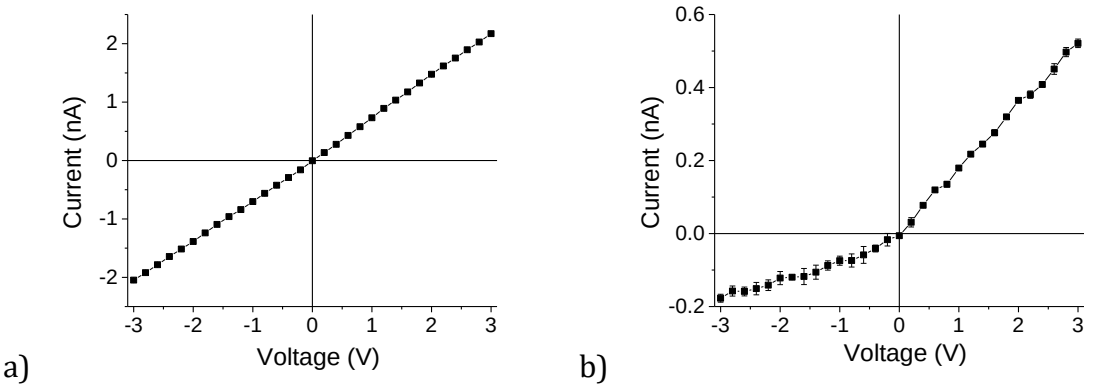

Figure 1.6 Current-voltage curves recorded in **(a)** 10 mM and **(b)** 100 mM LiClO4 in propylene carbonate through a glass nanopipette with an inner opening of 35 nm.

It is important to mention that the inverse current-voltage curves in glass nanopipettes were observed before for an organic electrolyte, tetraphenylarsonium tetraphenylborate (TPAsTPB) [74], dissolved in a range of organic solvents. Since large cations were reported before to adsorb to surfaces [85], it was proposed that adsorption of TPAs+ to walls of glass pipettes created an effectively positive surface charge [52], leading to this rectifying behavior. Rectification of currents carried by TPAsTPB was reported for sub-mM concentrations of the electrolyte, thus in conditions in which formation of ion-pairs was suppressed. This study, though exotic in its choice of electrolyte, promotes confidence that the effect we observe is not an artifact of recording but a robust physical phenomenon.

Section 1.3 – *Possible Mechanisms for Rectification in Propylene Carbonate*

As stated before, this inverse rectification was outside our initial expectations, which proposed linear I-V scans. However, the phenomenon could be explained with the existing model for ion current rectification in conical nanopores [24]: instead of a negative surface charge, the effective surface charge in our pores must be positive. Two mechanisms were

explored as the basis of the rectification observed with the $LiClO_4$/PC solutions. The first one, similar to the model presented by Yin et al. [74] and Cruz-Chu et al., [52] considered the possibility of lithium ion adsorption to the polymer and glass surfaces, which could lead to effectively positive surface charge. The second hypothesis focused on the importance of the solvent, namely its adsorption could render the pore walls a finite dipole moment [86, 87].

In order to test these hypotheses, different experiments were conducted, each focusing on a separate mechanism. Lithium ions in aqueous solutions were indeed found to adsorb to negative charges on the polymer surface, thus we considered whether, in propylene carbonate, lithium could show preferential binding to partial negative charge on the oxygen of the carboxyl group [75], leading to the formation of effectively positively charged pore walls. Experiments were therefore performed in $NaClO_4$ and KCl solution in propylene carbonate, because potassium ions were shown not to exhibit the tendency to bind to surfaces and sodium ions only bind to a lesser degree [75]. Figure 1.7 compares current-voltage curves recorded in 10mM $LiClO_4$, $NaClO_4$, and KCl solutions. This set of results demonstrates that the presence of the reverse rectification is not cation or anion dependent, although the rectification degree varied for the different salts.

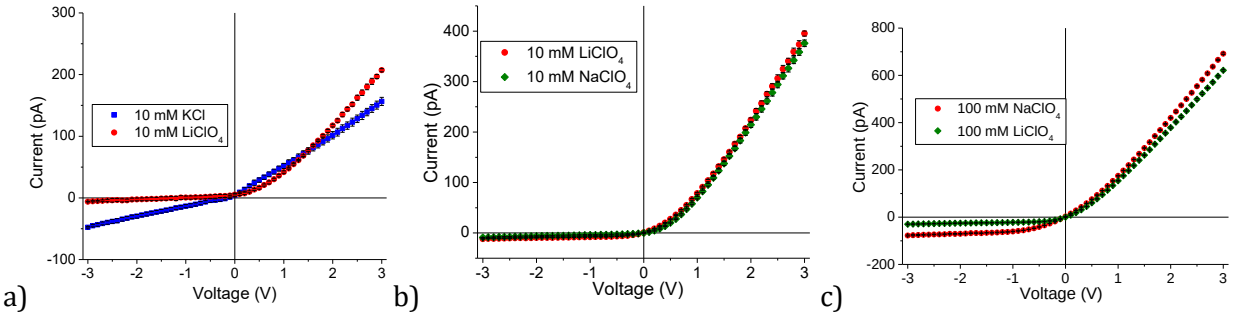

Figure 1.7. Current-voltage curves through a single polycarbonate nanopore with openings of **(a)** 10 nm (tip) and 470 nm (base) recorded in 10 mM KCl and 10 mM $LiClO_4$ and **(b-c)** 10 nm (tip) and 700 nm (base) recorded in **(b)** 10 mM $LiClO_4$ and 10 mM $NaClO_4$ in propylene carbonate and **(c)** 100 mM $LiClO_4$ and $NaClO_4$

This suggests that the ion current rectification observed in propylene carbonate salt solutions does not solely arise from cation adsorption or charge inversion, although adsorption of lithium could be responsible for enhanced rectification in the lithium salt. Due to limited solubility of KCl in propylene carbonate, studying a range of salt concentration was not possible. Similarity between sodium and lithium perchlorate solutions may be explained by sodium also having a tendency to bind to polymer surfaces, though experiment and modeling predicted this to a significantly lesser degree than lithium [45]. Because sodium has excellent solubility in propylene carbonate, 100mM solutions of $LiClO_4$ and $NaClO_4$ were also compared (Fig. 1.7c) and $NaClO_4$ was observed to have similar concentration dependence trends to $LiClO_4$.

The other explanation we pursued to explain the effect of ion current rectification in propylene carbonate was a possibility that pore walls in this solvent contain a positive dipole moment due to adsorption of propylene carbonate molecules to the polymer surface. A previous study with TiO_2 surfaces in contact with propylene carbonate, revealed that the adsorption occurred via the carbonyl oxygen of propylene carbonate, so that the carbon with positive partial charge pointed away from the surface [87]. In another set of experiments performed with thin films of $LiCoO_2$ in contact with propylene carbonate, two preferential configurations for the solvent adsorption were identified [88]. One configuration was similar to the one identified for TiO_2 surfaces, while in the other, the carbonyl oxygen with partial negative charge pointed to the solution. We considered this effect because propylene carbonate has a dipole moment of ~5 Debyes, (~2.7 times higher than the dipole moment of water), which might be strong enough to exert a significant effect on local ionic concentrations in a nanopore environment.

As shown in the literature developed for biological membranes, which often feature surface dipoles, even without net charge of the membrane, the surface dipoles can cause the formation of finite electrical potential in the solution, creating an electrical double layer with modified local ionic concentrations [89, 90]. The modeling predicted that a complex surface with positive dipole moment and negative surface charge can behave as an effectively positive or negative surface depending on the relative dipole and surface charge densities. In the limit of low surface potentials, the equation for electric potential, φ, at a distance z from a wall containing surface charges of density, σ, and dipole density of, υ, present within a layer of thickness, l, has the following form [90]:

$$\varphi(z) = \frac{4\pi}{\varepsilon k}[\sigma \cosh(kz) - \upsilon k sinh(kz)]e^{-kl}, \text{for } 0 < z < l \qquad (1.3)$$

where k is the inverse Debye length and ε stands for the dielectric constant.

For larger distances, $z > l$, the electric potential assumes the following form as a function of $(z - l)$:

$$\varphi(z - l) = \frac{4\pi}{\varepsilon k}[\sigma \cosh(kl) - \upsilon k sinh(kl)]e^{-kl}e^{-k(z-l)} \qquad (1.4)$$

So that the effective surface charge of the wall equals to:

$$\sigma_{eff} = [\sigma \cosh(kl) + \upsilon k sinh(kl)]e^{-kl} \qquad (1.5)$$

suggesting that the electric potential indeed results from the density of surface charges and the density of surface dipoles. Note that in the absence of the polarizable layer, $l = 0$, or dipole moment, $\upsilon = 0$, σ_{eff} converges to the surface charge density, σ ($\cosh(0) = 1$), considered in the Poisson-Boltzmann approach without polarizability.

Eqns. (1.3) – (1.5) also explain the salt concentration dependence of the ion current rectification shown in Figure 1.4. As the $LiClO_4$ increases, the electrical double-layer thickness, k^{-1}, decreases, diminishing the surface potential, which is responsible for

modulations of local ionic concentrations in the pore and ion current rectification. Equation (1.5) also predicts that presence of dipoles with positive dipole moment, even with $\sigma = 0$, is sufficient to render the surface potential positive; possible adsorption of Li^+ (in the absence of carboxyl group deprotonation) would lead to finite and positive values of σ, increasing further the potential's magnitude. Equation (1.3) also predicts that addition of negative surface charges due to deprotonation of carboxyls is expected to reverse the direction of rectification to the behavior shown in Figure 1.3.

This theoretical approach does not consider polarizability of the membrane because dipoles induced in the pore material were found to influence ionic current through nanopores primarily in cases where the product of the pore opening radius and the inverse Debye length, kr_{pore}, was small, ~3 [76]. In the systems considered here, e.g. Fig 1.4.a, ion current rectification was observed even in 500mM $LiClO_4$, thus with the pore radius of 5nm, the product of kr_{pore} equals ~12. For the 35nm in diameter glass pipette rectifying in 10 mM $LiClO_4$ (Fig. 1.5.a) kr_{pore} is ~6.

These results led us to consider experiments that, not only examine the interplay between surface charge and dipoles, but also the effect of dipole strength on rectification phenomena in nanopore systems.

Section 1.4 – *Probing Possible Dipole Adsorption with I-V Curves and SICM*

Considering the possibility of re-introducing surface charge by means of deprotonating carboxyl groups, experiments were performed to explore this by gradually increasing the content of water in a mixed solution with PC. The expectation for these experiments was that, as water was re-introduced to the system, the negative surface charge

of the deprotonated carboxyl groups would counter and eventually supersede the effective positive charge from adsorbed dipoles. This would be signaled by a change in rectification, from favoring positive to negative voltages.

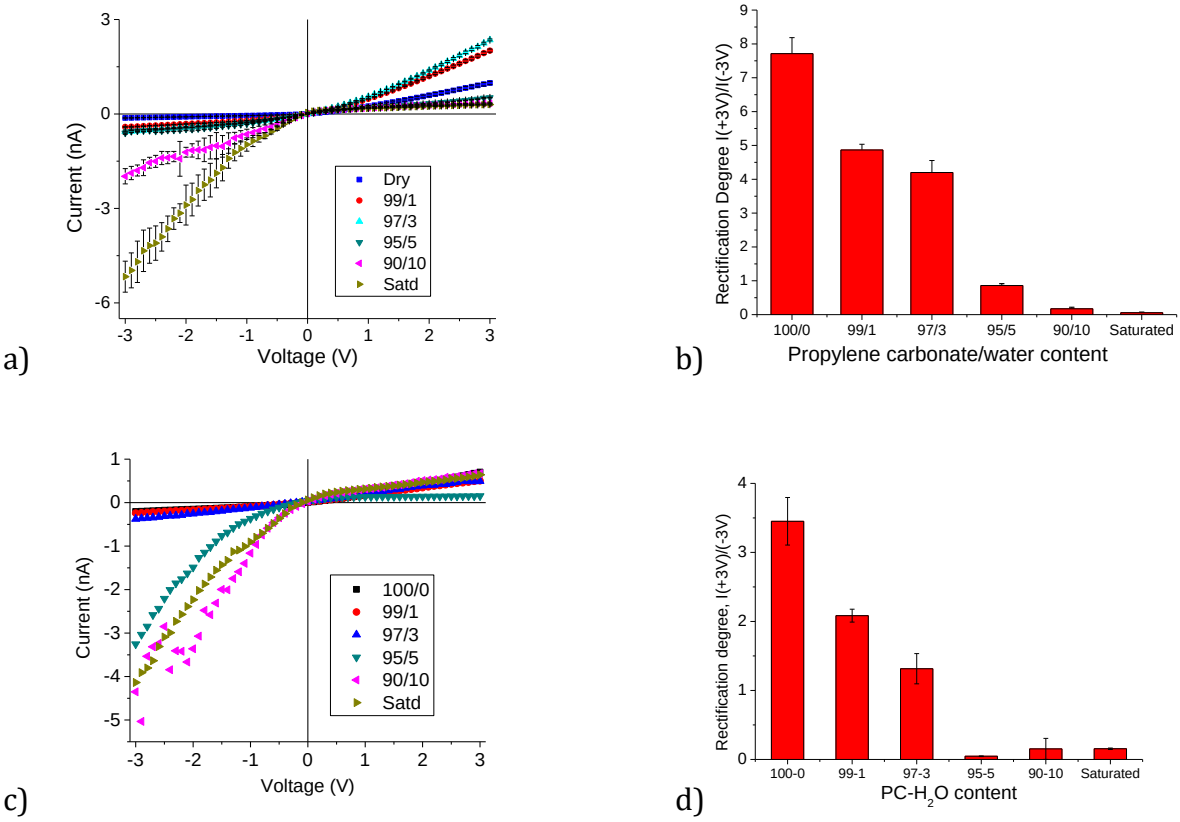

Figure 1.8 (a) Current-voltage curves recorded in 100mM $LiClO_4$ through a single polycarbonate pore with an opening of 60 nm (tip) and 440nm (base). The solutions were prepared in propylene carbonate with different levels (% by volume) of water content from 0% (dry propylene carbonate) to saturated water. With 5% water content the I-V curve was nearly linear marking indicating switching the direction of current rectification. **(b)** Rectification degree calculated based on data shown in **(a)** as I(+3V)/I(-3V). **Figures 1.7 (c-d)** Similar data and calculations for a pore with openings of 50nm (tip) and 410nm (base). While the data has more irregularities, the trend is similar: as water content increases, the rectification phenomenon changes polarity from favoring positive to negative voltages.

Example sets of recordings for two independently prepared nanopores are shown in Figure 1.8. The experiments were performed using a standard solution of 100mM $LiClO_4$ in

a variety of PC/H_2O solutions: dry, 99/1, 97/3, 95/5, 90/10, and saturated. As reported before for the organic electrolyte TPAsTPB in glass pipettes [74], water content had a direct impact on the rectification in a simple inorganic salt of $LiClO_4$ in polymer nanopores as well. For the pore shown in Figure 1.8, there is a threshold with ~5% water content when the recorded current-voltage curves are nearly linear. With 10% water content by volume, the pore rectifies definitively in the same direction as in an aqueous conditions.

It is important to note, however, that the inverted rectification in our system is present at water levels that are three orders of magnitude higher than in the system of TPAsTPB in glass nanopipettes (~1:10 vs. ~1:10,000) [74]. We think that the reported here robustness of the inverted rectification with respect to the presence of water is an indirect evidence that the rectification is caused by the presence of a high density of dipoles caused by the adsorbed solvent.

Another way to probe for the dipole effect on rectification is altering the dipole moment of the solvent. Two organic solvents with lower dipole moments were chosen for comparison with PC: acetonitrile (D=3.9) and tetrahydrofuran (D=1.7). Glass pipettes were used for these experiments because of their chemical stability in a wide range of chemical conditions. Figure 1.9 shows current-voltage curves of two 35 nm pipettes recorded in 10 mM $LiClO_4$ in acetonitrile (Fig. 1.9b) and tetrahydrofuran (Fig. 1.9c). Notably, the pipettes exhibited similar, inverted rectification in the two organic solvents with high dipole moment (Figure 1.8a.ii and Figure 1.8b), and ohmic behavior in tetrahydrofuran (Figure 1.8c), pointing to the importance of the solvent dipole moment in the properties of ion transport through nanopores.

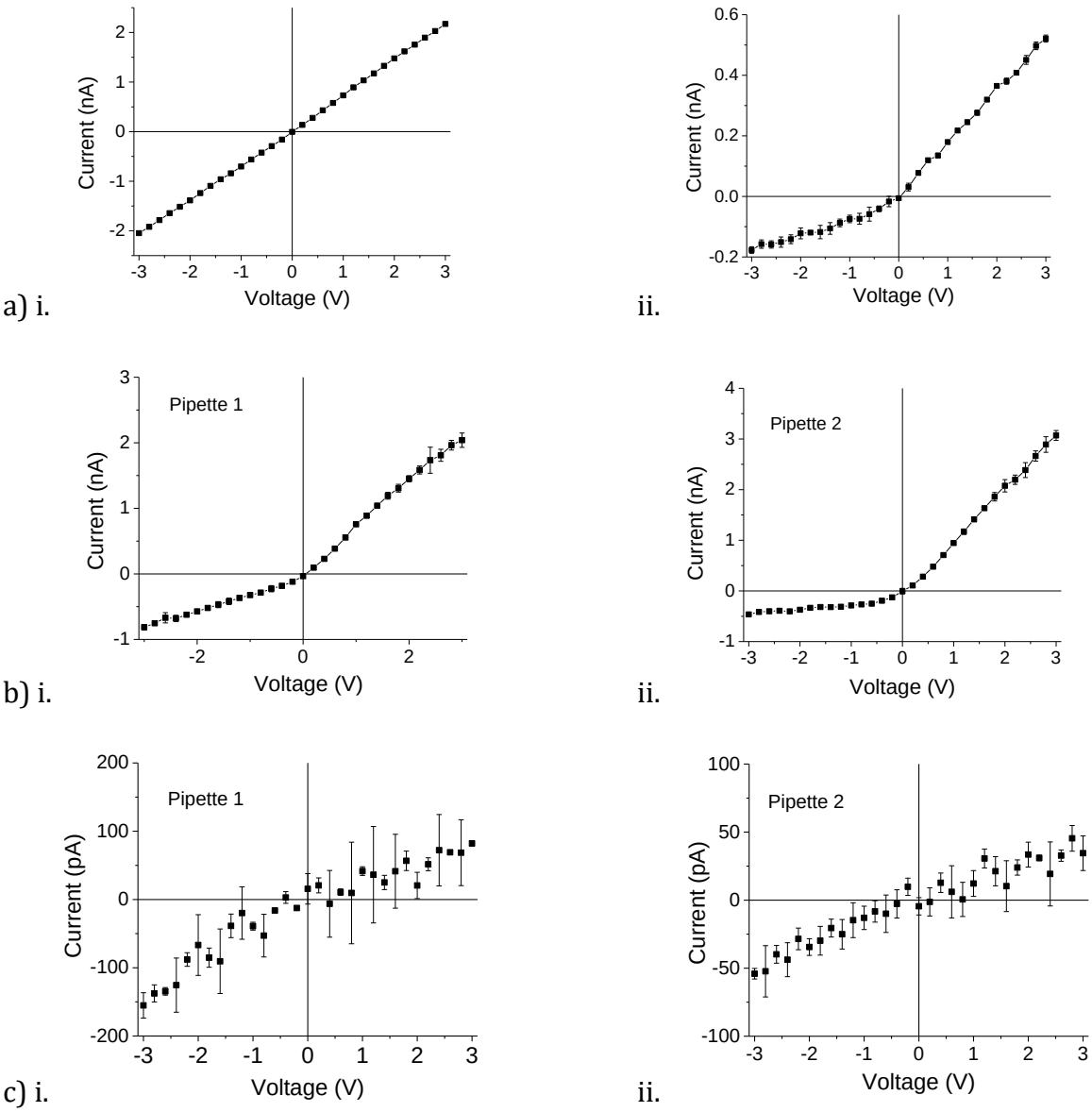

Figure 1.9 Current-voltage curves through two ~35 nm in in diameter glass nanopipettes recorded in 10 mM $LiClO_4$ in **(b)** acetonitrile, and **(c)** tetrahydrofuran. **1.9 (a)** is data previously shown in Figure 1.5 taken in **i.)** 100mM $LiClO_4$/PC and **ii.)** 10mm $LiClO_4$/PC. It is displayed here for comparison with the other solvents.

Equation (1.5) indeed predicts that the effective surface charge density due to the presence of dipoles will diminish with the decrease of the dipole moment. Table 1.1 shows effective surface charge calculated for a flat surface in contact with 10 mM 1:1 salt in the three organic solvents, assuming the solvent molecules are adsorbed at the density of three

molecules per nm^2 in a configuration in which the atom with partial positive charge faces the solution. The polarizable layer, *l*, was assumed to have a thickness of 2 nm due to the presence of surface roughness, and in case of track-etched polymer pores, dangling ends of the polymer chains [91]. Thus the layer containing dipoles is expected to be larger than the size of surface groups and solvent molecules. This is a simplified picture of our experimental system, but it provides a qualitative argument for the possible existence of an effective positive charge in solvents with high dipole moment. The calculations also indicate that adsorption of positive ions can have a large influence on the electrical properties of surfaces.

	Effective surface charge, σ_{eff}, calculated from eq. (3), C/m^2		
Surface charge, σ, due to Li^+ adsorption, C/m^2	Propylene carbonate (D=4.9)	Acetonitrile (D=3.9)	Tetrahydrofuran (D=1.7)
0	0.0060 C/m^2	0.0048 C/m^2	0.0021 C/m^2
0.008 (1 per 20 nm^2)	0.01107 C/m^2	0.0098 C/m^2	0.0071 C/m^2
0.016 (1 per 10 nm^2)	0.0161 C/m^2	0.0149 C/m^2	0.0122 C/m^2

Table 1.1. Effective charge densities of a flat surface calculated from eq. (3) for *l*=2 nm, assuming three solvent molecules are adsorbed per 1 nm^2. Three cases of additional surface charge originating from Li^+ adsorption were considered.

The presence of an effectively positive surface potential can also be provided experimentally using the scanning ion conductance microscope (SICM) technique [76, 92, 93]. The measurement constitutes recording current-voltage curves when a glass nanopipette approaches a surface (see inserts on Fig. 1.9a,b). At far distances, only the rectification of the pipette is observed. However, as the pipette draws near the surface (~10s

of nm), surface charge on the surface may interact with the ion current, causing rectification [76, 92]. The preferential direction of rectification, similar to nanopores, is dependent on the polarity of the surface charge: negative surface charge produces higher currents at negative voltages, positive surface charge produces higher currents at positive voltages.

The experiments were performed in 100 mM $LiClO_4$ thus at conditions at which the pipettes do not rectify. When the pipette is far away from the surface, an ohmic behavior is observed, because the local ionic concentrations at the pipette entrance are unaffected by the presence of a charged surface. Observing an asymmetric current-voltage curve provides evidence that the pipette is within tens of nm from the surface, and that the surface is charged. Figure 1.9 shows scanning ion conductance measurements for polymer and glass surfaces in aqueous and propylene carbonate solutions of $LiClO_4$. The experiments confirmed that the effective surface charge has an opposite sign in the two solutions. In aqueous solutions, the current-voltage curves exhibited higher negative currents, consistent with a negative surface potential. By contrast, in polypropylene carbonate, current-voltage curves exhibited higher positive currents, which, in our electrode configuration, indeed indicate positive surface potential. Similar results were obtained in $LiClO_4$ solution in acetonitrile (Figure 1.9c). Measurements in THF could not be performed due to low signal-to-noise ratio in these conditions.

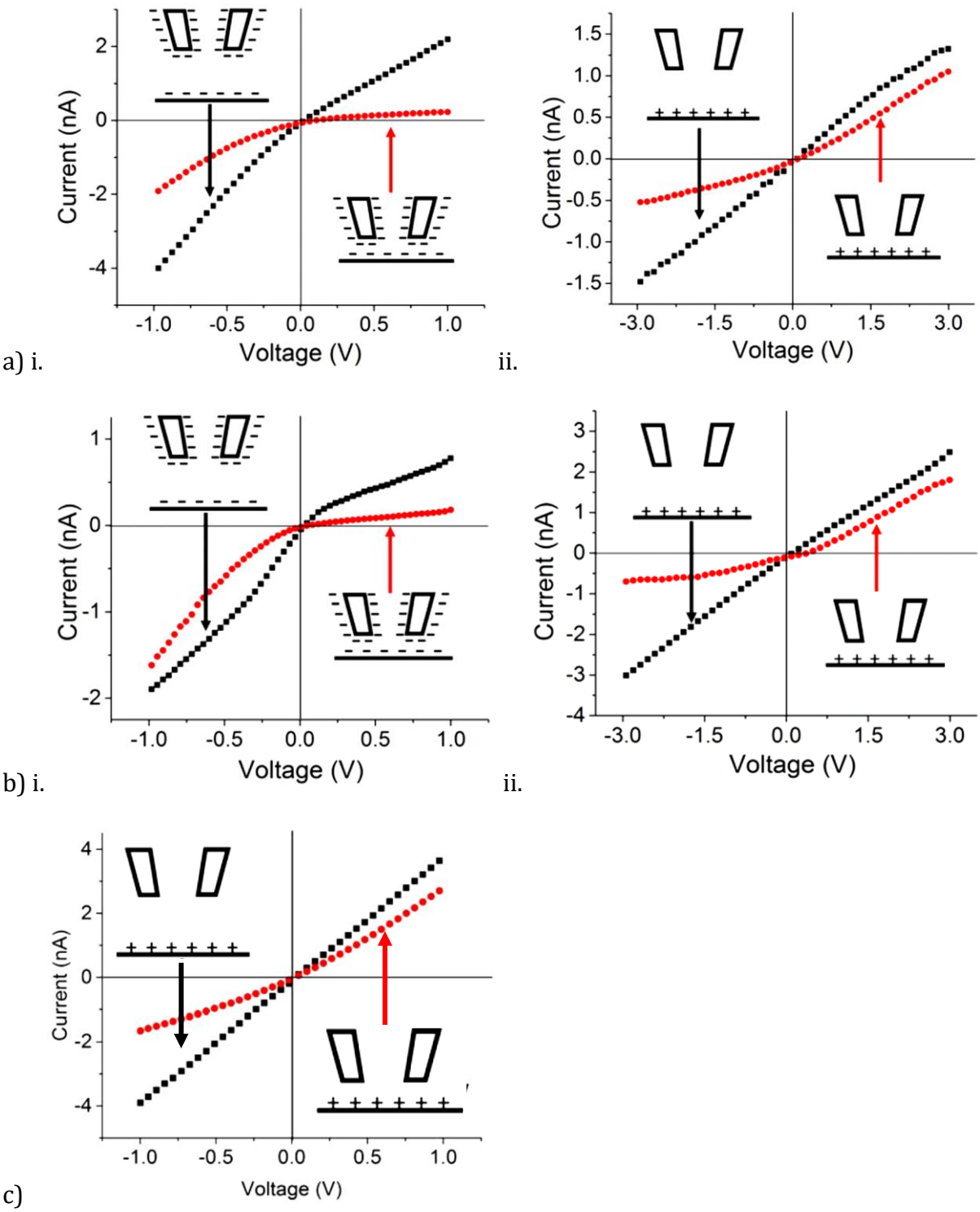

Figure 1.10. Scanning ion conductance measurements performed on **(a)** polycarbonate and **(b)** glass surfaces in aqueous (i) and propylene carbonate (ii) solutions of $LiClO_4$. **(c)** shows an additional experiment performed in a 100mM solution of $LiClO_4$ in acetonitrile on a glass surface with similar, but less pronounced results.

Our experiments in $LiClO_4$ and salt of other cations (see Figure 1.6) suggest that the positive potential in propylene carbonate and acetonitrile solutions results from both adsorption of Li^+ ions as well as solvent dipoles. The results from the Scanning Ion Conductance Microscopy (SICM) confirm the results of effective positive surface charge in organic solvent and further suggest a cause linked to both Li^+ ions and solvent dipoles, giving us two different physical methods of confirmation.

Section 1.5 – *Confirmation from Modeling and Conclusions*

In addition to physical techniques, we also consulted computer modeling as a means to confirm our experiments from a theoretical direction. The modeling program Comsol was utilized for this endeavor. Poisson-Nernst-Planck equations (1.6-8) were solved using the Comsol Multiphysics 4.3 package.

$$\varepsilon_0 \varepsilon \nabla^2 \varphi = e(C_+ - C_-) \tag{1.6}$$

$$J_i = -D_i \left(\nabla C_i + \frac{z_i e C_i}{k_B T} \nabla \varphi \right) \tag{1.7}$$

$$\nabla \cdot \left(\nabla C_i + \frac{z_i e C_i}{k_B T} \nabla \varphi \right) = 0 \tag{1.8}$$

A single 10 μm long conically shaped nanopore had opening diameters of 15 and 500 nm, respectively. The surface charge density of the pore walls was calculated as shown in Table 1. Fine triangular mesh of 0.5 nm was used close to the charged walls. In the remaining parts of the modeled structures, the mesh was reduced to the point when no change in the observed concentration profiles and currents was observed upon further mesh decrease. The dielectric constants were taken equal to 64, 37.5 and 7.58 for Propylene Carbonate, Acetonitrile and THF, respectively. Diffusion coefficients 2×10^{-9} m^2/s were used for both

cations and anions. This model was devised to answer the question of whether the positive potential due to the possible presence of dipoles alone can indeed induce ion current rectification in conically shaped nanopores. We assumed 3 dipole molecule present at 1 nm^2 of pore walls for all three considered solvents (as calculated in Table 1), and no adsorbed lithium ions. The calculated current-voltage curves in 10 mM $LiClO_4$ (Figure 1.10) are in a qualitative agreement with our experimental findings and predicted a more ohmic behavior in tetrahydrofuran.

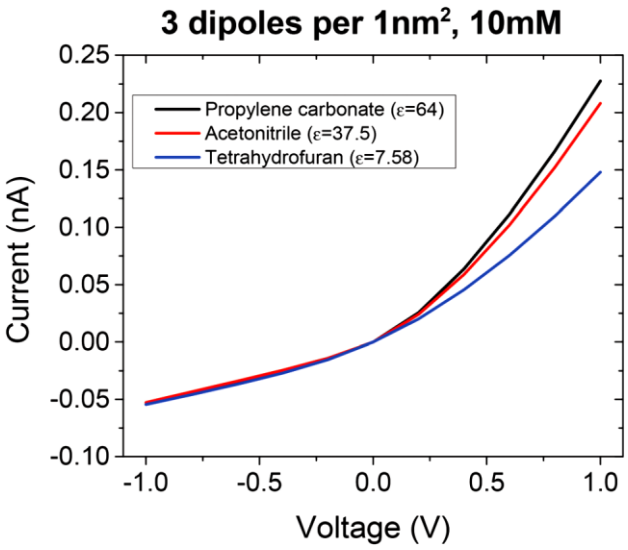

Figure 1.10 shows numerical solutions of Poisson–Nernst–Planck equations predicting current–voltage curves through a single conical nanopore in 10 mM $LiClO_4$ in three organic solvents. The modeled nanopore had openings of 15 nm and 500 nm.

In our various nanopore systems, we explain the rectification observed by two effects: (i) adsorption of Li^+ to the pore walls, and (ii) finite dipole moment of the pore walls by adsorbed solvent molecules. However, these evidences, both experimental and theoretical, strengthen the second explanation and point to a new prospect for man-made systems: surface dipole moment in nanofluidic systems can impact ion transport and can even have meaningful interplay with surface charges. The importance of surface dipoles on properties

of biological membranes and channels has been known for a long time [89, 90], however, the effect of dipoles has not been considered yet for transport properties of man-made systems, with exception of a theoretical study, which indeed predicted surface-dipole modified ionic concentrations in a nanopore when electrical double layer thickness is comparable to the pore radius [76, 94]. Future work with pores containing dipoles could become the basis for new ionic devices controlling transport of ions, molecules and water. For the purposes of this work, however, demonstrating polymer pores were stable in new kinds of electrolyte was a key insight which led to boldness in proposing experiments to come.

Chapter 2: Solid-State Ionic Diodes in Conical Nanopores with $LiClO_4$-doped PMMA Gel Electrolyte

Having established polymer nanopores of both polycarbonate and polyethylene terephthalate (PET) remain stable in an organic electrolyte, i.e. propylene carbonate (PC), efforts to expand the range of testable electrolyte were invigorated. A strong motivation for this was to demonstrate that outcomes and principles established in aqueous solutions, whose physical and chemical properties are well-studied, could be transferred to systems with less background in nano-fluidic literature. Among these outcomes is included developing man-made, nano-fluidic ionic circuitry [67], which is inspired by several biological processes e.g. nerve signaling, vision, and olfactory sense [39, 40]. As was stated earlier, biomimetic channels [41, 42] utilizing a physiologically similar electrolyte system (i.e. aqueous solutions of KCl and NaCl), have been reported, as well as other ionic devices resembling standard electrical equivalents, e.g. pn- junctions [43-45], pnp and npn-transistors [46-47], diode and transistor-based logic circuits [48-50]. Developing similar devices in other electrolytes could expand the range of applications for nanopore technology, serving to model and potentially increase compatibility with systems which do not operate well in aqueous environments, such as electrical energy storage [57].

Understanding nano-fluidics in electrical energy storage devices has gained interest in recent years since the Lee and Goodenough discovery of high capacitance (~200 F/g) nano-powdered manganese dioxide [1], which has been shown to have a highly porous nanostructure [7, 8, 9]. This has led to several studies attempting to leverage nanostructures for capacity improvement [5, 95], with some systems reporting specific capacitances in

excess of ~500 F/g [96]. However, these nanostructures have also demonstrated standard electrode breakdown phenomena in liquid electrolytes [57] as well as delamination [97], physical lift off of electrode material from its current collector. To mitigate stability and safety issues of liquid electrolytes, batteries and super capacitors often operate in solid electrolytes. One candidate material for solid electrolytes is $LiClO_4$-doped poly(methyl methacrylate) (PMMA) gel, due to its relatively high conductivity (~10^{-3} S/cm) and tunable viscosity [60, 61]. Recently, the gel has shown remarkable ability in preserving mesoscale battery electrodes past 100k cycles, demonstrating stability for long-term application [97].

In this chapter, we will present a system of a single nanopore filled with a solid electrolyte of $LiClO_4$-doped PMMA, which functions as a rectifier. The system does not contain any interface with a liquid electrolyte, thus the gel-filled nanopore functions as a solid ionics diode. This system is very different from reported before organic diodes, which require organic semiconductors and electronic transfer within [98]. The solid-state diode presented here rectifies the current in a wide range of $LiClO_4$ concentrations and produces stable ion current signals as well as fast switching. The solid-state ionic rectifier can find application to energy conversion from electrical fluctuating signals and storage procedures [99] and help understand ionic transport in solid electrolytes.

Section 2.1 – *Preparing and Testing PMMA Gels and Nanopore Samples*

The preparation of the gel started with the liquid electrolyte of $LiClO_4$ in propylene carbonate (PC) in various concentrations (depending on the type of experiments). A 5 mL aliquot of $LiClO_4$ in dry propylene carbonate (PC) was mixed with PMMA (with different w/w % mass- 2.6 g for 30% PMMA, and 2.0 g for 25% PMMA). The mixture was subjected to

vigorous stirring at 115°C. The mixture was left to cool down to room temperature in a desiccator and was subsequently transformed to the gel state. To apply the electrolyte to the pre-characterized pores, the gel was warmed to 75-90 ˚C and 0.1 mL was drop-cast onto both sides of the membrane. The membrane was allowed to sit in an open-air, room temperature environment for ~20hr before testing to ensure complete filling of the pore.

Current–voltage curves through all pores (PET) were recorded with a Keithley 6487 picoammeter/voltage source and Ag/AgCl pellet electrodes (A-M Systems, Sequim, WA). In conical nanopores, the ground electrolyte was placed at the side of the membrane with the narrow opening. Figure 2.1 shows pictures of the experimental set-up which was used during tests with the 6487 Keithley Picoammeter

a)  b) 

Figure 2.1 shows the membrane in the experimental set-up after it has been deposited with gel. The membrane is suspended between supporting O-rings on a glass slide and the pellet Ag/AgCl electrodes are placed directly into the gel on both sides of the membrane. There is no connection between the two sides via gel leaking around the edges, thus all recorded current is through the nanopore.

Ion current in time was recorded using Axopatch 200B and 1322A Digidata (Molecular Devices, Inc.) at 20 kHz sampling frequency and 2 kHz low-pass Bessel filter. Voltage was changed between −2 V and +2 V with 200 mV steps and at each voltage level, the current was recorded for 20 s. Current–voltage curves were obtained by averaging the last 0.5s of

recordings at each voltage. The fast-switching experiments were also performed using the Axopatch 200B assembly, which was programmed to produce driving square waves with varying frequency and a 2V amplitude.

Section 2.2 – *$LiClO_4$-PMMA Ion Transport Experiments in Cylindrical Nanopores*

In order to test ion transport through pores filled with gel electrolytes, experiments were first performed with cylindrical pores prepared by track-etching [22, 24]. The sizes for the cylindrical pores ranged from 400-1100nm in diameter. The measurements allowed us to provide evidence that continuous filling of a single pore with the $LiClO_4$-doped PMMA gel is indeed possible. Figure 2.2 shows recordings for single cylindrical pores after drop-casting the gel on both sides of the membrane; the gel was doped with 100 mM $LiClO_4$. We found the best results for cylindrical pores using a gel containing 25% (by wt.) PMMA. Two Ag/AgCl electrodes were placed directly into the gel as shown above (Figure 2.1).

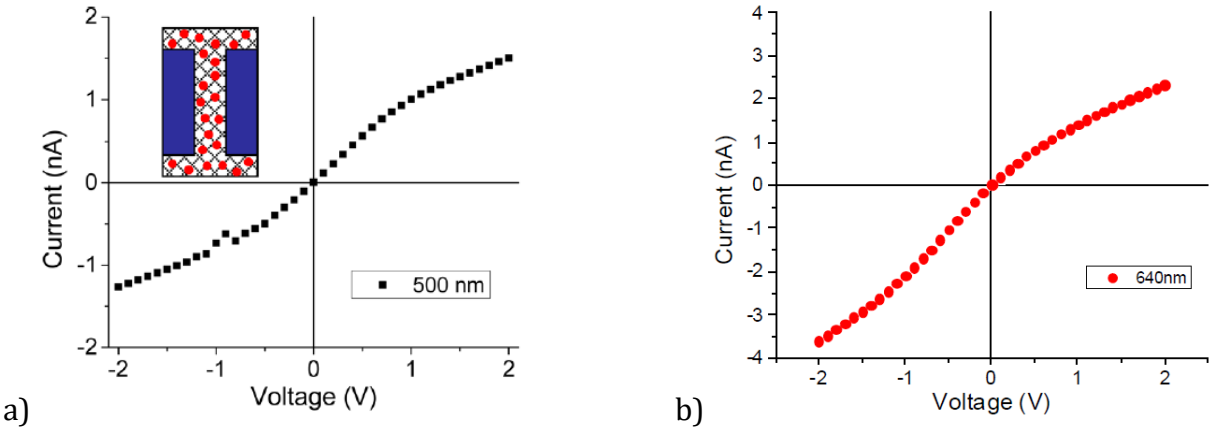

Figure 2.2 I-V response of two cylindrical pores filled with 100 mM $LiClO_4$-PMMA gel. **(a)** A 500 nm pore and **(b)** a 640 nm pore. As expected, overall system conductance scales with size. Conductivity was calculated relating the measured resistance with pore geometry, assuming cylindrical shape, by eqn. (1.1). The cross-hatched texture is to represent the PMMA gel inside the nanopore, with the red speckles to indicate lithium doping.

The measured current–voltage curves with known pore geometry allowed us to calculate the conductivity of the gel in the pore to be σ = 0.5 mS/cm, thus in good agreement with bulk studies [100]. The recorded current is indeed due to the presence of ions in the gel since filling a pore with PMMA gel without $LiClO_4$ led to significantly lower currents (Figure 2.3). The finite values of the current with an undoped gel result from finite electronic conductivity of the PMMA gel. The ratio of ionic conductivities in the doped and undoped cases is 10. Thus, according to our measurements, the electronic contribution to the total measured current reaches ~10% when the gel is doped with $LiClO_4$, again in excellent agreement with previous bulk studies of PMMA [100].

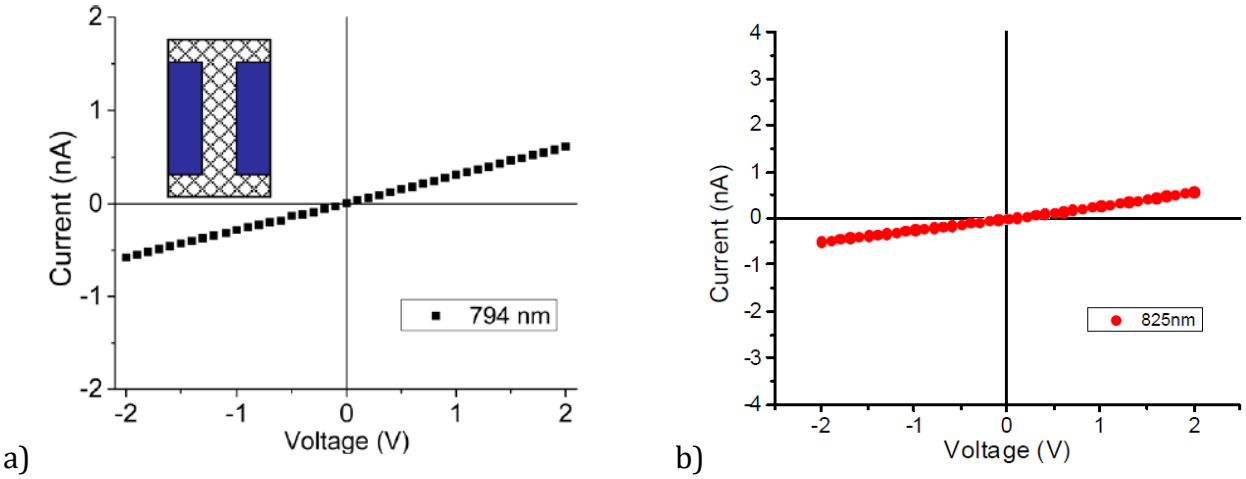

Figure 2.3 I-V response of two cylindrical pores filled with blank PMMA gel, containing only propylene carbonate without salt. **(a)** A 795 nm pore and **(b)** an 825 nm pore. Because of the similarity in size, it is difficult to observe system conductance scaling with size. Despite the much larger size of these pores, the observed conductivity is significantly lower than the pores in Figure 2.2 ($\sigma_{doped}/\sigma_{blank} \sim 10$). The cross-hatching is meant to indicate PMMA gel inside the nanopore, and the absence of red speckles indicates a blank sample.

These initial studies in cylindrical nanopores demonstrated that nanopores could support the gel electrolyte and that several of the bulk properties of the PMMA gel were preserved at the sub-micron scale.

Section 2.3 – *Solid State Diodes in Conical Nanopores with $LiClO_4$-PMMA Gel*

With successful control experiments in cylindrical nanopores, our next experiments featured conically-shaped nanopores, with the consideration that further constricting the electrolyte would reveal properties unique to nanoscale lengths. Conical pores varied from 340nm–1200nm at the base (wide opening) and 10–60nm at the tip (narrow opening). In conical pores, a 30% PMMA (by wt.) gel was shown to have the best results. It was initially expected that PMMA would render no surface charges on the nanopore and that conductivity could be calculated based on semi-conical conductance.

Figure 2.4 shows recordings through a single conically shaped nanopore after drop-casting $LiClO_4$-doped PMMA gel on both sides of the membrane. Transport properties of the pore were examined using two experimental approaches. First, similar to the data shown in Figures 2.2 and 2.3, current–voltage curves were measured using a Keithley picoammeter. The data revealed that the shape of the nanopore played a crucial role in the system behavior, so that the pore rectified. The character of the I–V curve was consistent with the presence of a net positive surface charge on the walls.

We also wanted to probe stability of the ion current in time and recorded signals with sampling frequency of 10 kHz. The voltage was changed between −2 V and +2 V with 0.2 V steps; at each step, the current time series was measured for 20 s. The recordings revealed that the ionic diode is capable of providing stable rectifying signals; no decay or signal

fluctuations were observed. We believe the excess of the gel on both sides of the membrane serves as an ionic reservoir. Due to presence of only a single pore in the membrane, in the time frame of the experiments, the reservoir did not suffer ion depletion. Thus, the currents did not exhibit any decay even after minutes of recordings at one voltage. Averaging of the time signals allowed us to plot an I–V curve and compare it with the Keithley recordings. Excellent agreement of the two data sets confirms the system stability over long recordings.

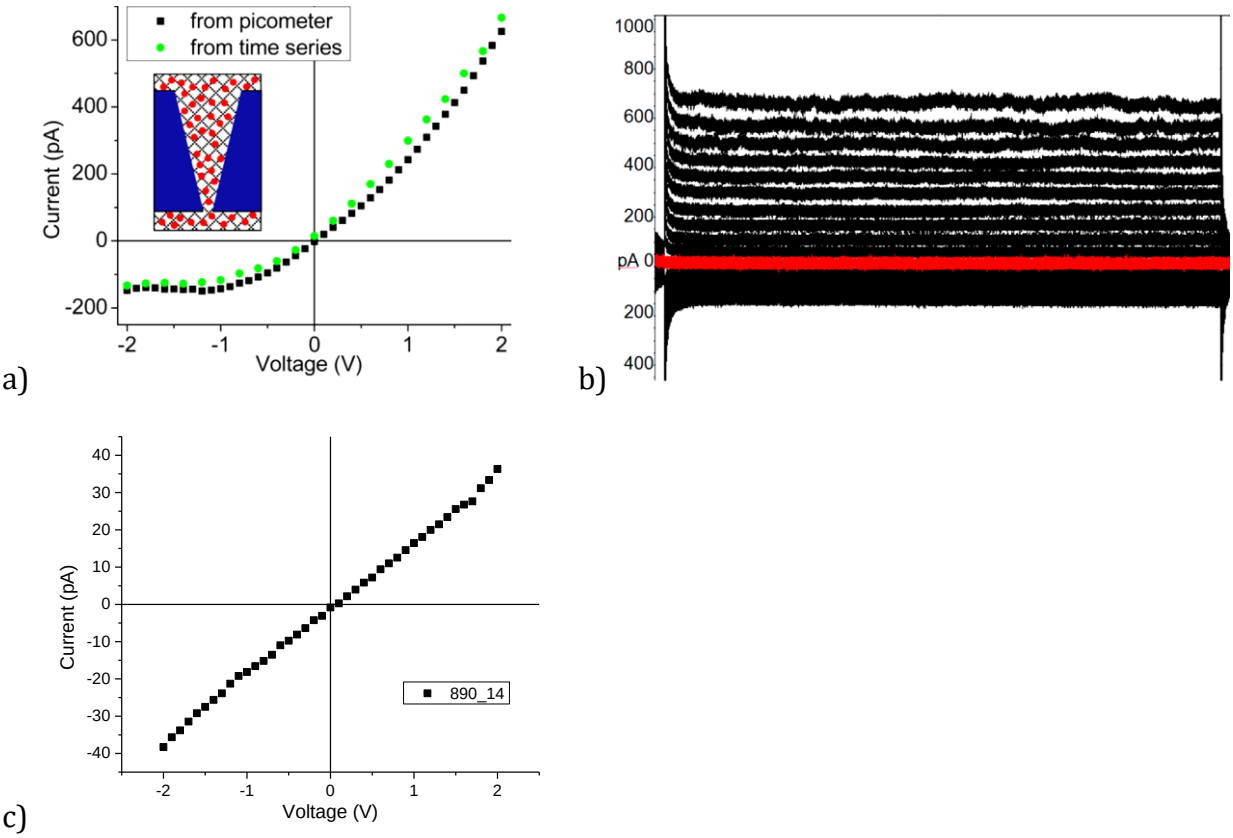

Figure 2.4 (a) I–V curves through a conically shaped nanopore drop cast with 1 M LiClO4 PMMA gel recorded with picoammeter/voltage source (black squares) and obtained by averaging ion current traces (recorded with 10 kHz sampling frequency) shown in **(b)** (green circles). Opening diameters of this pore were 610 and 22 nm, for base and tip, respectively. **(b)** 20 s long signals of ion current in time recorded between −2 V and +2 V with 200 mV steps. The cross-hatch texture is to represent PMMA gel, with the red speckles indicating lithium doping. **(c)** I-V curves through a conically shaped pore with undoped PMMA gel demonstrating absence of rectification, thereby confirming rectification as a property of ionic current.

In order to confirm that the gel filled the entire volume of the pore, an I–V curve of a conical nanopore drop cast with an undoped PMMA gel was measured as well (Fig. 2.4c). Linear I–V curve and much smaller current provided evidence that the I–V ion current data shown in Figure 2.4a-b present ionic movement through the PMMA gel in the pore. As in the case of cylindrical pores, the residual conductance observed with an undoped PMMA is due to electronic conduction, which is not rectified.

Additional tests were conducted to probe the current switching capability of the solid-state ionic diode. Figure 2.5 demonstrates stable, repeatable current switching between positive and negative voltages driven by a 0.1 Hz square wave. Similar scans at lower frequencies were tested with equal success, but after 0.2 Hz the frequency response of the system capacitance began dominating the signal. This demonstrates the viability of the system as fast-response nano-ionic circuitry.

a)

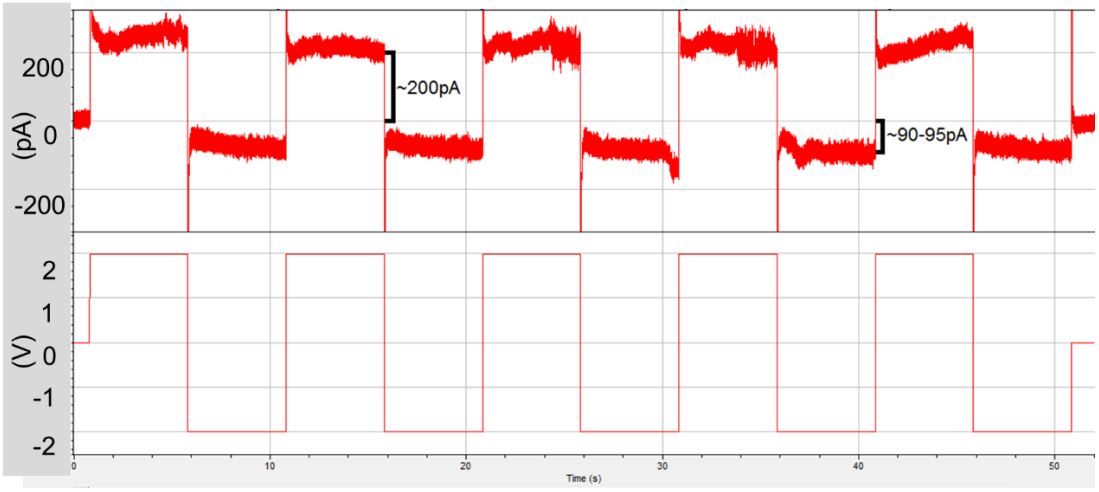

Figure 2.5 A conical nanopore filled with doped PMMA gel driven at 0.1 Hz by a 2 V amplitude square wave. Note that clear 'high' states and 'low' states are observed when the voltage switches between positive and negative. Also, the current response in the system generally stabilizes in under 2 s after the pulse changes polarity, indicating fast-switching capability.

A set of conically shaped nanopores with similar opening diameters and filled with PMMA gel with different $LiCO_4$ concentrations (between 100 mM and 1 M) allowed us to understand the role of salt concentration on the ion current rectification. Figure 2.6 demonstrates system rectification over a range of ion concentrations but also seems to suggest rectification does not have strong dependence on bulk concentration as found in liquid electrolytes [20, 54, 55].

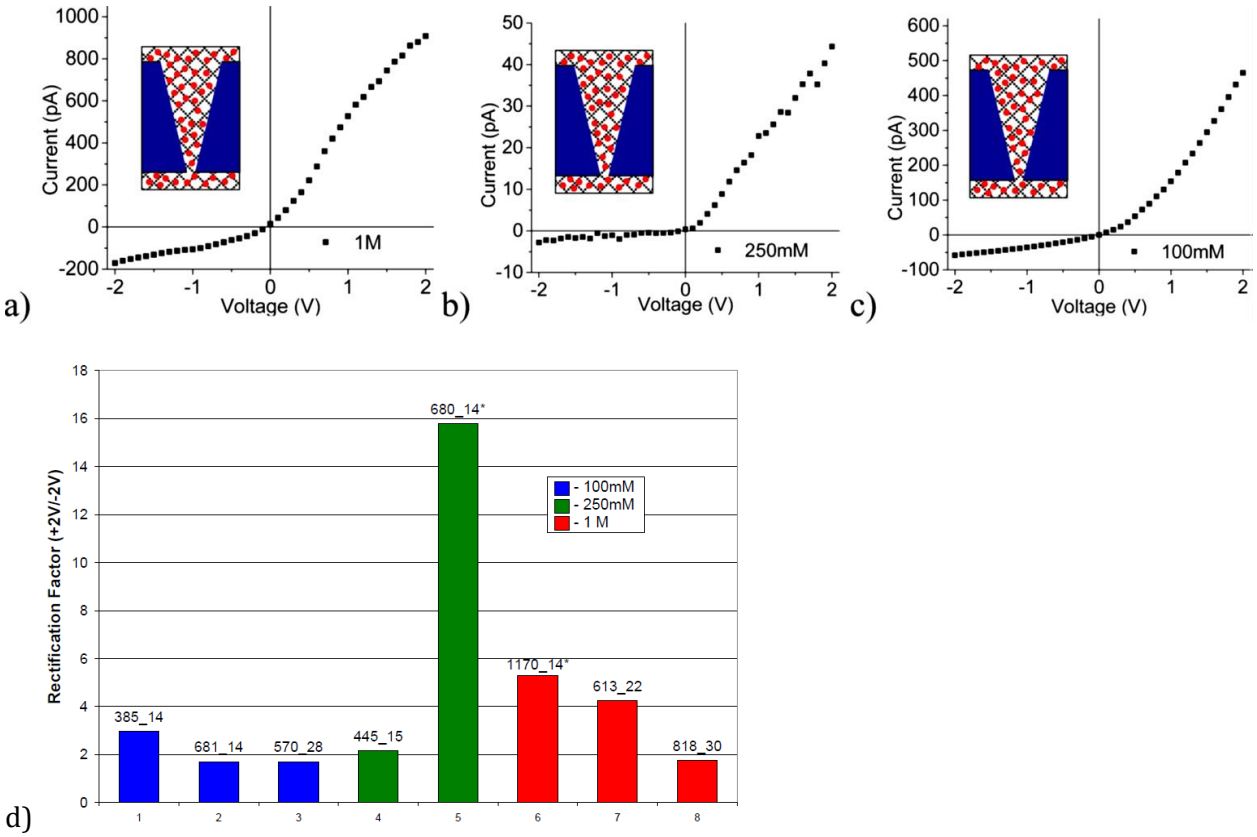

Figure 2.6 (a-c) I-V curves through three different conically shaped nanopores filled with PMMA gel doped with **(a)** 1 M, **(b)** 0.25 M, and **(c)** 0.1 M $LiClO_4$. Opening diameter of the pores (base and tip) were **(a)** 1170 nm and 14 nm, **(b)** 680 and 14 nm, and **(c)** 350 and 44 nm. All of these pores show significant rectification factor ($I_{+2V}/I_{-2V} > 5$) despite their differences in opening diameter and ionic concentration. The cross-hatch texture is to represent PMMA gel with the red speckles indicating lithium doping. **(d)** shows rectification factor for eight different conical nanopores with tip opening diameters less than or equal to 30. The data suggest lack of clear concentration dependence of ion current rectification, providing evidence that it is the internal porous structure of the gel that influences current characteristics. The speckling frequency is not indicative of concentration.

The lack of clear dependence of rectification on the salt concentration in the gel is further evidenced by recordings obtained for six additional nanopores in Figure 2.6d; the anomalously high rectification obtained with one nanopore deposited with 250 mM $LiClO_4$-PMMA (Figure 2.6b) stems most probably from favorable local arrangement of PMMA gel in this particular pore, and very small values of the current (few pA) for negative voltages. Presence of rectification even at high salt concentrations in the gel is consistent with earlier reports pointing to the formation of ion pairs when the salt concentration in PMMA is increased [101]. Consequently, the number of mobile ions does not increase with the increase of the salt concentration in the gel [100], providing less screening of the surface charges, and enabling rectification.

Section 2.4 – *Modeling Space Charge to Understand PMMA Gel Rectification*

Ion current rectification exhibited by conical nanopores filled with PMMA suggests that the structure of the PMMA gel matrix might play a significant role in transport properties of the gel-nanopore system beyond the effects from surface charges on the pore wall. This is especially evident in recordings for a conical nanopore shown in Figure 2.6c; its opening diameter of 44 nm assures that the pore walls surface charges are screened, thus the pore's transport properties are dominated by the gel. It is known that PMMA gel has mostly an amorphous character [102], which is partially dependent on its composition both in terms of PMMA and electrolyte concentration. Previous studies also revealed that even in bulk PMMA gels doped with salts, the measured current is primarily due to anions with transference numbers for lithium of ~0.2 [61, 103]. The low transference numbers can be caused by interactions of Li^+ with carbonyl groups in PMMA; complexation of Li^+ ions with

the gel was indeed demonstrated experimentally using, e.g., XRD, FT-IR, and Raman spectroscopy. [102, 104-106] We hypothesize that the complexed ions can lead to the formation of effective positive surface charge of the gel matrix, whose presence is suggested by I–V curves of nanopores filled with PMMA (Figure 2.6).

Previous Brunauer–Emmett–Teller (BET) and X-ray powder diffraction (XRD) studies revealed that gel electrolytes contained pores/voids with effective diameter as large as ~10 nm [107, 108]. If the gel structure and ionic concentrations were homogeneous throughout the whole pore volume, the system would not rectify. Asymmetric current–voltage curves require breaking symmetry so that for one voltage polarity, enhancement of ionic concentration occurs, while for the opposite polarity, a depletion zone is formed [14, 20, 51, 53, 55].

In order to probe the origin of rectification in the gel-filled conically-shaped nanopores, we consider a model of ionic conductivity consisting of two components: (i) the surface component that originates from counter-ions which neutralize the effective surface charge of the voids, and (ii) bulk conductivity through parts of the porous structure that is filled with bulk electrolyte [109]. We postulate the relative contribution of the surface and bulk conductivities to the measured ion current depends on the pore diameter thus is different in the narrow and wide openings of the pore. Consequently, concentrations of charge carriers will vary along the pore axis. This hypothesis is supported by earlier experimental findings on the dependence of conductivity of gel electrolytes on the dimension of pores in which they were embedded [63]. Gel electrolytes embedded in membranes with sub-100 nm pores were found to exhibit higher conductivity than in micron-sized pores; this

observation could be caused, e.g., by pore diameter-dependent arrangement and concentration of the gel components [110, 111] as well as of mobile ions.

Based on the studies of pore diameter dependent ionic conductivity [63], we assumed that, due to the nanoconstriction of the narrow opening of a conically shaped nanopore, the tip region features a higher density of mobile charges compared to the wide opening. This inhomogeneous distribution of mobile charges could be, e.g., a result of a lower local PMMA concentration at the pore tip. A higher density of mobile charges at the tip could also be treated as a model of a system in which an enhanced ionic conductivity is caused by other effects such as higher mobility of ions due to nanoscale induced arrangement of PMMA molecules, shown before for other polymer electrolytes [63, 110, 111].

Current–voltage curves through a conically shaped pore filled with a gel can be predicted by solving the following set of Poisson–Nernst–Planck (PNP) equations:

$$J_i = -D_i \left(\nabla C_i + \frac{z_i e C_i}{k_b T} \nabla \varphi \right) \quad (2.1a)$$

$$\nabla \cdot J_i = 0 \quad (2.1b)$$

$$\varepsilon_o \varepsilon \Delta \varphi = -[e(C_+ - C_-) + \rho(z)] \quad (2.1c)$$

where J_i is a flux due to one type of ions, characterized by diffusion coefficient, D_i, ε_o is vacuum permittivity, and ε is dielectric constant of the medium assumed to be equal to 64. Note that the Poisson equation (Eqn. 2.1b) has been modified to include space charge, $\rho(z)$, in the pore volume due to the presence of charged porous gel. In order to consider the dependence of the concentration of mobile charges on the pore diameter, we assumed the density of the space charge, $\rho(z)$, changes according to the following function [46]:

$$\rho(z) = \rho_o \left(\frac{dL}{Dz + dL} \right)^n \quad n = 0.5, 1, 2, 4 \quad (2.2)$$

where ρ_o is the concentration of space charge at the tip, and d and D and the diameters of the tip and the base opening, curves for a pore with diameters of 50 and 500 nm obtained by solving Eqns. 2.1 and 2.2 numerically using the Comsol Multiphysics 4.3 package. The modeled current–voltage curves are in qualitative agreement with the experimental data (Figure 2.7) and predict ion current rectification for all values of n considered.

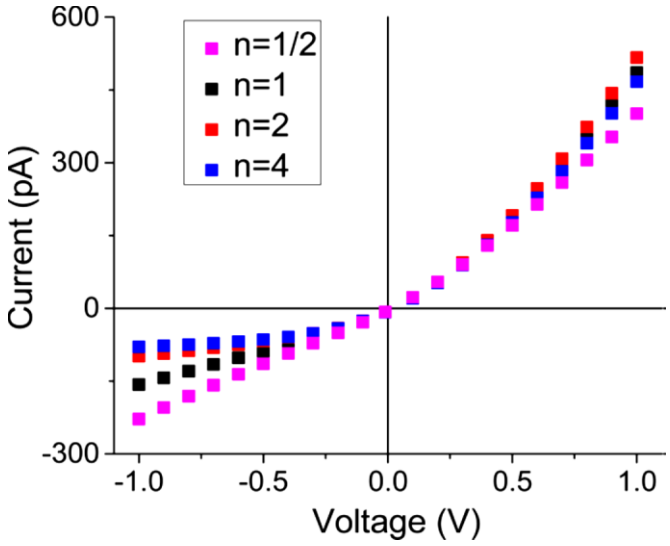

Figure 2.7 Numerically modeled I–V curves using Comsol through a conically shaped nanopore with opening diameters of 50 and 500 nm. Presence of the charged PMMA gel was modeled by introduction of additional space charge term, $\rho(z)$, whose dependence on the axial position, z, is given in Eqn. 2.2. The legend gives values of the coefficient, n, in Eqn. 2.2.

These experiments in PMMA gel demonstrate initial findings for a solid-state ionic diode and pave the way for future work with similar electrolytes in polymer pores and other potential substrates [17, 112]. Several questions were generated by these studies which led to the suggestion of new mechanisms to explain observed phenomena, chief of which is the observation of rectification without apparent concentration dependence and the proposed space charge correction. The insights gained from these experiments, as will be shown in the next chapter, were informative for the next, and more complicated, system we studied.

Chapter 3: Nanopores in Compatible $LiClO_4$-PMMA Gel and $LiClO_4$-PC Liquid Electrolyte System

The initial studies of $LiClO_4$-PMMA gel in nanopore systems illuminated important ion transport properties of the gel at nanoscale lengths. However, one of the key aspects we wanted to continue investigating was gel conductivity in different experimental arrangements. An important observation from the initial studies by Le et al with the MnO_2 mesorod-PMMA gel system was that of reduced capacitance [97] compared to earlier findings by Yan et al using MnO_2 mesorods and liquid organic solvents [96]. The liquid electrolyte MnO_2 system demonstrated almost 10x the capacitance exhibited by the gel-MnO_2 (60 F/g - Le vs. 600 F/g - Yan). Part of the reason for this may be the size of the electrodes used, as previous experiments in MnO_2 have shown that cross-sectional diameter plays a significant role in capacitance, e.g. δ-phase MnO_2 wires with shell thickness ~70nm outperformed similar wires of thickness ~175nm (450 F/g vs. 150 F/g @ 100mV/s) [96, 113]. Other studies have elucidated material thickness and density as a possible mechanism limiting active MnO_2, e.g. β-phase MnO_2, which has dense crystal structure, 1.89Å, demonstrated less capacitance (100 F/g) than δ-phase, whose interlayer distance is 7Å (325 F/g) [7, 8, 113]. It is not, however, clearly understood what effect the gel electrolyte could have on the system performance.

$LiClO_4$/PMMA gel has been studied for its bulk properties and its conductance is known to be similar to bulk conductivity of $LiClO_4$ in propylene carbonate [100, 101]. However, it has also been demonstrated that nanoscale architectures, such as conical nanopores, have the ability to modulate ionic concentrations inside their structure due to

the nanoscale and surface charge properties [15, 20, 23-28, 51, 52]. Since δ-MnO_2 is formed of several tendril-like structures and layers [7, 8], synthetic meso- and nanopores could provide insight on the ionic transport properties of $LiClO_4$/PMMA gel in such structures. It has been confirmed through experiment that drop-cast deposition of PMMA-based gels on both sides of cylindrical and conical nanopores in polyethylene terephthalate (PET) films result in a complete filling of the nanopore [63, 66]. It has also been shown that the gel can pass both ionic and electronic currents [100-102], and that the conical geometry leads to rectification phenomena of the ionic transport [66]. Thus, nanoconstriction does not measurably impact the conductivity of the gel system and, in some cases, can augment ionic conductance of a polymer electrolyte [63].

Here we disclose a series of experiments utilizing both cylindrical and conically shaped polymer nanopores implanted with $LiClO_4$/PMMA gel of varying concentrations to understand the transport response of the gel when in contact with a compatible electrolyte i.e. $LiClO_4$/propylene carbonate (PC). We selected polyethylene terephthalate (PET) nanopores because they have shown robustness in recent experiments involving the $LiClO_4$/PMMA gel and have already demonstrated ion transport properties such as rectification in gel-only systems [66]. This work provides direct results for materials testing and discusses mechanisms regarding the interaction of gel-liquid systems. This will allow us to test interfacial characteristics between the gel and liquid electrolyte in nanoconfinement, the ion transport properties of gel-liquid electrolyte systems, and also whether gel systems are permeable to liquid electrolyte exposure. We hope to provide initial research and perspective on a middle ground approach to increasing cell capacitance by studying a hybrid system composed of liquid and gel components.

Section 3.1 – *Gel-liquid systems in cylindrical nanopores*

The first pore system we approached in studying hybrid gel-liquid systems were cylindrical pores. A simple geometry was a useful simplification to answer important questions regarding the gel-liquid system, such as whether PMMA gel matrix at the sub-micron scale can 'hold' its initial doping concentration in the presence of liquid $LiClO_4$-PC electrolyte. A straightforward experiment to examine this property is a one-sided drop-cast on a membrane followed by probing ionic current in a liquid electrolyte system. Figure 3.1a shows a schematic of the planned experiment. Even though, in the one-sided drop-cast experiment, the depth of the gel penetration into the pore is not known, we expect it to be at least half of the pore length. Our previous experiments with samples subjected to drop-casting on both sides of the membrane provided evidence that the whole pore volume became filled with the gel [66]. It is therefore reasonable to expect at least half the volume would be filled by a one-sided drop-cast. The work in the previous chapter was performed without the liquid electrolyte and allowed us to examine the combination of ionic and electronic conductivity through the gel.

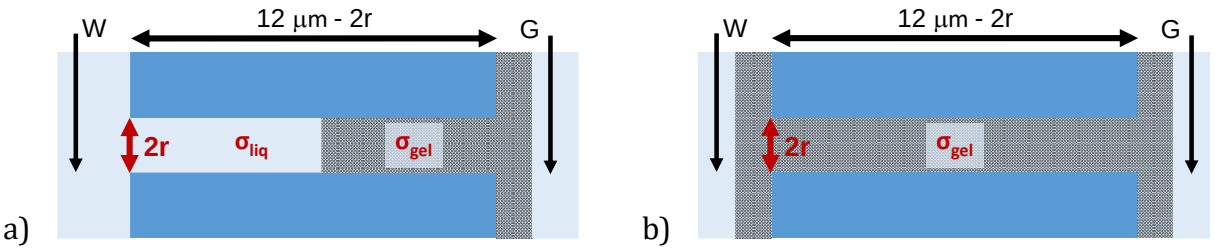

Figure 3.1. Scheme of experiments in which single pore membranes subjected to **(a)** one-sided or **(b)** double-sided gel dropping were placed in contact with liquid electrolyte of $LiClO_4$ in propylene carbonate. Note the regions containing the working and counter electrodes are macroscopic reservoirs with liquid electrolyte thus they do not significantly contribute to the system resistance. W and G indicate working and ground electrodes, respectively

Experiments with cylindrical pores entirely filled with gel, via double-sided gel casting, were performed as well (Figure 3.1b). These samples were used in control experiments to observe change of the pore resistance before and after exposing it to the liquid electrolyte. We expected that if the gel was unaffected by the liquid electrolyte, I-V measurements would be similar in the immersed and gel-only cases, and would show no dependence based on the concentration of the liquid electrolyte. Experiments were performed with PMMA doped with 100 mM $LiClO_4$ as well as undoped PMMA gel. The bulk solution was $LiClO_4$ in propylene carbonate ($LiClO_4$-PC); the salt concentration was varied between 10 mM and 1 M.

a) 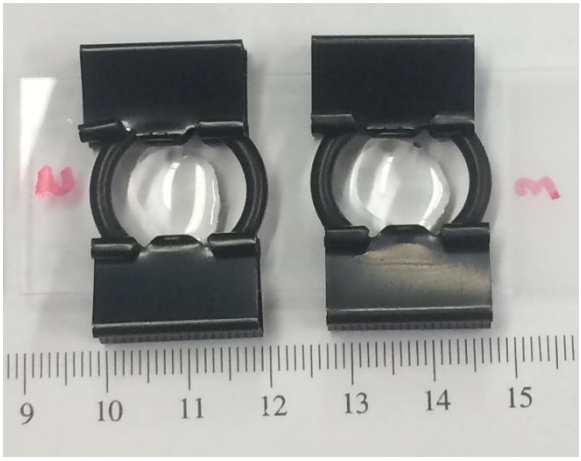

c) 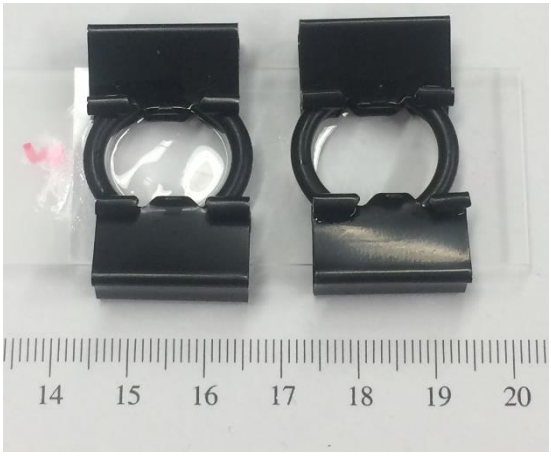

Figure 3.2 Photographic images of a glass slide upon which two samples of gel have been placed. The progression from **(a)** to **(b)** demonstrates how the gel can spread due to plasticizing with the propylene carbonate as the gel fills the constraining O-ring. No significant loss of the gel has been observed. The red numbers on the glass slide indicate the percent composition PMMA: '2' marks 25% (w/w), used in cylindrical pore samples, and '3' marks 30%, used in conical samples.

At first we checked stability of PMMA gel in contact with solutions of $LiClO_4$ in propylene carbonate. The gel was deposited on a glass slide and observed using a microscope and camera before and after exposing the gel to propylene carbonate (Figure 3.2). These

experiments were aimed at understanding the possibility of our gel spreading since propylene carbonate is known to be a PMMA gel plasticizer [114]. Indeed, the gel did spread after exposure to the solvent, however the gel layer remained continuous.

In order to assure that the mesoscopic structure of the gel quickly equilibrates when exposed to liquid PC and does not change during measurements, current-voltage curves were recorded using the following order. We started with 100 mM $LiClO_4$ in PC, followed by probing lower concentrations down to 10 mM, we re-measured the 100 mM conditions and finally increased the salt concentration to 1 M $LiClO_4$. For some samples, after the set of measurements was completed we checked the currents at 100 mM $LiClO_4$ one more time. The three sets of 100 mM salt would not typically differ more than 10%, providing evidence for a stable structure of the PMMA gel in contact with PC. Each set of current-voltage curves was recorded after ~1 minute equilibration of the system with a given salt concentration. Four scans were performed at each concentration and the reported I-V curves are the average of the last three scans.

The polymer samples with PMMA gel were visually examined after I-V recordings. As in the case of the glass side, the gel spreading on the polymer surface was evident as well, and we confirmed lack of visible loss of the gel. For pores entirely filled with the gel, we expected no loss of gel *from the inside* of the pore, since the gel in the pore was protected *via* the thick layers on the polymer surfaces.

Figure 3.3 shows I-V curves recorded for two samples with single pores, subjected to PMMA gel casting and exposed to bulk electrolyte of $LiClO_4$ in PC. The salt concentration of the liquid electrolyte was varied between 10 mM and 1 M. One sample (Fig. 3.3a-c) was subjected to PMMA gel drop-cast on one side only, and the gel was undoped. The second

sample (Fig. 3.3d-f) was entirely filled with gel, which had been doped with 100 mM $LiClO_4$ during its preparation. The first feature of the two nanopore membranes is a clear dependence of the I-V curves on the salt concentration in the bulk, regardless of gel doping: higher currents were recorded for higher concentrations of the salt in the liquid electrolyte.

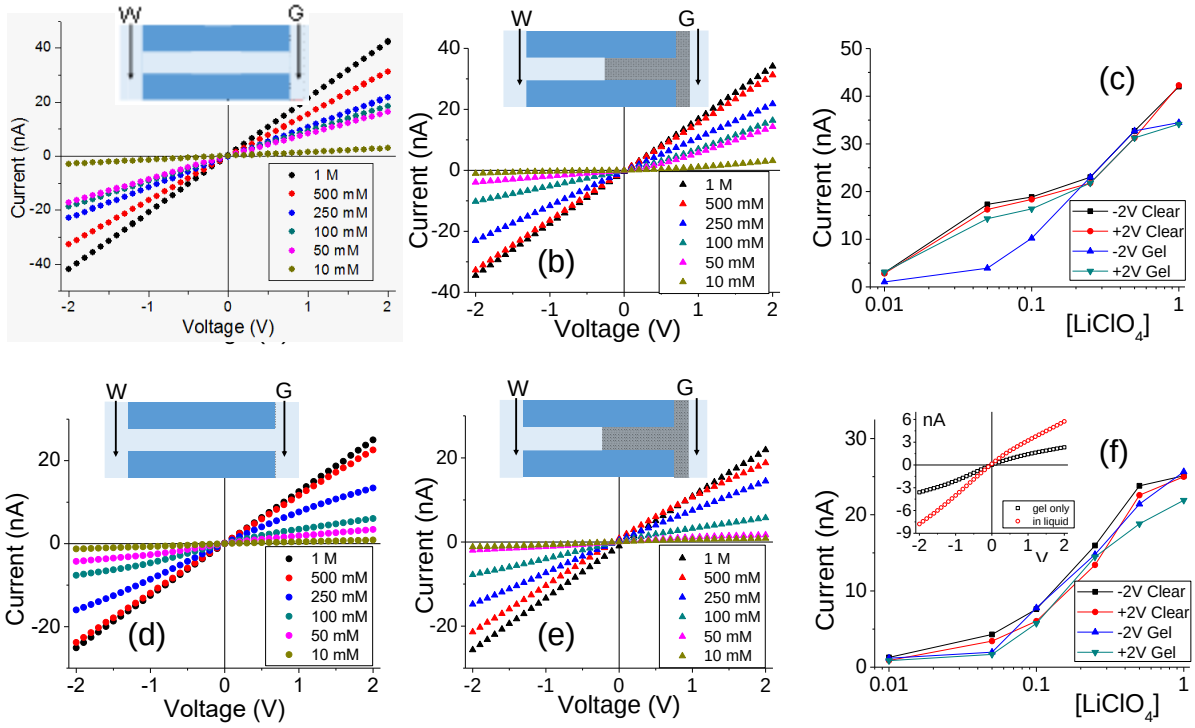

Figure 3.3 (a-c) Ion current through a 790nm in diameter cylindrical pore subjected to one-sided casting of undoped PMMA. **(d-f)** Experiments with a 640nm pore after it had been filled with PMMA gel doped with 100mM $LiClO_4$ (drop-casting had been performed on both sides of the membrane). Insets show state of the pore during the I-V scan. Inset on 3f shows I-V measurements of gel-only case and the immersed sample (100mM $LiClO_4$/PC).

In the samples subjected to gel casting on one side of the membrane, concentration dependence is expected since the gel infiltration may not be through the entirety of the pore. However for the pores that were entirely filled with PMMA, the presence of a clear concentration dependence of the current gives the first evidence that the ion transport properties of the gel do not remain unaffected by the liquid electrolyte. Similar values of pore

conductance before and after gel infiltration, independent of whether the pore was subjected to drop-casting with an undoped gel or with PMMA that contained $LiClO_4$, constitute the most surprising finding. This observation also suggests that once a PMMA gel is immersed in the liquid electrolyte, its conductivity becomes dominated by the bulk solution. Figure 3.3f also reports ion current measured before immersing the pore in liquid electrolyte with electrodes placed directly into the gel, as reported by us before. These gel-only measured conductance was significantly lower compared to the recordings in liquid electrolyte.

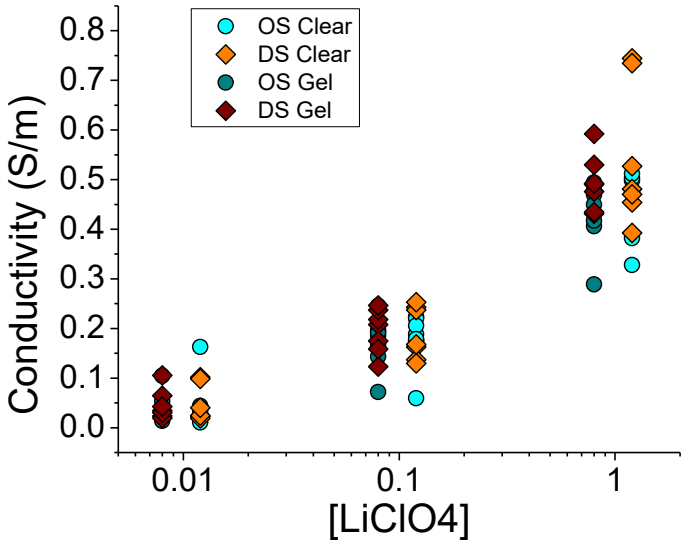

Figure 3.4 Summary of conductivities for 15 independently prepared single-pore membranes with one-sided (n=8) and double-sided (n=7) gel configurations; conductivities of the same pores before gel deposition are shown as well. The lack of distinct difference between gel and clear samples, or between these two gel configurations strongly suggests a high degree of permeability for PMMA gel to multiple levels of concentration when immersed in compatible electrolyte $LiClO_4$-PC.

Figure 3.4 summarizes several tested single cylindrical pores (n = 15) and their ionic conductivities before and after gel deposition in three standard concentrations (1 M, 100mM, and 10mM) of $LiClO_4$/PC. Ionic conductivities were calculated by assuming the pore geometry to be cylindrical and relating the pore resistance (obtained from I-V curves) with

its diameter and length, leaving conductivity as the only unknown. The figure shows a spread of conductivities, with no clear groupings to distinguish one-sided or double-sided samples or doping concentration in the PMMA. The data also highlight the statistical similarity between clear and gel-deposited cases when in contact with liquid electrolyte on both sides. This, along with the dependence of recorded current on concentration of the bulk electrolyte (Figure 4.3), suggests the PMMA gel is highly permeable to the liquid electrolyte.

An evidence of PMMA affecting ion transport was observed in one-sided drop-cast samples as ion current rectification; asymmetric I-V curves were especially pronounced in lower concentrations of $LiClO_4$ in the liquid electrolyte (Figure 3.5). In addition, cylindrical pores drop-cast with an undoped PMMA rectified to a greater degree than pores whose one side was drop-cast with 100 mM $LiClO_4$ doped PMMA. The rectification direction observed is consistent with effective positive surface charges in the PMMA gel voids and on the pore walls [65, 66], so that higher currents correspond to anions moving from the gel side to the open pore entrance (not covered with gel).

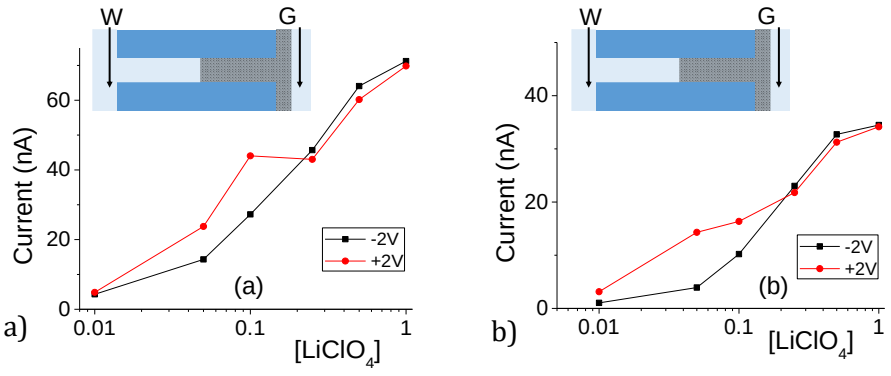

Figure 3.5 Ion current at +/- 2V for two cylindrical samples which have been deposited with gel on one side only: **(a)** 1100nm with doped gel, **(b)** 790nm with blank (undoped) gel. The doped PMMA gel in **(a)** contained 100mM $LiClO_4$. Salt concentration in the liquid electrolyte was changed between 10 mM and 1M. Ion current rectification was observed for both samples at lower salt concentrations in the liquid; rectification degrees were higher in the **(b)** undoped PMMA sample.

The presence of positive charges was previously suggested by our experiments with conical nanopores utilizing $LiClO_4$-PC and $LiClO_4$-PMMA gels [65, 66]; the excess charge could originate from adsorption of lithium ions as well as PC molecules, whose high dipole moment can impart effective charge. Existence of ion current rectification suggests that the local ionic concentrations in the gel are voltage polarity dependent [15, 20, 23-28, 51, 52], becoming enhanced for positive voltages, and depleted for negative voltages. We believe an undoped gel in contact with liquid electrolyte allows for more significant difference in ionic local concentrations for both voltage polarities compared to a gel that had been prior doped with a salt. Rectifying I-V curves also support our hypothesis that, while the PMMA gel is permeable to the liquid electrolyte, its porosity can still have an impact on the ionic current if the ionic strength of the electrolyte fails to screen surface charges. In addition, there could be significant difference in ion mobility inside the PMMA structure versus the bulk-like open pore conditions [63, 110, 111], which could affect ion current rectification as well.

Further tests were conducted to determine if exposing pores with PMMA gel to a liquid electrolyte only from one side is sufficient to observe an enhanced ionic transport of the system from the gel-only system explored in the earlier chapter. The schematic in Figure 3.6a illustrates how this would be accomplished for a one-sided gel deposition: one electrode was secured in the gel-cast side, while the open end was exposed to a reservoir of $LiClO_4$ electrolyte with the electrode freely suspended in the liquid. For a gel sample subjected to gel casting on both sides, the only difference would be the pore being completely filled with gel and one side being exposed to liquid electrolyte (Figure 3.6b). This set of tests will be referred to as a Gel-Liquid-Interface (GLI) experiment, and the results are shown in Figure 3.6. We found that conductance of nanopore membranes subjected to a one-sided gel drop-

cast is less sensitive to the salt concentration in the liquid electrolyte, and lower than when the pores were exposed to liquid electrolyte on both sides. A similar qualitative conclusion can be drawn from the data recorded for samples subjected to the gel drop-cast on both sides, with exception that in this case rectification of ion currents was observed.

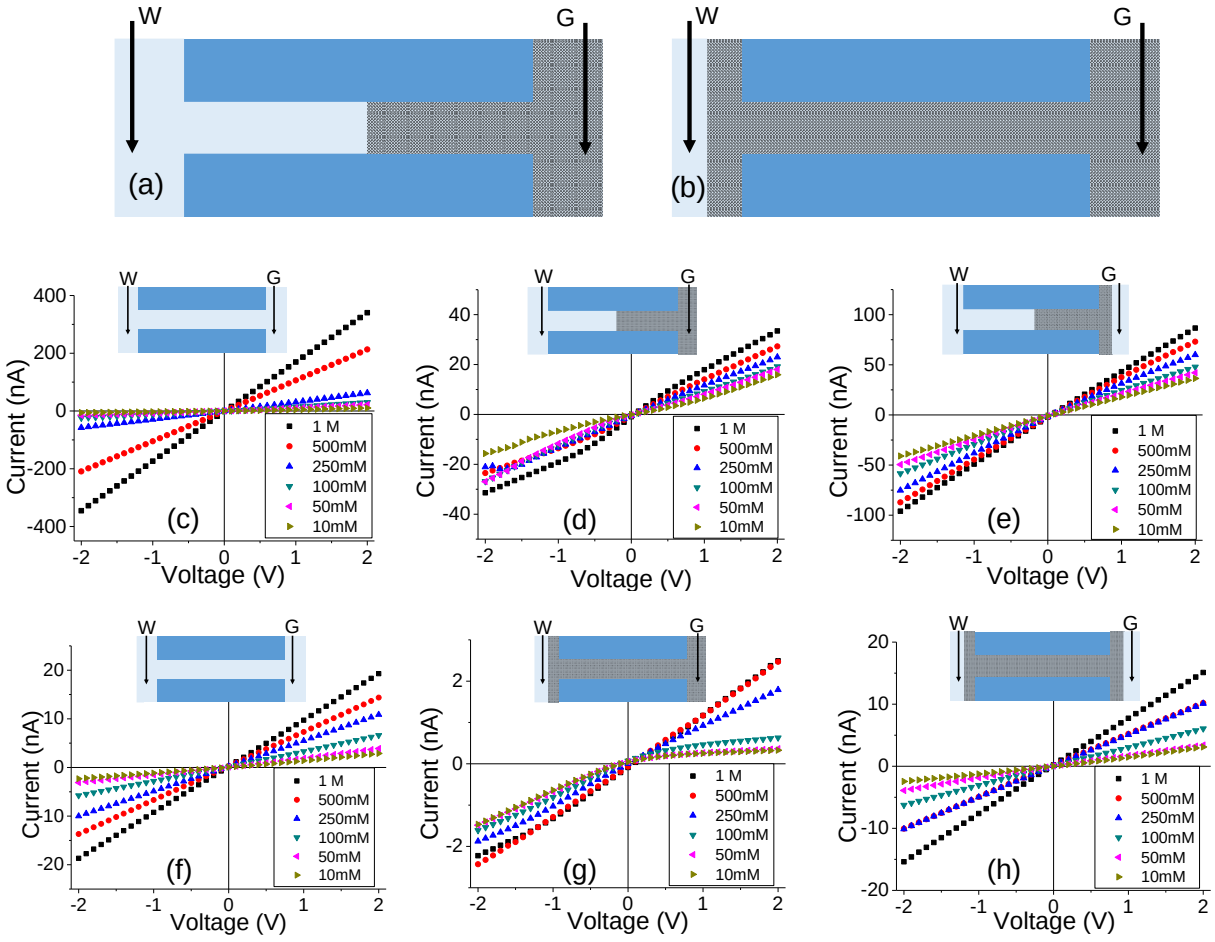

Figure 3.6 (a, b) Schematics of an experiment, called GLI, in which one side of the membrane was exposed to solution. Two electrodes were used in the measurements: one was embedded in the gel, the other one was located in the liquid. **(a)** Scheme of a pore subjected only to a one-sided drop of PMMA gel; **(b)** Scheme of a pore filled with PMMA. **(c-e)** Results for a cylindrical pore with an opening of 1060 nm in diameter subjected to gel deposition on one side; **(c)** recordings before depositing the gel; **(d)** measurements in the GLI mode, and **(e)** data obtained when both sides of the pore were placed in contact with a liquid electrolyte. **(f-h)** recordings performed with a 440 nm in diameter pore filled with PMMA gel doped with 100 mM $LiClO_4$.

In order to interpret the asymmetric I-V curves we recall that ionic conductivity of doped PMMA is lower than the conductivity of liquid electrolyte. Thus, when the membrane is in contact with liquid on one side only, at opposite voltage polarities ions are sourced from media of different conductivities. The effect is similar to the previously reported finding of ion current rectification induced in geometrically symmetric silica nanochannels placed in contact with a salt gradient in aqueous conditions [115]. The key requirement for the silica channel and our systems is the presence of surface charges and nano-confinement, which make the pores at least partly ion selective. For one voltage polarity, the majority carriers are sourced from the side of the pore in contact with a medium of lower conductivity, lower salt concentration in the silica channel system, and gel electrolyte in our case. For the opposite voltage polarity, majority carries are sourced from the opposite side of the membrane in contact with a medium of higher conductivity. The effect of ion current rectification observed in pores filled with PMMA gel provides yet another evidence that the gel contains interconnected voids with excess positive surface charges.

Section 3.2 – *Gel-liquid experiments in conical nanopores*

Experiments with cylindrical nanopores allowed us to verify that PMMA gel is porous and permeable to ions from the interfacing liquid electrolyte. A conical geometry of pores offers an easy access to nanoscale, and enables one to probe effects the gel exerts on ion transport when placed on the narrow and/or wide opening [116]. For conical nanopores, stable ion current signals were observed after increasing the weight percent of PMMA to 30%. As demonstrated before, this PMMA concentration also allowed full infiltration of the gel into the pore, so that the whole volume of conical nanopores was filled with the gel. As

with cylindrically shaped pores, experiments with one-sided and double-sided gel casting were performed, using doped and blank PMMA gels.

In our previous chapter, we reported that conical nanopores filled with gel and studied as an ionics solid system without liquid electrolyte, function as an ionic rectifier [66]. In addition, as shown in Chapter 1, an as prepared nanopore filled with liquid PC based electrolyte rectifies the current as well [65]. Thus, we expected conical nanopores with PMMA gel (drop cast on one side or two-sides) and in contact with liquid electrolyte would also rectify, however with degree that is modulated by the gel placement. Previous studies in aqueous KCl solutions indeed revealed that rectification of conical nanopore membranes was sensitive to the placement of agar hydrogels on one or two membrane surfaces [116]. In contrast to the previous report, the gel in our samples infiltrated the pores changing the overall nanostructure of the system, and we operate in entirely non-aqueous conditions.

Figure 3.7 shows representative samples of conically shaped nanopores after drop cast on the tip (and base) side only, as well as a nanopore filled with the gel entirely. The PMMA used was doped with 100 mM $LiClO_4$, and all samples were placed in contact with liquid electrolyte on both sides. Comparison with conductance of the clear pore, i.e. before gel deposition, is also shown. All conical nanopores examined exhibited the effect of ion current rectification with the currents for positive voltages higher than currents for negative voltages. This observation is in agreement with the existence of effective surface charges in the gel, as evidenced by our earlier experiments [66] as well as literature data [117]. The highest degrees of rectification were observed for pores subjected to drop-casting of the gel only on the tip side of the pore, similar to the observations with the agar hydrogel system.

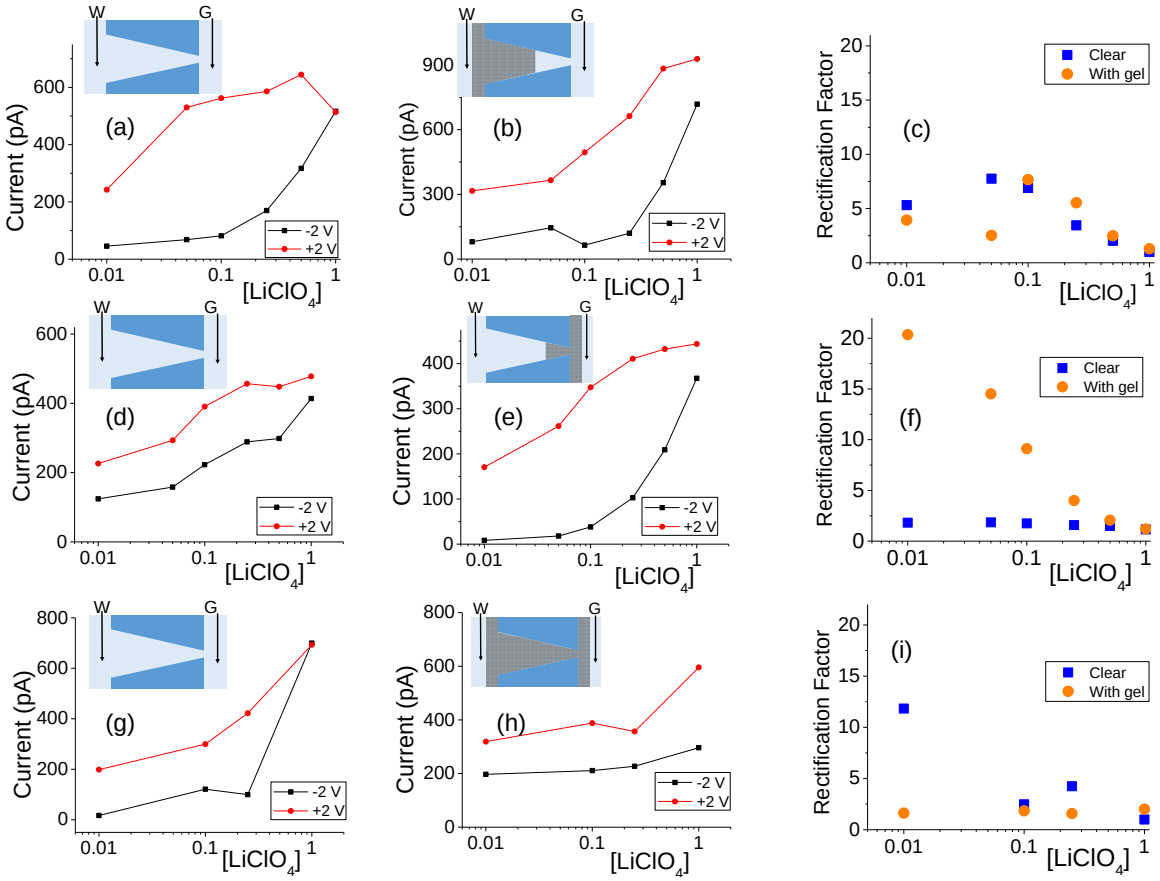

Figure 3.7. **(a-b)** Recordings with a single conical nanopore with opening diameters of 440nm (base) and 55nm (tip) subjected to gel drop-casting on the base side; the gel was doped with 100 mM $LiClO_4$. **(d-e)** Results from a pore with dimensions of 808nm (base) and 18nm (tip) subjected to one-sided casting of blank (undoped) gel. **(g-h)** Measurements for a pore with dimensions 354nm (base) and 44nm (tip) filled with doped gel (100mM $LiClO_4$). **(c, f, i)** Rectification degrees calculated as a ratio of currents at +2V and -2V for pores before and gel deposition in each case.

In terms of system conductance for an immersed sample before and after gel deposition, a large number of samples (n = 8) for one-sided pores and (n = 15) double-sided pores exhibited a reduced conductivity (Figure 3.8) after the gel was deposited. However, a statistically significant number of samples showed enhanced conductivity, which may be linked to rectification phenomena.

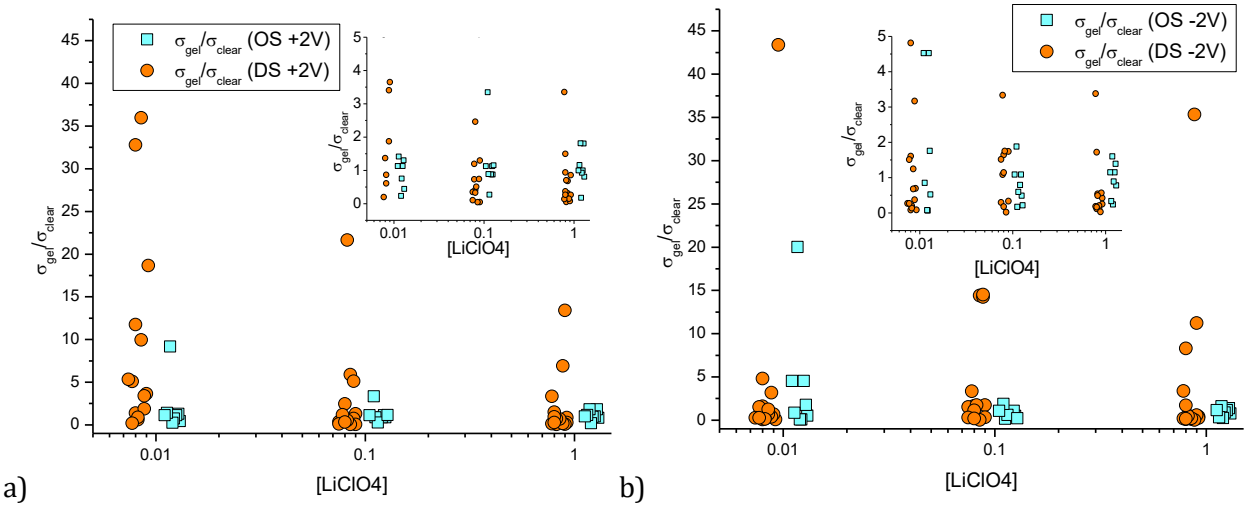

Figure 3.8 Summarizes the ratio of conductivities in immersed conical systems before and after drop-cast of PMMA gel at the extremes in polarity. A majority of samples in both gel configurations show similar or reduced conductivity after gel addition, however, there are cases where the gel conductivity is higher than that of the clear pore case. Jitter and insets added to clarify sample clusters.

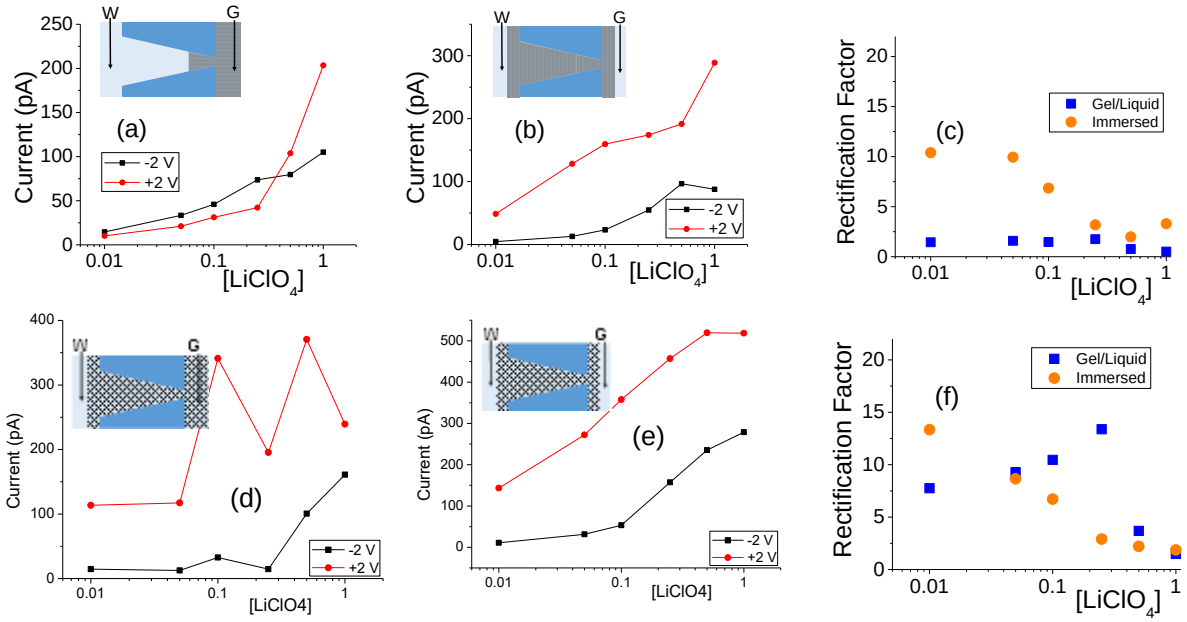

Figures 3.9. **(a-b)** Recordings with a single conical nanopore with opening diameters of 515nm (base) and 16nm (tip); this pore was subjected to one-sided drop cast of PMMA gel doped with 100 mM $LiClO_4$. **(d-e)** Measurements from another conical nanopore (1000nm (base) and 13nm (tip)), filled with PMMA gel. The base side was initially exposed to liquid electrolyte for the GLI test. **(c,f)** Rectification degrees calculated from currents at +2V and -2V for both GLI and IMM cases respectively.

We also performed GLI experiments in conical pores in the following configurations: (i) one-sided gel drop cast on the tip side, and (ii) pores filled with the gel in which the tip or base side was exposed to liquid electrolyte. Figure 3.9 details the findings and compares the GLI experiment to the immersed case and tracks rectification. The GLI experimental results follow the pattern shown in cylindrical pores as they all exhibit lower system conductance as compared to the immersed condition. This GLI experimental set-up also allowed us to probe the interplay of the two mechanisms for ion current rectification originating from (i) geometrical asymmetry of a nanopore with excess surface charges, and (ii) asymmetry in medium conductivities on both sides of the membrane.

The GLI experiments for the double-sided gel samples suggest that the rectification properties are dominated by the structural asymmetry of the pore. The dominant role of the conical shape is especially evident in recordings in which the base side of the pore was in contact with liquid electrolyte, and the other electrode was placed directly in the gel on the tip side. In our electrode configuration, for positive voltages the majority carriers – anions – are sourced from the tip side, thus from a medium with lower conductivity, and yet, positive currents are higher than negative currents.

The exception in the GLI experiments is one-sided gel samples on the tip side where the based side faces the liquid. Conical nanopores with the gel drop cast on the tip side (Fig. 3.9a) feature nearly ohmic behavior for lower concentration of $LiClO_4$ in the liquid on the base size, and some rectification for concentrations of 500 mM and 1 M. We postulated that the effect of weaker rectification stemmed from the location of the gel/liquid interface in the pore [116, 118] (Figure 3.10), which could be equivalent to a shorter conical pore. Rectification of conical pores is known to decrease with the decrease of pore length [56],

thus with a partial gel infiltration, the influence of the geometrical rectification can be expected to be less dominant compared to a pore entirely filled with the gel. Ion current rectification occurring at higher $LiClO_4$ concentration was puzzling, but could be explained by possibility of a higher effective surface charge of the gel caused by Li adsorption [105].

Section 3.3 – *Modeling the gel-liquid system: competing mechanisms*

In order to illustrate the interplay of the two mechanisms, geometric [51] and asymmetric conductivity [116], the system was subjected to numerical modeling based on the Poisson-Nernst-Planck equations [44, 56]. Due to axial symmetry of the system, 1D model along the pore axis, *z*, was considered. Presence of gel in the part of conical nanopore filled with PMMA was captured *via* introduction of space charges, ρ(z), added to the Poisson equation, as reported before [44]:

$$J_i = -D_i(\nabla C_i + \frac{z_i e C_i}{k_B T}\nabla\varphi) \tag{3.1a}$$

$$\nabla \cdot J_i = 0 \tag{3.1b}$$

$$\varepsilon_o \varepsilon \Delta\varphi = -\left[e(C_+ - C_-) + \rho(\mathrm{z})\right] \tag{3.1c}$$

where J_i is a flux due to one type of ions, characterized by diffusion coefficient, D_i, ε_0 is vacuum permittivity, and ε is dielectric constant of the medium assumed to be equal to 64. As modeled in our earlier manuscript, the axial dependence of the space charge was assumed:

$$\rho(\mathrm{z}) = \rho_0\left(\frac{dL_{\mathrm{int}}}{D_{\mathrm{int}} z + dL_{\mathrm{int}}}\right)^n \quad n=0.5,\ 1,\ 2,\ 4 \tag{3.2}$$

where ρ_0 is the concentration of space charge at the tip, and d and D_{int} and the diameters of the tip and pore diameter at the location of the gel/liquid interface (Figure 4.10), respectively. ρ_0 was taken equal to 10^7 C/m^3 which corresponds to charge concentration of ~0.1M. The base side of the pore was in contact with a liquid salt solutions of 0.1 M. In order to distinguish the gel and liquid bulk, diffusion coefficients of Li^+ and ClO_4^- ions differed by a factor of 10. The length of the pore infiltrated with gel, $L_{inf,}$ ranged between 0 and 12 μm.

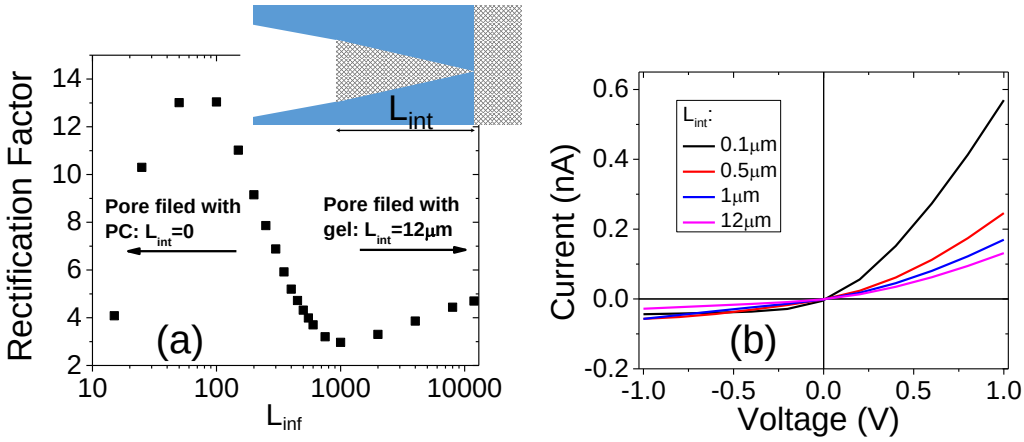

Figure 3.10. **(a)** Rectification factor calculated from **(b)** Numerical solutions to 3.1-2 plotted as I-V curves over -1 V - +1 V. Inset is a scheme of a nanopore system filled with two mediums of differing diffusion coefficients, subjected to numerical modeling.

Figure 3.10a shows how rectification factor calculated as I(+1 V)/I(-1 V) depends on L_{int}. The modeling confirmed that as in the case of a conical pore in contact with liquid electrolyte on both sides of the membrane, rectification is the strongest for a L_{int} below 500 nm. Note, however that the modeling predicted a dominant role of the geometric asymmetry over the mobility differences in the gel and liquid electrolyte. The nearly linear I-V curve observed in our experiments suggests that the gel placed on the tip side, infiltrated the pore at the depth of the order of magnitude of a micrometer.

Section 3.4 – *Discussion of findings*

Experiments with meso and nanopores containing PMMA gel revealed that ionic conductivity of the gel became dominated by the salt concentration in the liquid bulk solutions in contact with the pores. Even a pore filled with an undoped gel placed in contact with liquid salt solution exhibited conductances comparable to these in a control experiment of the same pore performed before gel infiltration. The effect of the gel on ionic transport was however clearly observed via ion current rectification consistent with a model of a porous structure of the gel [102] with effective positive charges [64]. Inserting gel into mesopores preserved large magnitudes of the current characteristic of the large pores, but rendered the pores' transport properties to have characteristics of nanoscale structures.

The system of mesopores filled partly or entirely infiltrated with PMMA gel presents an important model system showing that nano-scale properties such as rectification can be induced in microstructures by infiltrating them with a nanoporous gel. The structure of PMMA gel is not known in detail but Environmental SEM (ESEM) was attempted on $LiClO_4$-PMMA to discover structural details of the gel. However, at chamber pressure of 20mbar and controlled temperature of 10^oC, evaporation of the PC plasticizer dried the surface of the PMMA and caused the sample to bubble, preventing images from being taken of the native gel surface. However, earlier studies suggest the gel contains nanoscale voids [102], whose surface charge can originate from complexing Li^+ ions with carbonyl group of PMMA [105]. It is possible that the number of complexed ions increases with the increase of salt concentration in the bulk electrolyte. This hypothesis would explain the results for conically shaped nanopores drop cast at the tip side only and studied in the GLI mode; this system exhibited rectification whose direction was dependent on the salt concentration in the liquid

side. For higher Li^+ concentration in the bulk, the effective positive charge in PMMA would increase, enhancing the asymmetry that stems from pore asymmetry [114].

We also believe that the increased conductance of the gel system in contact with a liquid electrolyte can provide a route to obtain batteries with not only increased lifetime but also capacitance.

Chapter 4: Ion Transport for Manganese Oxide at Different Oxidation States

These studies of model electrolyte in model nanoconfinement have provided data related to fundamental questions regarding surface charge and ion transport. While they can serve as a guide to inform design principles in nanostructured battery components, it is prudent to consider other model systems which include components of the electrodes themselves. We have focused our efforts on probing structure of a cathode material MnO_2, which is known to contain voids [75, 119]. We were interested in measuring ionic resistance of the voids, which is expected to impact the power output of a battery.

A nanofabrication technique to obtain such components relies on electrodepositing materials in nanopores: template deposition [120, 121]. A wide spectrum of materials can be electrodeposited, including metals [122-124], metal oxides [125], and polymers [125], as well as composite structures such as PEDOT/MnO_2 coaxial structures [3]. The main use for this technique has been to deposit a desired material in the nanopore template, then etch away the membrane to access the wires. However, there are cases where removal of the template is not needed. For example, the template can serve as a separator in fully integrated nanobatteries [5]. The template can also be used to confine materials to the nanoscale, to investigate their ionic transport properties and geometry, as was demonstrated for MnO_2 mesorods previously [9].

MnO_2 is a popular material for energy storage devices, due to its high theoretical capacitance and low cost. When electrodeposited, it has a porous structure as recently revealed by microscopy and electrochemical measurements [9]. MnO_2 has come under

investigation in recent years due to the discovery of its supercapacitor nature at the nanoscale [1]. In order to capitalize on this property, many designs have focused on densely packed nanostructures utilizing conductive additives or scaffolds to boost electrical conductivity, and thus improve power density [8]. The dense packing paradigm highlights the relevance of our studies of nanoconfined electrolyte since power is not just limited by electric conductivity, but also by ionic access *in* and *around* these porous, densely packed structures. In order to optimize ionic conductivity in the MnO_2 nanovoids, methods are needed to quantify it, and to understand how the conductivity may change during charging and discharging [10].

Here we use the template method to electrodeposit a single MnO_2 mesorod in a single-pore polymer membrane as well as millions of rods [126] in a multipore polymer membrane. In contrast to a previous study [9], the MnO_2 in this case is not a static plug, but serves as a model nanoscale electrode. It is connected to an external circuit so that its oxidation state can be electrochemically altered before subsequent ionic conductivity measurements. The recorded ion currents reflect ionic transport through the porous structure of the material, thus they are de-coupled from the electronic transport. This method provides a unique platform for understanding how structural and electrochemical changes could influence ion access to active material during the charging and discharging of a supercapacitor.

Section 4.1 – *Nanopore template preparation*

Obtaining nanopore templates for the deposition of manganese oxide followed the track-etch protocol which has been previously described (see Ch.1, Sec. 1.1). The specific etch protocol used 0.5 M NaOH at 70^{o}C, which causes the pore opening to increase linearly

with time at a rate of ~100nm/30min [81]. The single pore templates used had diameter between 150 and 500nm in size. The multipore membranes used in these studies are commercially available; we used Whatman multipore polycarbonate membranes with 200nm diameter pores with a pore density of $\sim 10^8$ pores/cm^2.

In order to electrodeposit material inside these nanopore templates and retain an electrical contact with the material for controlling its oxidation state, one side of the membrane was sputtered with ~50-100nm of gold. This was done in accordance with an approximation model of gold atoms scattering through a solid angle into a nanopore. A simplified two-dimensional model based on azimuthal scattering cannot be used because it assumes a full range of lateral scattering (Θ_s) which is limited by pore width at a given depth (Fig. 4.2). By lateral scattering, we mean the full range of polar angles in the plane defined by an axis through the azimuthal angle and the horizontal axis (Fig. 4.1).

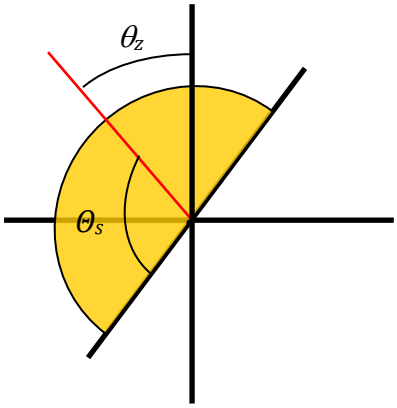

Figure 4.1 Pictorial representation of azimuthal and lateral scattering angles

What follows from this is an involved, but numerically solvable, geometry problem visualized in Figure 4.2a. One way to use the model is to solve for film thickness at a given depth, *d*, inside the nanopore (radius, *r*). For chosen *d* and given *r*, we may calculate an angle, θ_{zmax}, which dictates the maximum range of azimuthal scattering:

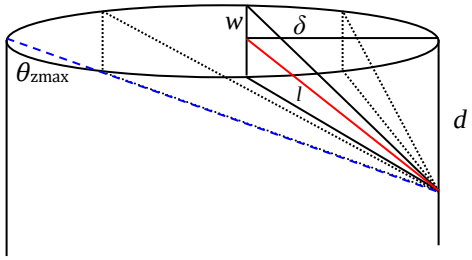

Fig. 4.2a

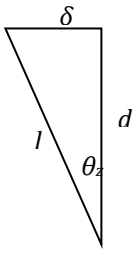

Fig. 4.2.b

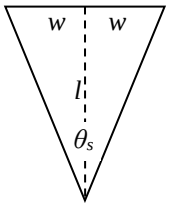

Fig. 4.2.c

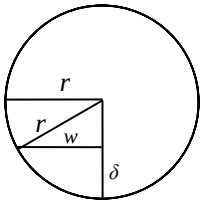

Fig. 4.2.d

Figure 4.2 (a) Scheme of the geometry that comes out of assuming a three-dimensional scattering. The scheme indicates how lateral scattering angle, θ_s, into the cylinder increases, then decreases, in accordance with the pore geometry. **Figures 4 (b-d)** further define variables in the geometry which is useful in framing and solving Equation 4.2.

$$\theta_{zmax} = \tan^{-1}\left(\frac{2r}{d}\right) \qquad (4.1)$$

At a given θ_z, we identify a range of lateral scattering angles, θ_s, dependent on the width of the pore, w, (Fig. 4.2a, the three triangles and Fig. 4.2c). Since θ_s is dependent on θ_z, we may propose a general equation (4.2) to solve for film thickness at a given depth, λ_d:

$$\lambda_d = \lambda_o \frac{\theta_{z\,max}}{\pi} \int_0^{\theta_{z\,max}} \Theta_S(\theta_z) d\theta_z \qquad (4.2)$$

The expression $\Theta_S(\theta_z)$ represents the equation for lateral scattering angle based on azimuthal scattering angle, θ_z. But since θ_z is itself dependent on d and r, the equation must be determined based on these two known factors. Figures 4.2.b-d depict the necessary geometric steps for clearly framing the desired equation. From this, we can accurately define radial entry point, δ, and scattering path, l, in terms of θ_z, as well as define width, w, in terms of δ and r:

$$\delta = \tan(\theta_z)\, d, \quad l = \frac{d}{\cos(\theta_z)}, \quad w = \sqrt{r^2 - (r-\delta)^2} = \sqrt{2r\delta - \delta^2} \qquad (4.3a\text{-}c)$$

By substitution, we can now frame $\Theta_S(\theta_z)$:

$$\theta_s = 2\tan^{-1}\left(\frac{w}{l}\right) = 2\tan^{-1}\left(\frac{\sqrt{2r\delta-\delta^2}\cos(\theta_z)}{d}\right) = 2\tan^{-1}\left(\frac{\sqrt{\left(2r-d\tan(\theta_z)\right)d(\tan(\theta)_z}\cos(\theta_z)}{d}\right) \quad (4.4)$$

Despite the deterministic geometry of the problem, the final expression is virtually impossible to solve analytically. However, a numerical solution is easily obtained by summation:

$$\lambda_d = \lambda_o \frac{\Delta}{\pi}\sum_{\theta_z=0}^{\theta_{zmax}} 2\tan^{-1}\left(\frac{\sqrt{\left(2r-d\tan(\theta_z)\right)d(\tan(\theta)_z}\cos(\theta_z)}{d}\right)/\pi \quad (4.5)$$

Δ represents the angle increment used in the summation, e.g. π/360; both lateral and azimuthal scattering are divided by π because we assume a homogeneous distribution of scattering angles for the free metal atoms in both the sputtering and evaporation deposition methods. We used Mathematica to perform this calculation at an angle increment of π/10000 for a variety of radial-length depths. What we found was an attenuating thickness. At $d = r/2$, homogeneous scattering yielded a result $\lambda_d = .19966\lambda_o$. A more complete treatment of results is shown below in Table 4.1 and Figure 4.3.

depth, d	λ_d/λ_o, $\theta_l = \pi$	λ_d/λ_o $\theta_l = 2\pi/3$	λ_d/λ_o $\theta_l = \pi/2$
$r/2$	0.19966	0.2995	0.3993
r	0.1205	0.18075	0.2410
$3r/2$	0.0784	0.1176	0.1568
$2r$	0.05387	0.0808	0.10774

Table 4.1. Simulated relative Au film thickness at different depths, *d*, of a pore with opening diameter of 200 nm (r = 100 nm). The values were obtained from eq. (*S*5). Figure 1 in the main manuscript plots λ_d/λ_o as a function of *d*. Different scenarios of maximum lateral scattering are considered in an attempt to account for how the width of the deposition chamber could affect particle scattering.

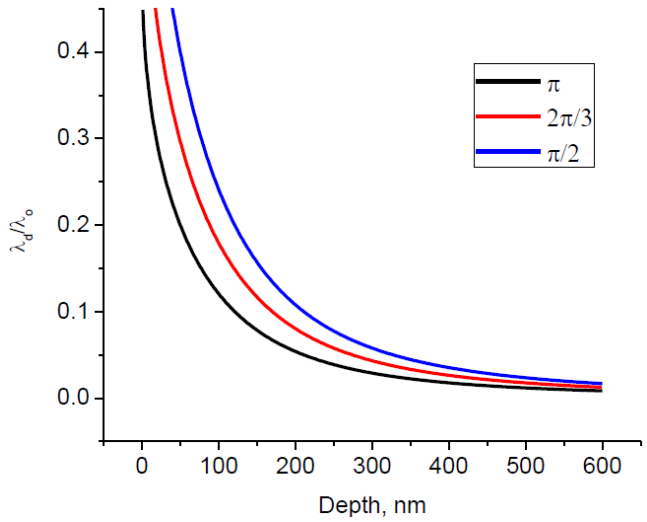

Figure 4.3 Numerical solutions to Eqn 4.5 expressed as a ratio of gold thickness at a given depth, λ_d, and gold thickness on the surface, λ_0. Three scattering conditions are considered. In case of the full hemisphere scattering (π) for a 200nm diameter pore, a 50nm thick surface layer is attenuated to 10nm thickness at d~60nm.

This lengthy discussion of gold penetration into a nanopore is relevant, because it is important to establish an effective working depth for the proposed electrode. An earlier study showed that a 10nm thick gold layer can serve as an electrode [127]; therefore, a 50nm thick sputtered surface layer of gold would yield a working distance of ~50-100nm into a 200nm pore. This gold layer completed the template preparations and provided a contact to electrodeposit MnO_2 inside the pore.

Section 4.2 – *Template deposition and confirmation by SEM, CV, and I-V scans*

The electrodeposition procedure used for depositing MnO_2 rods was established in a previous study [9]. The gold-sputtered pore was placed in contact with an external electrode and immersed in 100mM manganese acetate solution with the gold side sealed by a homemade containment unit (Figure 4.4).

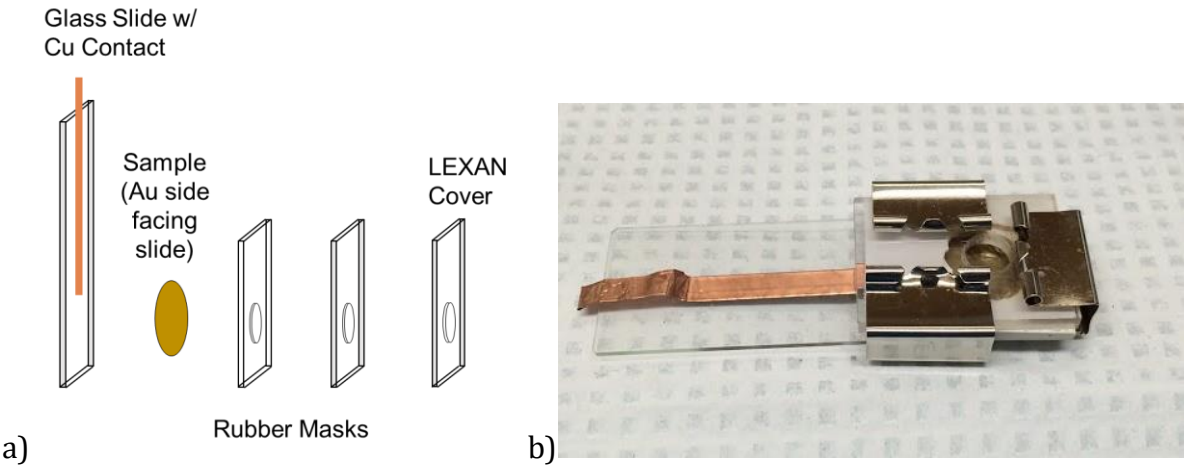

Figure 4.4 (a) Exploded schematic of containment unit designed to allow solution access to nanopore only through the unsputtered side. The copper tape contacts the gold on the membrane surface and serves as a working electrode. **(b)** Photograph of containment unit in use by a multipore membrane.

A CH Instruments 650C Electrochemical Analyzer was used as a three-probe potentiostat to hold the gold side at 0.6V vs. Ag/AgCl reference (Pt counter), which leads to the following electrochemical reaction:

$$Mn^{2+} + 2H_2O \rightarrow MnO_2 + 4H^+ + 2e^- \qquad (4.6)$$

At these parameters the MnO_2 rods grow at a rate of ~200nm/30sec [9]. For the initial experiments using aqueous solutions to probe ionic transport, MnO_2 rod length was grown to a length of ~1μm. Other experiments expanded the length explored from ~500nm - 2μm.

Electrodeposition was first attempted in multipore membranes. The presence of manganese oxide was then detected by four means. First, a visual discoloration would appear in the area of the membrane which had been exposed to the solution, turning from a golden color to brown. Second, cyclic voltammetry was performed in aqueous and propylene carbonate solutions of lithium perchlorate before and after deposition at different scan rates to demonstrate a change in system capacitance (Figure 4.5).

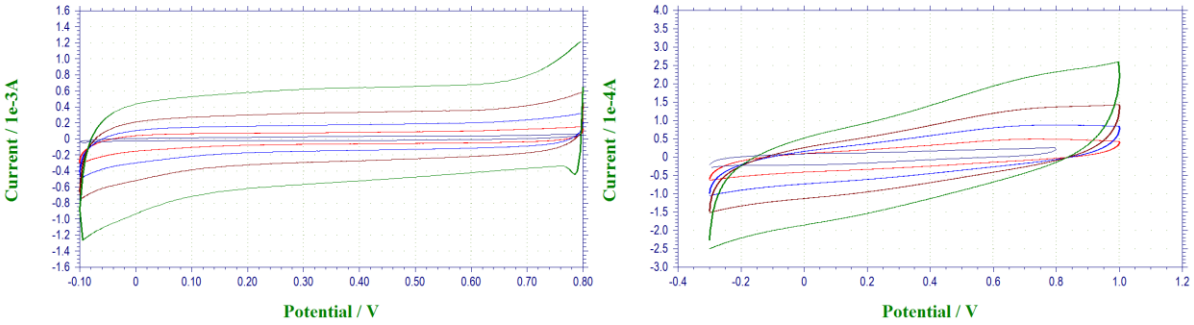

Figure 4.5 CVs demonstrating electrochemical reversibility in (left) 100mM $LiClO_4$ aqueous solution and (right) 100mM $LiClO_4$ propylene carbonate solution at scan rates of 100mV/s, 50mV/s, 25mV/s, and 10mV/s. The smallest scan on both CVs is the gold-sputtered multipore membrane's response to a 100mV/s sweep in the respective solutions. This is to demonstrate the change in capacitance resulting from the deposition of amorphous MnO_2 mesorods. The voltage window was restricted (-0.1V to 0.8V) in aqueous solution in an attempt to avoid excessive H_2 or O_2 evolution. The voltage window in the organic solution was widened to demonstrate reversibility in the regimes used for lithiation (-0.22V) and delithiation (+1V). All CVs were taken against a reference of Ag/AgCl in 3M KCl, using a CH Instruments 650C Electrochemical Analyzer and related software as a three-probe potentiostat.

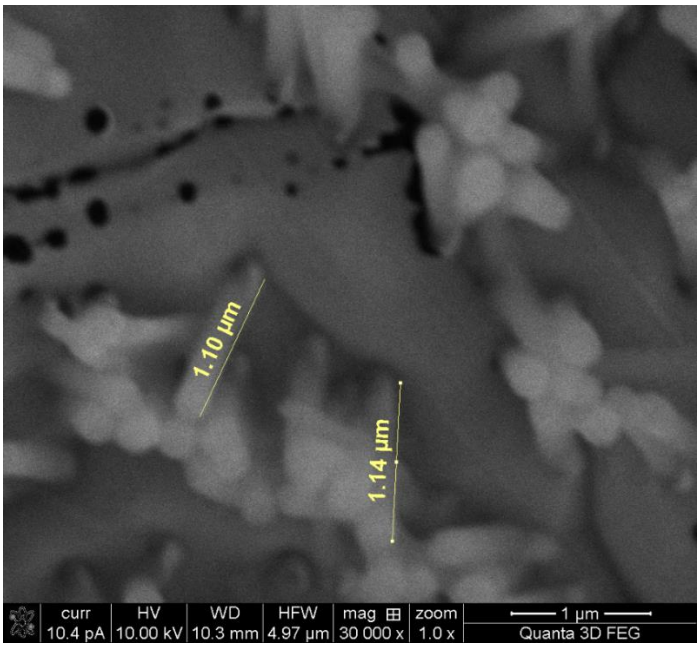

Figure 4.6 SEM images taken after the MnO_2 electrodeposition process was attempted on a commercial Whatman multipore (10^8/cm) film, which had been sputter coated with a 50nm thick layer of gold. Demonstrates viability of growing mesorods using the thin gold film technique

Another evidence for successful rod deposition was provided by current-voltage scans in aqueous 1 M KCl taken before and after deposition had taken place [9]. Lastly, SEM images were taken of MnO_2 rods using an FEG Quanta SEM/FIB after dissolving the polycarbonate template using dichloromethane (Figure 4.6). All of these means confirmed successful deposition of MnO_2 rods with the SEM images providing evidence that the rod length approximation we used was reasonable for the single pore systems.

Successful formation of a MnO_2 rod in the single pore systems was confirmed using two types of measurements. (i) First, we compared the ionic conductivity of a single pore before and after deposition of MnO_2. Similar to a previous report [9], the presence of a rod significantly increased the system resistance, as shown in Figure 4.7 for a ~1 μm long rod deposited in a 325nm diameter pore. This measurement also confirms the deposition forms a mesh with connected voids, so that the system still exhibits finite ionic conductance [9]. The samples demonstrated less dramatic changes in resistance than observed previously, possibly due to the effect of the gold electrode on the pore wall. The single pore/rod samples prepared for this study often featured ion current rectification, such that positive currents were higher than negative currents. Positive voltage in our electrode configuration indicates the anode located at the side of the membrane with deposited MnO_2 thus higher currents correspond to cations moving from the MnO_2 mesh to the open side of the template pore. The asymmetric current-voltage curves can be attributed to the negative surface charge of the MnO_2 and its nanometer-scale voids. The extended, micrometer length of the mesorod compared to the previous study (200 nm) also favours rectification. As shown recently, rectification of ion current in nanopores and nanovoids requires a certain minimum length of the pore with ionic selectivity characteristics [56]. The rectification of the examined MnO_2

rods can be compared to conically shaped nanopores [15, 20, 51], which also demonstrate preference in transporting cations from the small opening to the base of the cone.

(ii) The second measurement which confirmed successful deposition of single rods involved recording current-voltage curves for a wide set of KCl concentrations. For porous structures which carry excess surface charges on the pore walls, a saturation of ion current is observed such that further lowering of a bulk electrolyte concentration does not change the magnitude of the measured current [12, 41]. The currents start to saturate at conditions at which the pore radius approaches the thickness of the electrical double-layer. Similar to the study by Gamble et al, [9] ion current saturation was again observed in the samples prepared for this report. For the mesorod shown in (Fig. 4.7.b-c) the KCl concentration at which saturation occurred was ~10mM, which suggests the voids have opening of ~3-6nm.

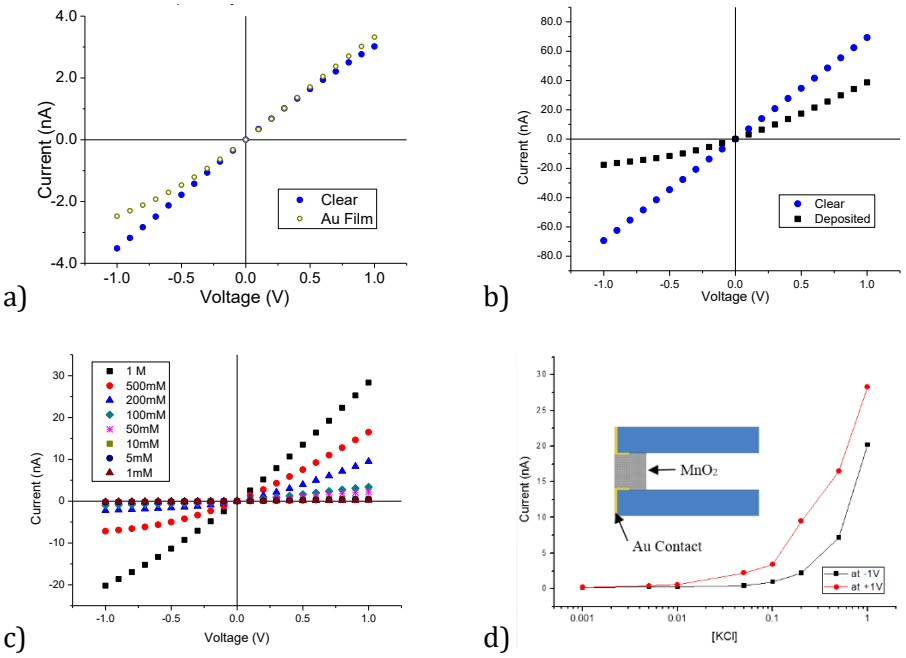

Figure 4.7 (a) I-V curves showing the difference in currents for a 210nm pore after being sputtered with 50nm Au on one side. **(b)** 325nm in diameter pore after MnO_2 deposition, as well as the resulting rectification behaviour. **(c)** I-V curves and **(d)** a semi-log plot of current vs. concentration of a single MnO_2 mesorod deposited in a 250nm in diameter pore. Saturation of ion current with bulk electrolyte (KCl) concentration occurs at ~10mM. The inset is a representation of the pore-rod system.

Section 4.3 – *Probing oxidation change of MnO_2 in aqueous electrolyte*

With thorough confirmation that MnO_2 was indeed inside our samples, we could then investigate the effect of changing the oxidation state of the MnO_2 on ion transport. After performing I-V curves for the newly deposited wires, some samples were selected for lithium insertion and discharge according to the equation:

$$MnO_2 + x\ Li^+ + x\ e^- \leftrightarrow Li_x(Mn_x^{3+}Mn_{1-x}^{4+})O_2 \qquad (4.7)$$

Insertion was carried out in non-aqueous (propylene carbonate, PC) 100mM $LiClO_4$ solution at -0.22 V vs. Ag/AgCl, a voltage which has been reported to produce a Li:Mn ratio of 1.0 [126]. Ion currents were measured in clear, deposited, 'lithiated', and 'delithiated' states of the samples in aqueous $LiClO_4$ solutions ranging from 1 M to 10mM in multipore samples for continuity with the lithiating electrolyte. Figure 4.8 shows photos of the two different set-ups used in our homemade conductivity cell for lithiation and delithiation as well as I-V scans.

a) 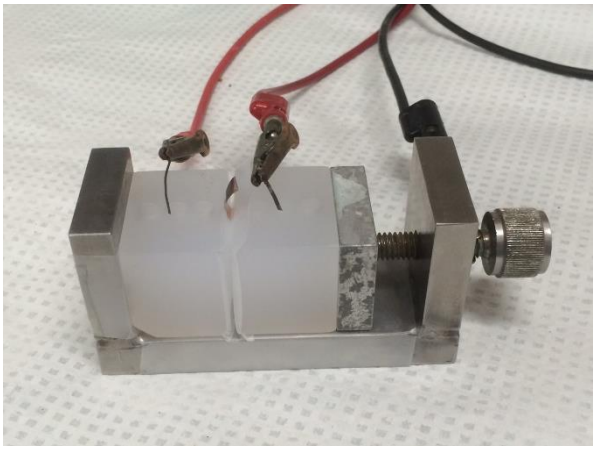 b) 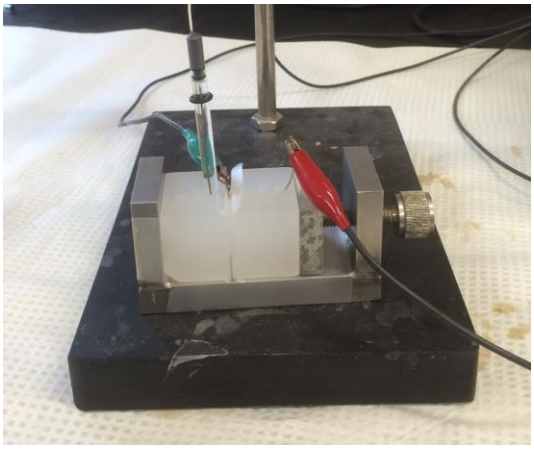

Fig. 4.8 (a) Picture of the two-probe measurement for a standard conductivity measurement. (Ag/AgCl rod electrodes for working and ground) **(b)** The three-probe set up for the lithiation and delithiation procedure (Working – *green*; Counter – *red*). Working electrode is electrically connected to Au sputtered membrane surface by means of Cu tape.

In multipore I-V scans, the oxidation state of the MnO_2 rods pointed toward conductive states associated with the intercalation or de-intercalation of lithium ions. Figure 4.9 shows bar graphs of two multipore samples. While we acknowledge that multipore samples are not identical and can vary in terms of overall pore density, the following trend can be seen in the samples shown: i) an initial decrease in system resistance following lithiation of the deposited sample, ii) a difference in resistance between lithiated and delithiated states which is somewhat reversible over the first two steps.

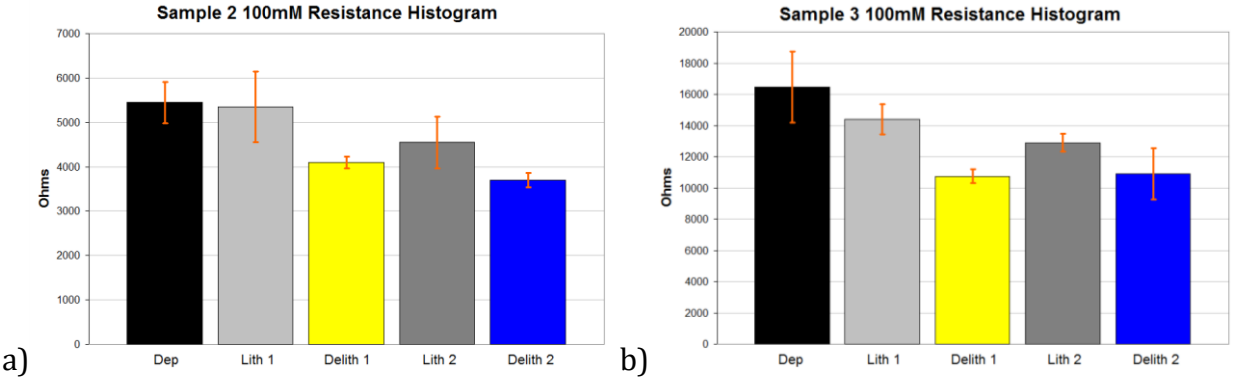

a) b)

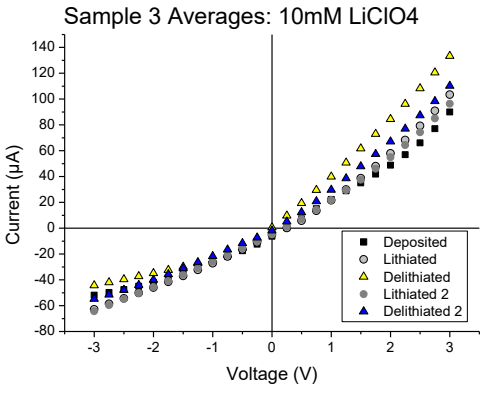

c)

Figure 4.9 (a-b) Averaged IV scans of two multipore samples over two cycles of lithiation and delithiation in 100mM aqueous $LiClO_4$ solution. Aqueous $LiClO_4$ was used to maintain compatibility with the lithiatiating solution of 100mM $LiClO_4$ in propylene carbonate. **(c)** An example of the rectification seen in lower concentrations of electrolyte in multipore samples. The initial delithiated state exhibits RF~3 while the second cycle lithiated state is RF~1.3, suggesting rectification could potentially be linked to oxidation state.

At lower concentrations of $LiClO_4$, however, some multipore samples exhibited rectification behavior (Figure 4.9c). Such rectification (4.9c Delithiated RF~3) could not be treated with the same data processing used in preparing the bar graphs, which took the average of the system resistance over most current measurements ($R = I_V/V$ where V = 1.5-3V). These results, which do not initially appear to fit with the other multipore data, point forward to the single pore experiments, where rectification is demonstrated to be a strong indicator of oxidation state in the MnO_2.

As was discussed for single pore MnO_2 rod samples, rectification was present after deposition, which has been linked to the extended length of the rod (~1μm) and the observed negative charge on the MnO_2 when immersed in aqueous solutions. Similar conditions for single pores were used regarding lithium insertion, but, for IV scans, KCl solutions ranging from 1 M to 1mM were used. KCl was the salt of choice due to nearly equal mobilities of the two ions. Figure 4.10 shows I-V curves for a 325nm diameter mesorod in three states: deposited, lithiated, and delithiated.

The change of the pore resistance is summarized in the form of bar graphs in Figure 5.b with currents for positive and negative voltages respectively. Lithiation of the rod causes a decrease of positive current and increase of negative current. This curtailing of rectification suggests a reduction of the excess negative charge on MnO_2. Subsequent discharge increases current for positive voltage polarity and increases the rectification effect. Similar behavior was found with independently prepared two MnO_2 mesorods subjected to two cycles of lithiation/delithiation. Figure 4.10c-d shows the recordings and summary obtained with a mesorod deposited in a single pore with an opening diameters of 240 nm, which suggests reversibility of the lithiation, delithiation processes.

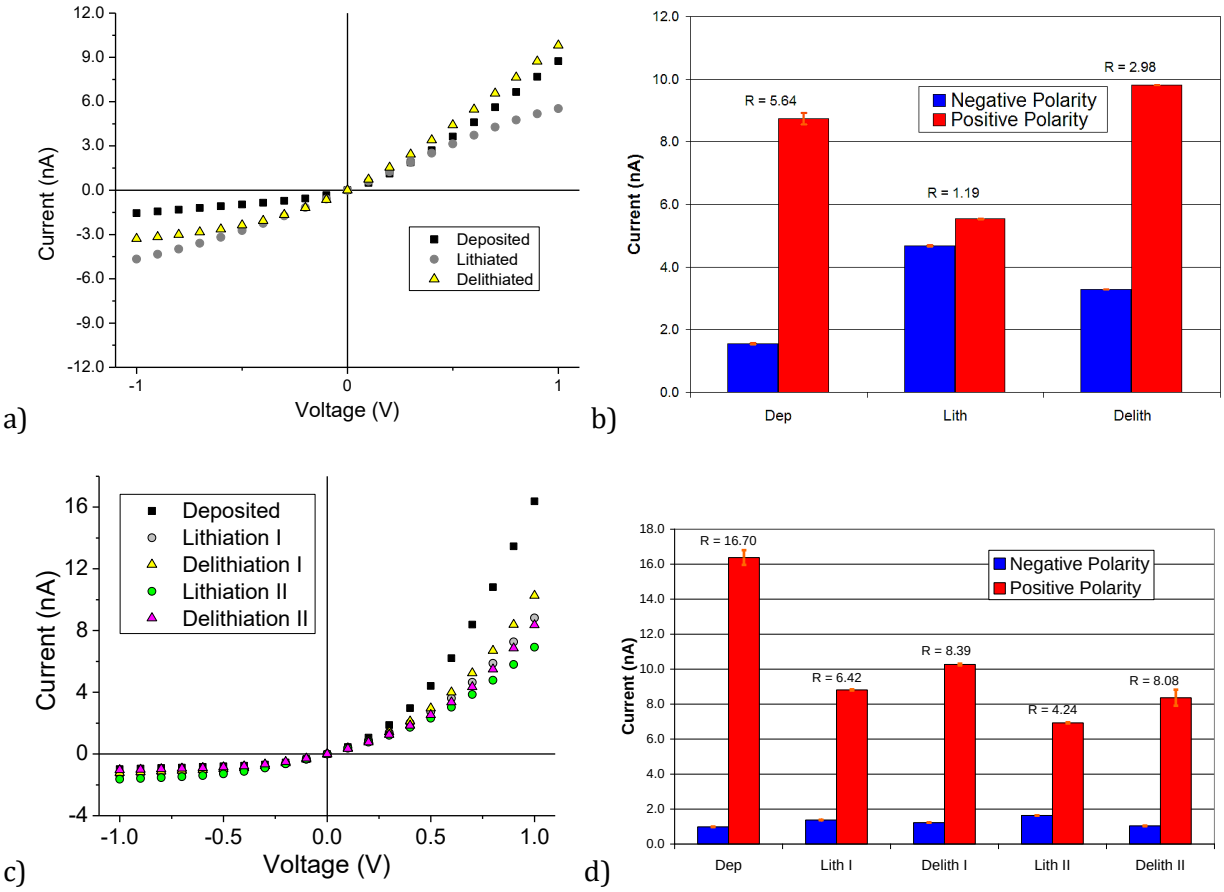

Figure 4.10 (a) Averaged I-V curves for forward and reverse scans of a MnO_2 rod at lithiated and delithiated states. **(b)** Histograms of ionic current at ±1V show the change in rectification factor, which is calculated: R = I (+1V)/I (-1V). **(c-d)** Similar measurements and summary histograms for ionic current in a 240nm pore, demonstrating cyclability.

In order to further probe the lithiation-induced changes in observed ionic conductance, surface charge on the MnO_2 rod at the lithiated state was also probed by measuring current voltage curves in a wide range of KCl concentrations. Similar to the as-deposited rods, currents through lithiated MnO_2 exhibited saturation at ~10 mM (Fig. 4.11); the measurements therefore indicate that the lithiated MnO_2 still carries negative surface charge on the voids, as suggested by the residual rectification properties shown in Fig. 4.10. A similar character of the saturation curves before and after lithiation allows us to conclude that the effective size of the voids in the material is not significantly affected by lithiation.

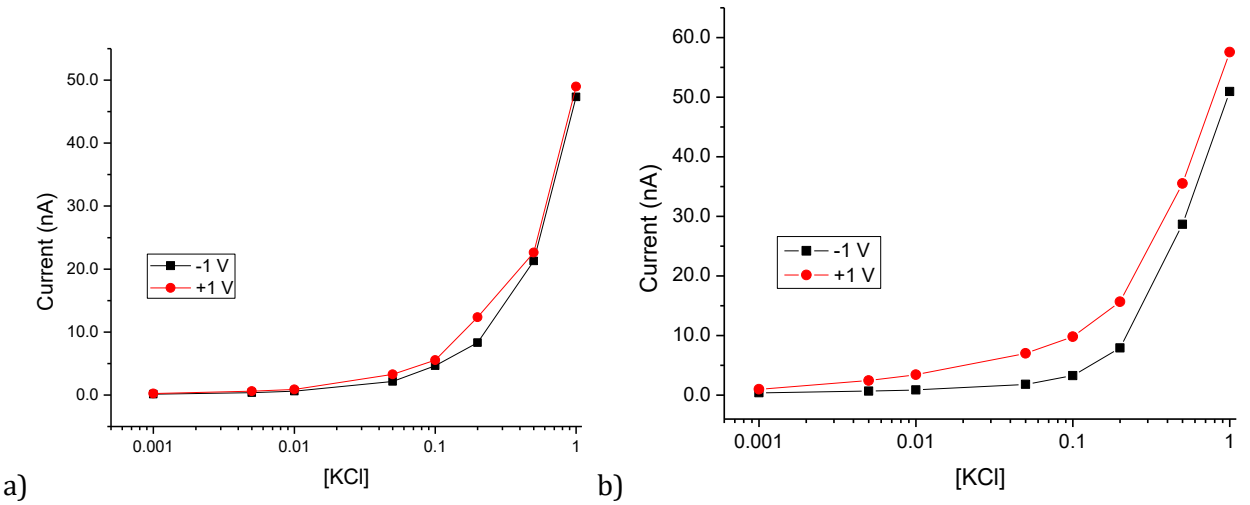

Figure 4.11 Saturation curves for a 325nm rod in its **(a)** lithiated and **(b)** delithiated states. The saturation in the MnO_2 rod demonstrates presence of surface charge and no significant changes to void size, as well as contrast between the two states.

Discharged saturation curves also demonstrate saturation, but at lower concentrations, possibly due to the difference in MnO_2 surface charge.

More detailed description of surface charge at different oxidation states was probed by the so-called reversal potential measurements. Reversal potential, V_{rev}, indicates the magnitude of a potential difference that develops across an ion selective membrane that is in contact with a salt concentration gradient. At room temperature, a 10-fold difference in ionic concentrations on both sides of a perfectly anion or cation selective membrane develops reversal potential equal to a Nernst potential of ~59mV. This is detected as an I-V curve not passing through the origin of the coordinate system, but rather being shifted to the right or left (depending on salt configuration as well as on anionic or cationic selectivity) by 59 mV. If there is no selectivity, with identical reference electrodes, the I-V curve goes through zero. If a membrane is partially selective, the shift occurs between 0 and 59 mV. A general description of ionic selectivity [39] is provided by the Goldman-Hodgkin-Katz

equation (4.8) which links the magnitude of the reversal potential with a ratio of effective diffusion coefficients of both ions in the pore, x:

$$V_{rev} = \frac{RT}{F} \ln \frac{x(K^+)_1 + (Cl^-)_2}{x(K^+)_2 + (Cl^-)_1} \quad where\ x = \frac{D^K_{pore}}{D^{Cl}_{pore}} \tag{4.8}$$

The subscripts in the equation represent the different sides of the MnO_2 rod. Figure 4.12 gives a simple schematic for our experiment. For the entirety of our experiment, the MnO_2 rod and the working electrode are on side 2 of the membrane. Therefore, a positive V_{rev} for a concentration arrangement of 0.1 M (side 1) and 10mM (side 2) indicates cation selectivity. Inversely, a negative V_{rev} for a concentration distribution of 10mM (side 1) and 0.1 M (side 2) also indicates cation selectivity.

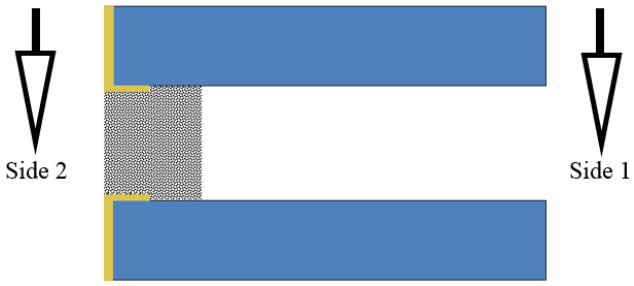

Fig. 4.12 Schematic of reversal potential measurement set-up.

S(1) / S(2)	Deposit	Lith I	Delith I	Lith II	Delith II
100 / 10*	+45mV	+33mV	+35mV	+30mV	+35mV
10 / 100	-50mV	-30mV	-30mV	-25mV	-25mV

Table 4.2. Full reversal potential measurements for a 250nm diameter mesorod as it passes through two charging cycles.
*The concentration configurations are given in concentration units of mM and are arranged where S(1) is side 1 and S(2) is side 2, which is the side of the deposited MnO_2. The electrode bias remained < ±3mV in all reversal potential measurements.

Selectivity of a 250nm diameter MnO_2 mesorod was probed using two electrolyte configurations: 0.1 M / 10mM and 10mM / 0.1 M (Table 1). Measurements for the initial deposition confirm the negative surface charge and cation selectivity (for 0.1M (1) / 0.01 M (2), eq. (4.8) yields x ~ 7).

In the 'lithiated' state, the sign of reversal potential measurements suggested MnO_2 still carried negative surface charge; a reduced magnitude of V_{rev} indicates, however, that some of the negative charge in the MnO_2 surface may be reduced by the presence of intercalated lithium. The reduction of V_{rev} is more pronounced in the case when the solution with higher KCl concentration was present on the side of the membrane with the mesorod. The enhanced dependence of the cation selectivity on the salt concentration in contact with the rod might be explained by the lowered overall negative charge on the manganese oxide. Since the excess concentration of counter-ions in the voids is a function of void diameter and surface charge density of the porous material [12, 41], after lithiation, the voids remain selective only at low salt concentrations. This is consistent with previous observations of MnO_2 in a lithium perchlorate solution, which suggest that there is some surface adsorption of lithium even without applied potential [126]. Therefore, significant differentiation of reversal potential between lithiated and delithiated states at these concentrations may not be detectable.

Section 4.4 – *Probing oxidation change of MnO_2 in non-aqueous electrolyte in multipore systems*

Having successfully shown oxidation state to impact ion transport through electrode material in aqueous conditions, the next step to consider was demonstrating the principle in organic solvent conditions. Aqueous electrochemistry is limited by a distinct voltage window (1.229 V) relating to the evolution of hydrogen and oxygen gases, and is therefore not suitable for most energy applications [128]. Thus, the new experiment would feature a model battery cathode material in model battery electrolyte: a full half-cell model system.

Again, we started with multipore MnO_2 sample studies to investigate the ion transport effects of oxidation state in organic solvent, i.e. $LiClO_4$/PC. The trend from the previous experiment was what we initially expected ($R_{dep} > R_{lith} > R_{delith}$), with the possibility of seeing rectification linked to oxidation state. However, given the positive nature of effective surface charge for nanopores in propylene carbonate, an initial assumption about rectification in MnO_2 might be that of the lithiated state possessing a positive rectification and the delithiated, or 'discharged', state having less rectification. Figure 4.13 shows an I-V scan from a multipore sample with deposited MnO_2 rods 1µm in length as well as a summary histogram tracking the resistances of several multipore samples over three cycles of insertion. Three sets of I-V curves in 100mM $LiClO_4$/PC over a window of -3V to +3V at each oxidation state were averaged together in similar fashion to the original aqueous studies to calculate resistance. As was seen before in aqueous studies, the resistance did change

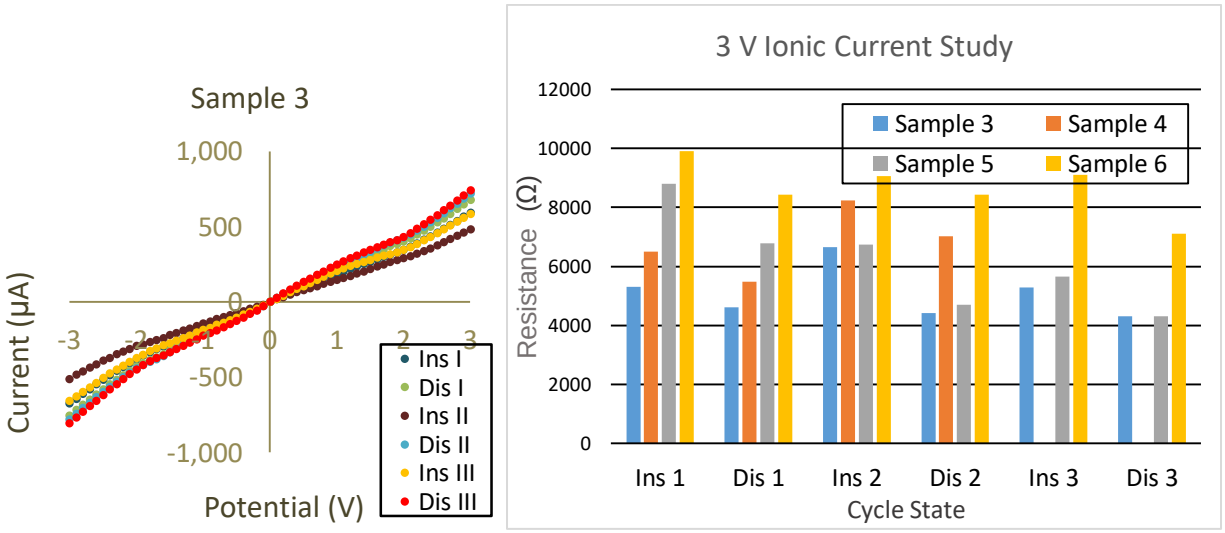

Figure 4.13 (a) Representative sample of a multipore membrane that was tested. Some variation in resistance is seen over the course of cycling, but the trend of $R_{ins(x)} > R_{dis(x)}$ is consistent, where x is the cycle number. **(b)** Four multipore samples are tracked through three cycles of lithium insertion and discharge. In all cases $R_{lith(x)} > R_{dis(x)}$, though exact reversibility was not detected, possibly due to material loss or other factors. All scans were conducted in 100mM $LiClO_4$-PC solution.

between oxidation states, with lithiated states having higher resistance than the discharged state. However, there was no clear presence of rectification in the MnO_2 samples, even when concentration of the probing solution was lowered to 10mM $LiClO_4$-PC.

In addition to these standard tests, some new lines of research were considered for non-aqueous electrolyte conditions. A technique referred to as contact-less electrochemistry [129] alerted us to the possibility that the large potential windows in our I-V scans could be causing oxidation and reduction in the MnO_2 rod. Given the apparatus we use to probe the MnO_2 rod, it is possible that a large percentage of the voltage drop over the pore-rod system occurs over the length of the rod (Figure 4.14a). This could lead to a difference in potential over the rod and lead to lithium insertion or discharge with a large transmembrane voltage. In other words, the multipore samples being tested at -3V to +3V could have undergone oxidation change during the I-V scans.

What followed was an investigation into the effect of transmembrane voltage on MnO_2 ionic resistance. We reduced the voltage window of primary I-V scans to significantly reduce the likelihood of this phenomenon (±100mV) and used those scans to calculate system resistance. The effect of transmembrane voltage was measured by subjecting the sample to I-V scans at increasing voltage windows ranging from ±200mV to ±3 V, then measuring the sample with the primary I-V scan protocol of ±100mV to track how the ionic resistance modulated as a result. From Figure 4.14b which summarizes measurements from four different samples, we see that there is a significant change in ionic resistance measured over the 100mV scan range after a scan range of -1 to +1 V is reached. This points to a physical change occurring in the system as a result of the broadened window.

a)

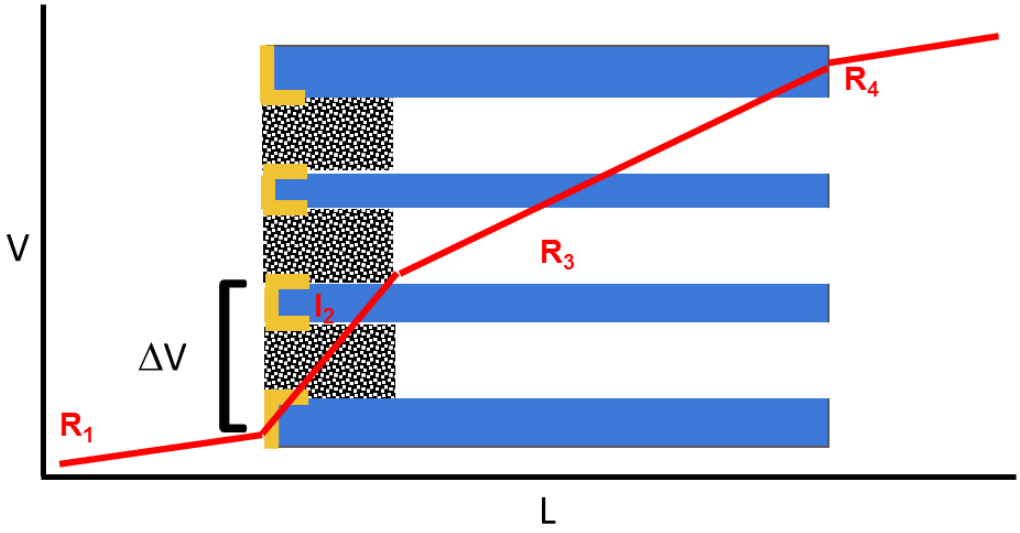

b)

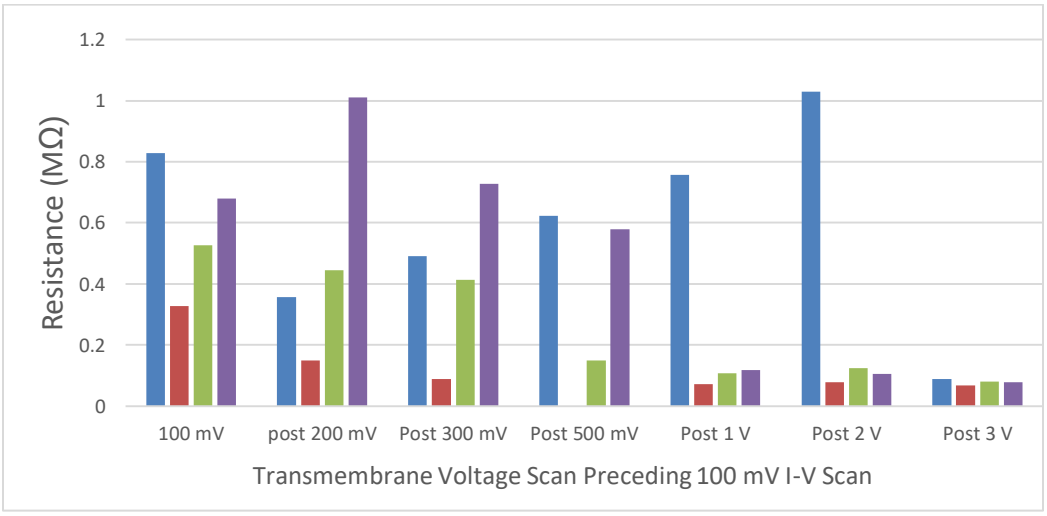

Figure 4.14 (a) Schematic of voltage drops in the multipore system. It has been proposed that insertion of lithium into the MnO_2 could happen without direct electrical contact provided the change in voltage over the length of the rod (ΔV) is sufficiently large to stimulate the insertion half-reaction. **(b)** Calculated resistances from four MnO_2 rod samples in 100mM $LiClO_4$-PC solution which have been probed by increasingly large I-V scan windows. A majority of samples experienced a significant change in system resistance between 200mV and 1 V, with all samples changing significantly after a 3V window had been achieved. (See also Appendix A for additional results related to rod length)

While the contact-less electrochemistry hypothesis is supported by this evidence, loss of material from the membrane could also contribute to the change in conductivity [97].

Another condition we considered in our multipore experiments was cycle number. It has been established that, in non-aqueous liquid electrolyte, a solid-liquid interphase (SEI) layer, which results from electrolyte breakdown, forms on the electrode material [130]. It can change the ionic resistance in the system and protect the electrode itself from breakdown [130]. This SEI layer is usually formed within the first several 10s of cycles, therefore extending the number of cycles for testing I-V response is of interest in the organic electrolyte for the MnO_2 rod system. Two multipore samples demonstrated a continuous decrease in resistance over 20 cycles (Figure 4.15). While it is not certain whether this is due to SEI formation (would usually increase ionic resistance) or material loss, the experiment suggested cycle number to be an important factor to consider for future experiments. No clear evidence of rectification was observed but it is possible that, if surface charge was small, the 100mM electrolyte concentration screened the surface charges [51].

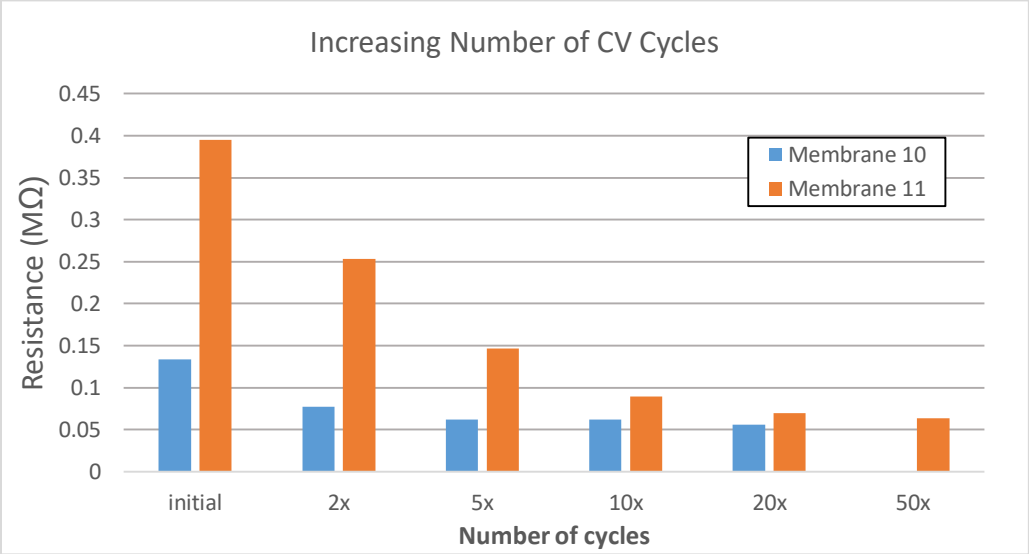

Figure 4.15 Summary bar graphs of resistance in 100mM $LiClO_4$-PC in two multipore samples over the course of cycling. CV window chosen for cycling was -0.4V to +1V vs. Ag/AgCl at a scan rate of 100mV/s. Resistance was measured using the average of three I-V scans over a -100mV to +100mV window.

Section 4.5 – *Probing oxidation change of MnO_2 in non-aqueous electrolyte in single pore-rod systems and conclusions*

For single pore samples studied in propylene carbonate conditions, we hoped that rectification would be observed from the change in oxidation state. To maintain continuity with our original experiments in aqueous electrolyte [64], we chose a -1V to +1V window for I-V scans to measure single MnO_2 rod-pore systems and -0.22 V and +1V vs. Ag/AgCl for lithiating and delithiating the MnO_2 rod respectively. While multipore-rod samples exhibited significant changes in ionic resistance from this scan window, single pore-rod samples did not. We do not yet have an explanation for this effect, and further studies are planned utilizing different deposition times and salt concentration in the testing set-up.

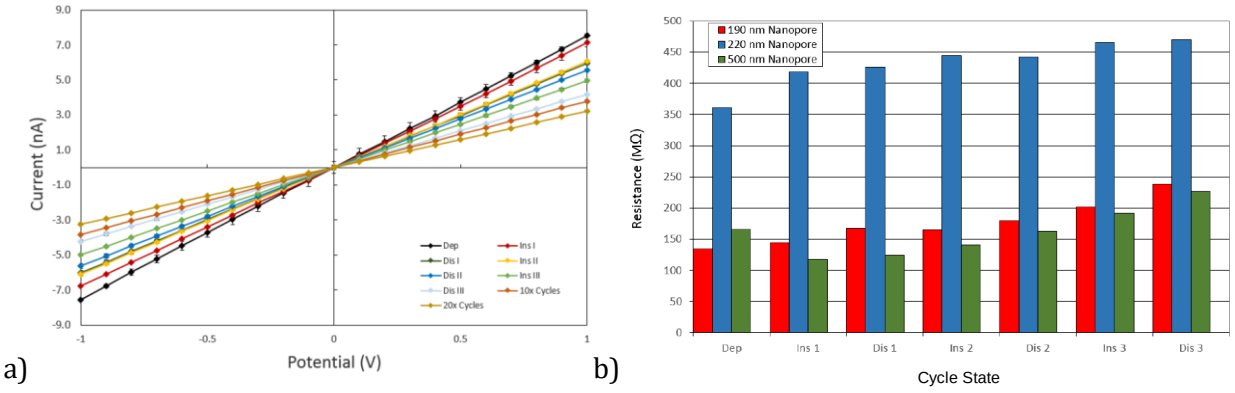

Figure 4.16 (a) I-V scans from a representative 190nm pore-rod system at different stages of insertion and discharge in 100mM $LiClO_4$-PC. The recordings at the 10th and 20th cycle were taken at the state of insertion. The electrolyte used was 100mM $LiClO_4$ in all tests. **(b)** Summary of calculated resistances for three samples with diameters of 190 nm (red), 220nm (blue), and 500nm (green). All samples show increase in resistance over the first three cycles, despite one sample showing an initial decrease in resistance after initial lithium insertion (500nm).

While the data is preliminary in nature, given the small number of samples tested (n < 10), a trend from cycling single MnO_2 rods was detected. Figure 4.16b shows resistance

data from three samples of varying pore width at different stages of lithiation, (Ins), or delithiation (Dis), over the course of the first three cycles. Unlike samples in aqueous electrolyte, no significant rectification phenomena were observed (Figure 4.16a). The previous chapter suggested that, for nanopores in PC electrolyte, the formation of positive effective surface charge resulted from the ordered dipoles on the pore surfaces. MnO_2, however, does not have regular pore geometry, and though the nanovoids are on the order of ~5nm in size, their random formation may disrupt dipole regular arrangement. Additionally, the MnO_2 structure may not preferentially favor a specific dipole orientation, or even adsorb the dipoles to begin with. However, even with lithium intercalation, which is expected to impart partial charge to the MnO_2, rectification still is not seen. More work must be done to explain whether this is a limitation of the MnO_2 material properties or the geometry of their structure.

However, despite not observing the expected phenomena of oxidation-state dependent rectification, each sample showed consistent increase in ionic resistance over the course of cycling (Fig. 4.16b). This trend was noted to continue in one sample up to the 20^{th} cycle (Fig. 4.16a). The increase in resistance can be explained by formation of an SEI layer in the MnO_2 structure as a result of cycling the rod the propylene carbonate-based electrolyte [130]. It has been shown that PC electrolyte can break down and form the SEI layer at an applied potential of 0.7V [131]. Thus it is reasonable to see an increase in resistance from such an effect in these samples which are cycled and measured solely in organic electrolyte. The MnO_2 rods cycled and then measured in aqueous electrolyte did not form a stable SEI layer, possibly due to the water exposure between cycles [132].

While it must be stressed that these findings regarding MnO_2 nanorods in $LiClO_4$/PC electrolyte are indeed preliminary, they can serve to guide future experiments that are more comprehensive in nature, looking at other factors which could probe surface charge and cycle dependence. Additionally, the stability in organic solvent could prove useful in expanding the MnO_2 pore-rod to other model battery electrolyte systems.

Chapter 5: Summary and Conclusions

Before we close, it seems appropriate to reflect on the major findings from these experiments and consider what more can be learned. The aprotic solvents work, both in PET nanopores and in the glass nanopipettes, demonstrated a unique possibility for nano-channel systems: another type of surface charge modulation, in a form of specifically adsorbed dipoles. More work in this area could be done in terms of experiments to directly quantify the effect of dipoles as well as explore the interplay between fixed surface charges and dipole adsorption. This line of study could continue from the experiment of $LiClO_4$-PC electrolyte with controlled H_2O dosage, which demonstrated surface charge modulation linked to H_2O content. This interplay could vary from material to material and solvent, which leads to a question regarding a quantitative governing principle for nanochannels of any material. Additionally, we pushed the envelope in terms of electrolytes capable of being used in polymer pores.

Experiments in the gel electrolyte, $LiClO_4$-PMMA, explored various arrangements of solid and solid-liquid electrolyte systems. We demonstrated the first solid-state nanoscale ionic diode, which led to new questions regarding the nature of charge arrangement in nanoconfined $LiClO_4$-PMMA system. Presence of surface charge is one of the conditions necessary to generate ionic rectification. Numerical modeling of nanoconfined gel demonstrated that varying volume charge, dependent on axial position, was sufficient to generate rectification and account for the lack of concentration dependence in rectification (a standard feature in most ionic rectifiers). However, systematic studies linked to tip opening size and other limiting factors such as gel concentration (which is variable) or gel type could be performed to see how far such rectifying effects could extend in the gel

electrolyte. These studies also opened a new field of understanding ionic transport in solid electrolytes at the nanoscale. The nanopore system with infiltrated solid electrolyte is unique, because the measured signal gives direct information on ionic current without the necessity to de-convolute it from the combined ionic and electronic signals.

Gel-liquid electrolyte systems aimed at proposing means to gain the advantages of both electrolyte types: high conductivity from liquid, and high mechanical stability from solid. For a gel fully immersed, we discovered that the gel-liquid system had an ionic response similar to liquid-only systems, suggesting a high degree of permeability of the gel to the compatible electrolyte. However, there was evidence that the gel structure could play a role in ion transport as asymmetric placement of the gel on a nanopore resulted in rectified currents. Asymmetric placement also served to modulate rectification of a pore which already demonstrated rectification from its asymmetric, i.e. conical, geometry. However, in the GLI experiments, the phenomena of ion transport in the gel-liquid system demonstrated other properties of rectification, which suggested a) nanostructure in the gel and b) significant changes in conductive states possibly linked to the sourcing of ions from one medium to the other. Since no successful imaging data was taken of the unbaked PMMA gel, it remains a point of interest to use these and other techniques to get meaningful sizing data, and explore how changing gel structure impacts the ion transport phenomena observed through these systems.

For manganese oxide, we expanded on previous research into its structure and surface charge properties by examining the effect of oxidation state, which can serve as a model for states of charge and discharge in battery systems. Probing in aqueous KCl solutions showed evidence that surface charge of MnO_2 does modulate with the intercalation

of lithium, impacting ion transport. While similar procedure did not yield similar results in organic solvent, preliminary findings did suggest cycling MnO_2 impacted its ionic conductivity, though a cause has yet to be determined. Additionally, with the result of long-term cycling shown for MnO_2 in $LiClO_4$-PMMA, experiments could also be conducted in a system containing MnO_2 and $LiClO_4$-PMMA, both of which are compatible with our pores.

In conclusion, there are many directions this line of research can take and much is yet unknown. But what is unknown can be made known if one has the courage to seek it.

References:

[1] H. Y. Lee and J. B. Goodenough, "Supercapacitor Behavior with KCl Electrolyte" *J. Solid State Chem.*, vol. 144, pp. 220-223 (April 1999)

[2] M. Stanley Whittingham, "History, Evolution, and Future Status of Energy Storage", *Proceedings of the IEEE*, vol. 100, pp. 1518-1534 (May 2012)

[3] J. Duay, E. Gillette, R. Liu and S. B. Lee, "Highly flexible pseudocapacitor based on freestanding heterogeneous MnO2/conductive polymer nanowire arrays" *Phys. Chem. Chem. Physics*, vol. 14, pp. 3329-3337 (January 2012)

[4] E. J. Menke, M. A. Thompson, C. Xiang, L. C. Yang and R. M Penner, "Lithographically patterned nanowire electrodeposition", *Nature Materials*, vol. 5, pp. 914- 919 (October 2006)

[5] C. Liu, E. I. Gillette, X. Chen, A. J. Pearse, A. C. Kozen, M. A. Schroeder, K. E. Gregorczyk, S. B. Lee & G. W. Rubloff, "An all-in-one nanopore battery array" *Nature Nanotechnology*, vol. 9, pp. 1031-1039 (September 2014)

[6] S. Santhanagopalan, A. Balram and D. D. Meng, "Scalable High-Power Redox Capacitors with Aligned Nanoforests of Crystalline MnO2 Nanorods by High Voltage Electrophoretic Deposition", *ACS Nano*, vol. 7 (3), pp. 2114-2125 (February 2013)

[7] S. Devaraj and N. Munichandraiah, "Effect of Crystallographic Structure of MnO_2 on Its Electrochemical Capacitance Properties", *J. Phys. Chem. C.* vol. (112), pp. 4406–4417 (February 2008)

[8] O. Ghodbane, J. L. Pascal, and F. Favier, "Microstructural effects on charge-storage properties in MnO_2 based electrochemical supercapacitors", *ACS Appl. Mater. Interfaces*, vol.1, pp. 1130-9 (May 2009)

[9] T. Gamble, E. Gillette, S. B. Lee, and Z. S. Siwy, "Probing Porous Structure of Single Manganese Oxide Mesorods with Ionic Current" *J. Phys. Chem. C,* vol. 117, pp. 24836-42 (November 2013)

[10] M. Le, Y. Liu, H. Wang, R. Dutta, W. Yan, X. Li, Y. Liu, J. C. Hemminger, R. Wu, and R. M. Penner, "*In-situ* Electrical Conductivity of Li_xMnO_2 Nanowires as a Function of 'x' and Size", *Chemistry of Materials*, vol. 27, pg. 3494-3504 (April 2015)

[11] A. van den Berg, H. Craighead and P. Yang, "From Microfluidic Applications to Nanofluidic Phenomena", *Chem. Soc. Rev.*, vol. 9, pp. 889–1220 (February 2010)

[12] R. B. Schoch, J. Han and P. Renaud, "Transport Phenomena in Nanofluidics", *Rev. Mod. Phys.*, vol. 80, pp. 839–883 (July 2008)

[13] K. Zhou, J. M. Perry and S. C. Jacobson, "Transport and Sensing in Nanofluidic Devices", *Annu. Rev. Anal. Chem.*, vol. 4, pp 321–341 (July 2011)

[14] S. Howorka and Z. S. Siwy, "Nanopore Analytics: Sensing of Single Molecules", *Chem. Soc. Rev.,* vol. 38, pp. 2360–2384 (June 2009)

[15] Z. S. Siwy and S. Howorka, "Engineered Voltage-Responsive Nanopores", *Chem. Soc. Rev.*, vol. 39, pp. 1115–1132 (March 2010)

[16] J. Li, D. Stein, C. McMullan, D. Branton, M. J. Aziz and J. A. Golovchenko, "Ion-beam Sculpting at Nanometer Length Scales", *Nature*, vol. 412, pp. 166–169 (February 2001)

[17] A. J. Storm, J. H. Chen, X. S. Ling, H. W. Zandbergen and C. Dekker, "Fabrication of Solid-State Nanopores with Single-Nanometre Precision", *Nat. Mater.*, vol. 2, pp. 537–540 (July 2003)

[18] M. D. Fischbein and M. Drndić, "Electron Beam Nanosculpting of Suspended Graphene Sheets", *Appl. Phys. Lett.*, vol. 93, pp. 113107 (August 2008)

[19] K. Liu, J. Feng, A. Kis and A. Radenovic, "Atomically Thin Molybdenum Disulfide Nanopores with High Sensitivity for DNA Translocation", *ACS Nano*, vol 8, pp. 2504–2511 (February 2014)

[20] C. Wei, A. J. Bard and S. W. Feldberg, "Current Rectification at Quartz Nanopipet Electrodes", *Anal. Chem.*, vol. 69, pp. 4627–4633 (November 1997)

[21] S. Umehara, N. Pourmand, C. D. Webb, R. W. Davis, K. Yasuda and M. Karhanek, "Current rectification with poly-l-lysine-coated quartz nanopipettes", *Nano Lett.*, vol. 6, pp. 2486–2492 (October 2006)

[22] R. L. Fleischer, P. B. Price and R. M. Walker, *Nuclear Tracks in Solids, Principles and Applications*, Univ. of California, Berkeley, Berkeley, CA (1975).

[23] Z. Siwy and A. Fulinski, "Fabrication of a Synthetic Nanopore Ion-Pump", *Phys. Rev. Lett.*, vol. 89, 198103 (October 2002)

[24] P. Y. Apel, Y. E. Korchev, Z. Siwy, R. Spohr and M. Yoshida, "Diode-like Single Ion-Track Membrane Prepared by Electrostopping", *Nucl. Instrum. Methods Phys. Res., Sect. B*, vol. 184, pp. 337–346 (November 2001)

[25] Z. Siwy, D. Dobrev, R. Neumann, C. Trautmann and K. Voss, "Electro-Responsive Asymmetric Nanopores in Polyimide with Stable Ion-Current Signal", *Appl. Phys. A*, vol. 76, pp. 781–785 (January 2003)

[26] P. Y. Apel, I. V. Blonskaya, O. L. Orelovitch, P. Ramirez and B. A. Sartowska, "Effect of Nanopore Geometry on Ion Current Rectification", *Nanotechnology*, vol. 22, 175302 (March 2011)

[27] C. C. Harrell, Z. S. Siwy and C. R. Martin, "Conical Nanopore Membranes: Controlling the Nanopore Shape", *Small*, vol. 2, pp. 194–198 (November 2005)

[28] M. Ali, P. Ramirez, S. Mafé, R. Neumann and W. Ensinger, "A pH-Tunable Nanofluidic Diode with a Broad Range of Rectifying Properties", *ACS Nano*, vol. 3, pp. 603–608 (February 2009)

[29] H. Kwok, K. Briggs and V. Tabard-Cossa, "Nanopore Fabrication by Controlled Dielectric Breakdown", *PLoS One*, vol. 9, e92880 (March 2014)

[30] N. A. W. Bell, C. R. Engst, M. Ablay, G. Divitini, C. Ducati, T. Liedl and U. F. Keyser, "DNA Origami Nanopores", *Nano Lett.*, vol. 12, 512–517 (December 2011)

[31] J. R. Burns, E. Stulz and S. Howorka, "Self-Assembled DNA Nanopores that Span Lipid Bilayers", *Nano Lett.*, vol. 13, pp. 2351–2356. (April 2013)

[32] B. J. Hinds, N. Chopra, T. Rantell, R. Andrews, V. Gavalas and L. G. Bachas, "Aligned Multiwalled Carbon Nanotube Membranes", *Science*, vol. 303, pp. 62–65. (January 2004)

[33] L. Sun and R. M. Crooks, "Single Carbon Nanotube Membranes: A Well-Defined Model for Studying Mass Transport through Nanoporous Materials", *J. Am. Chem. Soc.*, vol. 122, pp. 12340–12345. (November 2000)

[34] F. Fornasiero, H. G. Park, J. K. Holt, M. Stadermann, C. P. Grigoropoulos, A. Noy and O. Bakajin, "Ion Exclusion by Sub-2 nm Carbon Nanotube Pores", *Proc. Natl. Acad. Sci. U.S.A.*, vol. 105, pp. 17250–17255. (November 2008)

[35] H. Liu, J. He, J. Tang, H. Liu, P. Pang, D. Cao, P. Krstic, S. Joseph, S. Lindsay and C. Nuckolls, "Translocation of Single-Stranded DNA through Single-Walled Carbon Nanotubes", *Science*, vol. 327, pp. 64–67. (January 2010)

[36] C. Y. Lee, W. Choi, J. H. Han and M. S. Strano, "Coherence Resonance in a Single-Walled Carbon Nanotube Ion Channel", *Science*, vol. 329, pp. 1320–1324. (September 2010)

[37] J. Feng, K. Liu, M. Graf, M. Lihter, R. D. Bulushev, D. Dumcenco, D. T. L. Alexander, D. Krasnozhon, T. Vuletic, A. Kis and A. Radenovic, "Electrochemical Reaction in Single Layer MoS_2: Nanopores Opened Atom by Atom", *Nano Lett.,* vol. 15, pp. 3431–3438. (April 2015)

[38] C. Reece (2005) "An introduction to electrochemical impedance spectroscopy", https://www.jlab.org/conferences/tfsrf/Thursday/Th2_1-EIS%20intro%20Reece.pdf

[39] B. Hille, *Ion Channels of Excitable Membranes*; Sinauer Associates: Sunderland, MA, 2001

[40] F. M. Ashcroft, *Ion Channels and Disease*; Academic Press: Cambridge, MA, 1999

[41] S. W. Kowalczyk, T.R. Blosser, C. Dekker, "Biomimetic Nanopores: Learning from and about Nature", *Trends Biotechnol.* vol. 29, pp. 607–614 (August 2011)

[42] X. Hou, W. Guo, L. Jiang, "Biomimetic Smart Nanopores and Nanochannels", *Chem. Soc. Rev*. vol. 40, pp. 2385–2401 (February 2011)

[43] H. Daiguji, Y. Oka, K. Shirono, "Nanofluidic Diode and Bipolar Transistor", *Nano Lett*. vol. 5, pp. 2274–2280. (March 2005)

[44] I. Vlassiouk, Z. S. Siwy, "Nanofluidic Diode", *Nano Lett.* vol. 7, pp. 552–556. (February 2007)

[45] R. Karnik, C. Duan, K. Castelino, H. Daiguji, A. Majumdar, "Rectification of Ionic Current in a Nanofluidic Diode," *Nano Lett.* vol. 7, pp. 547–551. (March 2007)

[46] E. Kalman, I. Vlassiouk, Z. S. Siwy, "Nanofluidic Bipolar Transistors", *Adv. Mater.,* vol. 20, pp. 293–297. (January 2008)

[47] K. Tybrandt, K. C. Larsson, A. Richter-Dahlfors, M. Berggren, "Ion Bipolar Junction Transistors", *Proc. Natl. Acad. Sci. U. S. A.*, vol. 107, pp. 9929–9932 (May 2010)

[48] M. Ali, S. Mafe, P. Ramirez, R. Neumann, W. Ensinger, "Logic Gates Using Nanofluidic Diodes Based on Conical Nanopores Functionalized with Polyprotic Acid Chains", *Langmuir* vol. 25, pp. 11993–11997. (October 2009)

[49] K. Tybrandt, R. Forchheimer, M. Berggren, "Logic Gates Based on Ion Transistors," *Nat. Commun.*, vol. 3, pp. 871. (May 2012)

[50] J. H. Han, K. B. Kim, H. C. Kim, T. D. Chung, "Ionic Circuits Based on Polyelectrolyte Diodes on a Microchip", *Angew. Chem., Int. Ed.* vol. 48, pp. 3830–3833. (April 2009)

[51] Z. S. Siwy, "Ion Current Rectification in Nanopores and Nanotubes with Broken Symmetry Revisited", *Adv. Funct. Mater.*, vol. 16, pp. 735–746. (March 2006)

[52] E. R. Cruz-Chu, A. Aksimentiev and K. Schulten, "Ionic Current Rectification through Silica Nanopores," *J. Phys. Chem. C*, vol. 113, pp. 1850–1862. (January 2009)

[53] J. Cervera, B. Schiedt and P. Ramirez, "A Poisson/Nernst- Planck Model for Ionic Transport through Synthetic Conical Nanopores," *Europhys. Lett.*, vol. 71, pp. 35–41. (May 2005)

[54] J. Cervera, B. Schiedt, R. Neumann, S. Mafe, and P. Ramirez, "Ionic Conduction, Rectification, and Selectivity in Single Conical Nanopores," *J. Chem. Phys.*, vol. 124, 104706. (March 2006)

[55] H. S. White and A. Bund, "Ion Current Rectification at Nanopores in Glass Membranes," *Langmuir*, vol. 24, pp. 2212–2218. (January 2008)

[56] J.-F. Pietschmann, M.-T. Wolfram, M. Burger, C. Trautmann, G. Nguyen, M. Pevarnik, V. Bayer and Z. S. Siwy, "Rectification Properties of Conically Shaped Nanopores: Consequences of Miniaturization," *Phys. Chem. Chem. Phys.*, vol. 15, pp. 16917–16926. (September 2012)

[57] K. Xu, "Nonaqueous Liquid Electrolytes for Lithium-based Rechargeable Batteries," *Chem. Rev.*, vol. 104, pp. 4303–4417. (September 2004)

[58] P. Voelker, "Trace Degradation Analysis of Lithium-Ion Battery Components, R&D Magazine", (April 2014), http://www.rdmag.com/articles/2014/04/trace-degradation-analysislithium-ion-battery-components, (accessed August 2015).

[59] M. Yazid Saidi, C. Scordilis-Kelley and J. Barker, Stabilized Electrochemical Cell, US Patent, 5869207A, 1999.

[60] O. Bohnke, C. Rousselot, P. A. Gillet, C. Truche, "Gel Electrolyte for Solid-State Electrochromic Cell." *J. Electrochem. Soc.,* vol. 139, pp. 1862–1865. (July 1992)

[61] J. Vondrak, M. Sedlarikova, J. Reiter, T. Hodal, "Polymer Gel Electrolytes for Electrochromic Devices," *Electrochim. Acta*, vol. 44, pp. 3067–3073. (May 1999)

[62] A. C. Kozen, A. J. Pearse, C-F. Lin, M. Noked, and G. W. Rubloff, "Atomic Layer Deposition of the Solid Electrolyte LiPON", *Chem. Mater.*, vol. 27, pp. 5324-5331 (July 2015)

[63] S. Vorrey, D. Teeters, "Study of the Ion Conduction of Polymer Electrolytes Confined in Micro and Nanopores," *Electrochim. Acta*, vol. 48, pp. 2137–2141. (June 2003)

[64] T. S. Plett, T. Gamble, E. Gillette, S. B. Lee, and Z. S. Siwy, "Ionic Conductivity of a Single MnO_2 Mesorod at Controlled Oxidation States" *J. of Mat. Chem. A*, vol. 3, pp. 12858-12863, (May 2015)

[65] T. S. Plett, W. Shi, Y. Zeng, W. Mann, I. Vlassiouk, L. Baker, and Z. S. Siwy, "Rectification of Nanopores in Aprotic Solvents – Transport Properties of Nanopores with Surface Dipoles" *Nanoscale*, vol. 7, pp. 19080-19091, (October 2015)

[66] T. S. Plett, W. Cai, M. Le Thai, I. Vlassiouk, R. M. Penner, Z. S. Siwy, "Solid-State Ionic Diodes Demonstrated in Conical Nanopores," *J. Phys. Chem. C*, vol. 121, pp. 6170-6176 (March 2017)

[67] W. Sparreboom, A. van den Berg, J. C. T. Eijkel, "Principles and Applications of Nanofluidic Transport," *Nat. Nanotechnol.* vol. 4, pp. 713–720. (November 2009)

[68] M. Davenport, A. Rodriguez, K. J. Shea and Z. S. Siwy, "Squeezing Ionic Liquids through Nanopores," *Nano Lett.*, vol. 9, pp. 2125–2128. (April 2009)

[69] J. Feng, K. Liu, R. D. Bulushev, S. Khlybov, D. Dumcenco, A. Kis and A. Radenovic, "Identification of Single Nucleotides in MoS_2 Nanopores," *Nat. Nanotechnol*., vol. 10, pp. 1070-1076. (September 2015)

[70] G. Maglia, A. J. Heron, W. L. Hwang, M. A. Holden, E. Mikhailova, Q. Li, S. Cheley and H. Bayley, "Droplet Networks with Incorporated Protein Diodes show Collective Properties," *Nat. Nanotechnol.*, vol. 4, pp. 437–440. (June 2009)

[71] G. Nguyen, I. Vlassiouk and Z. S. Siwy, "Comparison of Bipolar and Unipolar Diodes," *Nanotechnology*, vol. 21, 265301. (June 2010)

[72] M. E. Gracheva, J. Vidal and J.-P. Leburton, "p-n Semiconductor Membrane for Electrically Tunable Ion Current Rectification and Filtering," *Nano Lett.*, vol. 7, pp. 1717–1722. (May 2007)

[73] R. Yan, W. Liang, R. Fan and P. Yang, "Nanofluidic Diodes Based on Nanotube Heterojunctions," *Nano Lett.,* vol. 9, pp. 3820–3825. (July 2009)

[74] X. Yin, S. Zhang, Y. Dong, S. Liu, J. Gu, Y. Chen, X. Zhang, X. Zhang and Y. Shao, "Ionic Current Rectification in Organic Solutions with Quartz Nanopipettes," *Anal. Chem.,* vol. 87, pp. 9070–9077. (July 2015)

[75] T. Gamble, K. Decker, T. S. Plett, M. Pevarnik, J.-F. Pietschmann, I. Vlassiouk, A. Aksimentiev and Z. S. Siwy, "Rectification of Ion Current in Nanopores Depends on the Type of Monovalent Cations: Experiments and Modeling," *J. Phys. Chem. C*, vol. 118, pp. 9809–9819. (April 2014)

[76] B. Zhang, Y. Ai, J. Liu, S. W. Joo and S. Qian, "Polarization Effect of a Dielectric Membrane on the Ionic Current Rectification in a Conical Nanopore," *J. Phys. Chem. C*, vol. 115, pp. 24951–24959. (November 2011)

[77] R. Spohr, Methods and Device to Generate a Predetermined Number of Ion Tracks, German Patent, DE2951376C2, 1983; R. Spohr, Methods and Device to Generate a Predetermined Number of Ion Tracks, US Patent 4369370, 1983.

[78] A. Adla, H. Fuess, and C. Trautmann, "Characterization of Heavy Ion Tracks in Polymers by Transmission Electron Microscopy." *J. Polymer Sci. Part B*, vol. 41, pp. 2892–2901 (October 2003).

[79] W. DeSorbo, "Ultraviolet Effects and Aging Effects on Etching Characteristics of Fission Tracks in Polycarbonate Films," *Nuclear Tracks*, vol. 3, pp. 13-32 (March 1979)

[80] Z. Zhu, Y. Maekawa, Q. Liu, and M. Yoshida, "Influence of UV Light Illumination on Latent Track Structure in PET," *Nuc. Inst. and Meth. in Phys. Res. Section B*, vol. 236, pp. 61-67 (May 2005)

[81] M. Pervarnik, K. Healy, M. E. Toimil-Molares, A. Morrison, S. E. Létant, and Z. S. Siwy, "Polystyrene Particles Reveal Pore Substructure as they Translocate" *ACS Nano*, vol. 6, pp. 7295–7302. (July 2012)

[82] E. Ferain, R. Legras, "Pore Shape Control in Nanoporous Particle Track Etched Membrane", *Nucl. Inst. and Meth. in Phys. Res. Section B*, vol. 174, pp. 116-122 (March 2001)

[83] K. Fujimoto, M. Doi and S. Kobayashi, "Etching Rate of Polycarbonate," *Jpn. J. Health Phys.*, vol. 25, pp. 221–226. (March 1990)

[84] J. Barthel, H.-J. Gores, G. Schmeer and R. Wachter, "Nonaqueous Electrolyte Solutions in Chemistry and Modern Technology," *Phys. Inorg. Chem.*, vol. 111, pp. 33–144. (1983)

[85] *Adsorption on Silica Surfaces*, Ed. E. Papirer, Marcel Dekker Inc., New York, 2000.

[86] H. Huang, M. Manciu and E. Ruckenstein, "The Effect of Surface Dipoles and of the Field Generated by a Polarization Gradient on the Repulsive Force," *J. Colloid Interface Sci*., vol. 263, pp. 156–161. (July 2003)

[87] H. Tatsumi, A. Sasahara and M. Tomitori, "Adsorption of Propylene Carbonate Molecules on a TiO_2 (110) Surface," *J. Phys. Chem. C*, vol. 117, pp. 10410–10416. (April 2013)

[88] H. Liu, Y. Tong, N. Kuwata, M. Osawa, J. Kawamura and S. Ye, "Adsorption of Propylene Carbonate (PC) on the $LiCoO_2$ Surface Investigated by Nonlinear Vibrational Spectroscopy," *J. Phys. Chem. C*, vol. 113, pp. 20531– 20534. (November 2009)

[89] M. L. Belaya, M. V. Feigel'man and V. G. Levadny, "Structural Forces as a Result of Nonlocal Water Polarizability," *Langmuir*, vol 3, pp. 648–654. (September 1987)

[90] M. Belaya, V. Levadny and D. A. Pink, "Electrical Double Layer near Soft Permeable Interfaces. 1. Local Electrostatics," *Langmuir*, vol. 10, pp. 2010–2014. (June 1994)

[91] Z. Siwy and A. Fulinski, "Origin of 1/f α Noise in Membrane Channel Currents," *Phys. Rev. Lett*., vol. 89, 158101. (September 2002)

[92] N. Sa, W.-J. Lan, W. Shi and L. A. Baker, "Rectification of Ion Current in Nanopipettes by External Substrates," *ACS Nano*, vol. 7, pp. 11272–11282. (November 2013)

[93] K. McKelvey, S. L. Kinnear, D. Perry, D. Momotenko and P. R. Unwin, "Surface Charge Mapping with a Nanopipette," *J. Am. Chem. Soc.*, vol. 136, pp. 13735–13744. (September 2014)

[94] K. Leung, "Ion-dipole Interactions are Asymptotically Unscreened by Water in Dipolar Nanopores, Yielding Patterned Ion Distributions," *J. Am. Chem. Soc.*, vol. 130, pp. 1808–1809. (January 2008)

[95] J. W. Long, B. Dunn, D. R. Rolison, H. S. White, "Three-Dimensional Battery Architectures," *Chem. Rev.* vol. 104, pp. 4463–4492. (August 2004)

[96] W. Yan, M. L. Thai, R. Dutta, X. Li, W. Xing, R. M. Penner, "A Lithographically Patterned Capacitor with Horizontal Nanowires of Length 2.5 mm," *ACS Appl. Mater. Interfaces* vol. 6, pp. 5018–5025. (March 2014)

[97] M. L. Thai, G. T. Chandran, R. K. Dutta, X. Li, R. M Penner, "100k Cycles and Beyond: Extraordinary Cycle Stability for MnO_2 Nanowires Imparted by a Gel Electrolyte," *ACS Energy Lett*. vol. 1, pp. 57–63. (April 2016)

[98] V. Coropceanu, J. Cornil, D. A. da Silva Filho, Y. Olivier, R. Silbey, and J. L. Bredas, "Charge Transport in Organic Semiconductors," *Chem. Rev.,* vol. 107, pp. 926–952. (March 2007)

[99] P. Ramirez, V. Gomez, J. Cervera, S. Nasir, M. Ali, W. Ensinger, S. Mafe, "Energy Conversion from External Fluctuating Signals Based on Asymmetric Nanopores," *Nano Energy*, vol. 16, pp. 375–382. (July 2015)

[100] Z. Osman, M. I. Mohd Ghazali, L. Othman, K. B. Md Isa, "AC Ionic Conductivity and DC Polarization Method of Lithium Ion Transport in PMMA-$LiBF_4$ Gel Polymer Electrolytes," *Results Phys*., vol. 2, pp. 1–4. (January 2012)

[101] A. M. M. Ali, M. Z. A. Yahya, H. Bahron, R. H. Y. Subban, M. K. Harun, I. Atan, "Impedance Studies on Plasticized PMMA-LiX [X: $CF_3SO_3^-$, $N(CF_3SO_2)_2^-$] Polymer Electrolytes," *Mater. Lett*. vol. 61, pp. 2026–2029. (April 2007)

[102] C. M. Mathew, K. Kesavan, S. Rajendran, "Structural and Electrochemical Analysis of PMMA Based Gel Electrolyte Membrane," *Int. J. Electrochem.* vol. 2015, 494308. (January 2015)

[103] J. Vondrak, M. Sedlarikova, J. Velicka, B. Klapste, V. Novak, J. Reiter, "Gel Polymer Electrolytes Based on PMMA," *Electrochim. Acta* vol. 46, pp. 2047–2048. (2000)

[104] P. Johansson, M. Edvardsson, J. Adebahr, P. Jacobsson, "Mixed Solvent and Polymer Coordination in PAN and PMMA Gel Polymer Electrolytes Studied by Ab Initio Calculations and Raman Spectroscopy," *J. Phys. Chem. B*, vol. 107, pp. 12622–12627. (October 2003)

[105] J. Y. Wang, W. Chen, T. P. Russell, "Ion-Complexation-Induced Changes in the Interaction Parameter and the Chain Conformation of PS-b-PMMA Copolymers," *Macromolecules*, vol. 41, pp. 4904–4907. (June 2008)

[106] X. H. Flora, M. Ulaganathan, R. S. Babu, S. Rajendran, "Evaluation of Lithium Ion Conduction in PAN/PMMA-based Polymer Blend Electrolytes for Li-Ion Battery Applications," *Ionics* vol. 18, pp. 731–736. (March 2012)

[107] A. M. Stephan, "Review on Gel Polymer Electrolytes for Lithium Batteries," *Eur. Polym. J.*, vol. 42, pp. 21–42. (January 2006)

[108] C. Svanberg, W. Pyckhout-Hintzen, L. Börjesson, "Network Structure of Poly(Methyl Methacrylate) – Based Gels and Gel Electrolytes," *Electrochim. Acta*, vol. 51, pp. 4153–4156. (May 2006)

[109] S. Mafé, J. A. Manzanares, P. Ramirez, "Modeling of Surface vs. Bulk Ionic Conductivity in Fixed Charge Membranes," *Phys. Chem. Chem. Phys.* vol. 5, pp. 376–383. (November 2002)

[110] S. H. Chung, Y. Wang, S. G. Greenbaum, D. Golodnitsky, E. Peled, "Uniaxial Stress Effects in Poly(ethylene oxide)-LiI Polymer Electrolyte Film: A ^{7}Li Nuclear Magnetic Resonance Study*," Electrochem. Solid-State Lett*. vol. 2, pp. 553–555. (September 1999)

[111] D. Golodnitsky, E. Livshits, A. Ulus, Z. Barkay, I. Lapides, E. Peled, S. H. Chung, S. Greenbaum, "Fast Ion Transport Phenomena in Oriented Semicrystalline LiI-P(EO)n-Based Polymer Electrolytes," *J. Phys. Chem. A*, vol. 105, pp. 10098–10106. (October 2001)

[112] I. Vlassiouk, P. Y. Apel, S. N. Dmitriev, K. Healy, Z. S. Siwy, "Versatile Ultrathin Nanoporous Silicon Nitride Membranes," *Proc. Natl. Acad. Sci. U. S. A.*, vol. 106, pp. 21039–21044. (December 2009)

[113] W. Yan, J. Y. Kim, W. Xing, K. C. Donavan, T. Ayvazian, R. M. Penner "Lithographically Patterned Gold/Manganese Dioxide Core/Shell Nanowires for High Capacity, High Rate, and High Cyclability Hybrid Electrical Energy Storage," *Chem. Mat.* vol. 12, pp. 2382. (May 2012)

[114] C-W. Kuo, W-B. Lin, P-R. Chen, J-W. Liao, C-G. Tseng, T-Y. Wu, "Effect of Plasticizer and Lithium Salt Concentration in PMMA-based Composite Polymer Electrolytes," *Int. J. of Electrochem. Sci.*, vol. 8, pp. 5007-5021 (April 2013)

[115] L. J. Cheng, and L. Guo, **"**Rectified Ion Transport through Concentration Gradient in Homogeneous Silica Nanochannels**,"** *Nano Lett.*, vol. 7, pp. 3165-71 (September 2007)

[116] L. Wang, H. Zhang, Z. Yang, J. Zhou, L. Wen, L. Li, and L. Jiang, "Fabrication of Hydrogel-Coated Single Conical Nanochannels Exhibiting Controllable Ion Rectification Characteristics" *Phys. Chem. Chem. Phys.* vol. 17, pp. 6367-6373 (January 2015)

[117] H. Falahati, L. Wong, L. Davarpanah, A. Garg, P. Schmitz, D. P.J. Barz "The Zeta Potential of PMMA in Contact with Electrolytes of Various Conditions: Theoretical and Experimental Investigation," *Electrophoresis*, vol. 35, pp. 870-882 (March 2014)

[118] F. Maletzki, H. W. Rosler, E. Staude "Ion Transfer Across Electrodialysis Membranes in the Overlimiting Current Range: Stationary Voltage Current Characteristics and Current Noise Power Spectra Under Different Conditions of Free Convection," *J. Membr. Sci.,* vol. 71, pp. 105–15 (July 1992)

[119] B-C. Yu, J-O. Lee, J. H. Song, C-M. Park, C. K. Lee, H-J. Sohn, "Nanostructured cobalt Oxide-Based Composites for Rechargeable Li-ion Batteries," *J. of Solid State Electrochem.* vol. 16, pp. 2631-2638 (August 2012)

[120] C. R. Martin, "Nanomaterials: a Membrane-Based Synthetic Approach," *Science*, vol. 266, pp. 1961–1966; (December 1994)

[121] C. J. Brumlik, V. P. Menon and C. R. Martin, "Template Synthesis of Metal Microtubule Ensembles Utilizing Chemical, Electrochemical, and Vacuum Deposition Techniques," *J. Mater. Res.*, vol. 9, pp. 1174–1183. (May 1994)

[122] C. Schönenberger, B. M. I. van der Zande , L. G. J. Fokkink, M. Henny, C. Schmid, M. Krüger, A. Bachtold, R. Huber, H. Birk, and U. Staufer, "Template Synthesis of Nanowires in Porous Polycarbonate Membranes: Electrochemistry and Morphologyc" *J. Phys. Chem. B*, vol. 101, pp. 5497–5505; (July 1997)

[123] M. E. Toimil-Molares, V. Buschmann, D. Dobrev, R. Neumann, R. Scholz, I. U. Schuchert and J. Vetter, "Single-Crystalline Copper Nanowires Produced by Electrochemical Deposition in Polymeric Ion Track Membranes" *Adv. Mater.,* vol. 13, pp. 62–65; (January 2001)

[124] T. W. Cornelius, J. Brötz, N. Chtanko, D. Dobrev, G. Miehe, R. Neumann and M. E. Toimil Molares, "Controlled Fabrication of Poly- and Single-Crystalline Bismuth Nanowires," *Nanotechnology*, vol. 16, pp. S246–S249. (May 2005)

[125] *Nanostructured Materials in Electrochemistry*, ed. A. Eftekhari, Wiley-VCH, Weinheim, 2008.

[126] J. Song, J. Duay, E. Gillette and S. B. Lee, "The Reversible Anomalous High Lithium Capacity of MnO2 Nanowires" *Chem. Commun*., vol. 50, pp. 7352–7355. (May 2014)

[127] S.-Y. Kishioka, J. Nishino and H. Sakaguchi, "Fabrication of Stable, Highly Flat Gold Film Electrodes with an Effective Thickness on the Order of 10 nm" *Anal. Chem*., vol. 79, pp. 6851–6856. (2007)

[128] C. Wessells, R. Ruffo, R. A. Huggins, and Y. Cui, "Investigations of the Electrochemical Stability of Aqueous Electrolytes for Lithium Battery Applications," *Electrochem. Solid-State Lett.*, vol. 13, pp. A59-A61 (March 2010)

[129] T. Uda, T. H. Okabe, Y. Waseda, K. T. Jacob, "Contactless Electrochemical Reduction of Titanium (II) Chloride by Aluminum," *Metall. and Mater. Trans B,* vol. 31, pp. 713 (August 2000)

[130] M. B. Pinson and M. Z. Bazant, "Theory of SEI Formation in Rechargeable Batteries: Capacity Fade, Accelerated Aging and Lifetime Prediction," *J. Electrochem. Soc.*, vol. 160, pp. A243-250 (December 2012)

[131] A. N. Dey and B. P. Sullivan, "The Electrochemical Decomposition of Propylene Carbonate on Graphite," *J. of Electroch. Soc*., vol. 117, pp. 222-224, (February 1970)

[132] A. M. O'Mahony, D. S. Silvester, L. Aldous, C. Hardacre and R. G. Compton, "Effect of Water on the Electrochemical Window and Potential Limits of Room-Temperature Ionic Liquids," *J. Chem. Eng. Data*, vol. 53, pp. 2884-2891 (November 2008)

[133] M.R. Powell, I. Vlassiouk, C. Martens, Z.S. Siwy, "Non-equilibrium 1/f noise in rectifying nanopores," *Physical Review Letters*, vol. 103, pp. 248104 (1-4) (2009)

Appendix A: Additional Studies of Multipore MnO_2 Samples and their Transmembrane Voltage Sensitivity

Additional transmembrane voltage tests of electrodeposited MnO_2 samples were done as a probe for contactless electrochemistry. The other lengths of MnO_2 that were tested were ~500nm and ~2μm. The data is showed here in Figure A.1:

a)

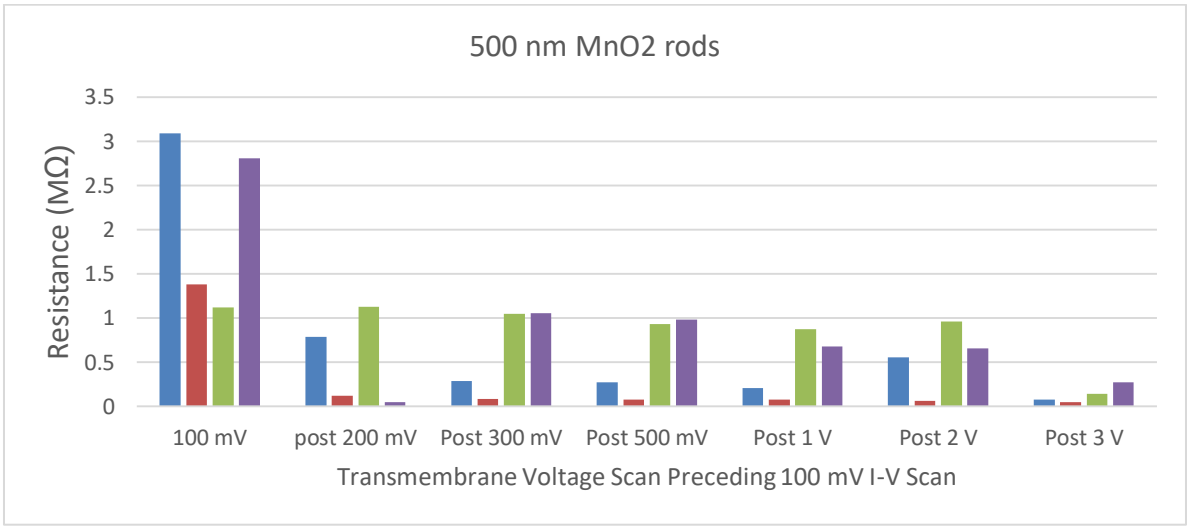

b)

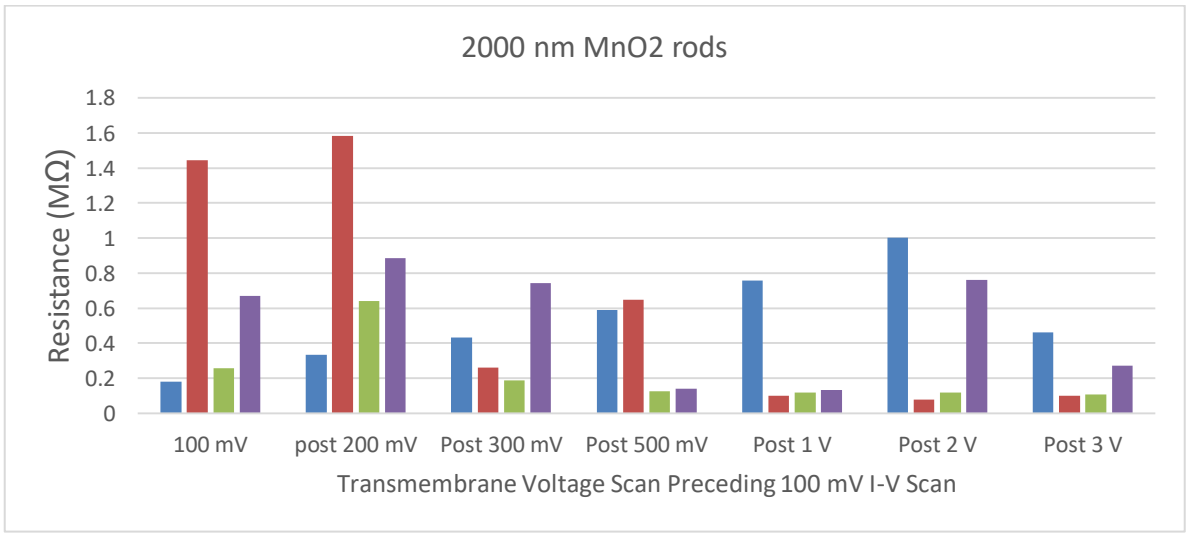

Figure A.1 Summary histograms of four multipore MnO_2 samples of two different rod lengths. In both samples, a uniform cut-off voltage is seen at 3 V. These measurements were taken in 100mM $LiClO_4$-PC solution.

Interestingly, the initial ionic resistance in the shorter MnO_2 samples is higher than in the longer rods, which is consistent with observations from previous studies [9, 64]. However, the shorter rods appeared to be more susceptible to transmembrane voltage as three out of four samples had markedly reduced resistance after the voltage window was widened to ±200mV (Fig. A.1a) whereas the longer rods had increased resistance (Fig. A.1b). That being said, a majority of ~2μm samples showed reduced resistance after ±500mV, save one sample which showed increased resistance through ±2V (which might point to similarity with the single pore experiments in Ch.4 Sec. 5). The small magnitude of the voltage window required to cause changes in ionic resistance, in addition to a small sample size (n = 4), seems to suggest that contactless electrochemistry may not be the only mechanism at play. Further studies are required to make clear this effect and its dependence on the length of deposited MnO_2 rods.